Nanostructuring and Ge redistribution in thin films of Silicon-Germanium by thermal oxidation

Ethan Schuyler Long

Thesis submitted in partial fulfillment
of the requirements for the degree of
Philosophiae Doctor

UiO : Centre for Materials Science
and Nanotechnology
University of Oslo

Department of Physics
University of Oslo

February 2013

Series of dissertations submitted to the
Faculty of Mathematics and Natural Sciences, University of Oslo
No. 1340

ISSN 1501-7710

Cover: Inger Sandved Anfinsen.
Printed in Norway: AIT Oslo AS.

Produced in co-operation with Akademika publishing.
The thesis is produced by Akademika publishing merely in connection with the thesis defence. Kindly direct all inquiries regarding the thesis to the copyright holder or the unit which grants the doctorate.

To Alexis, Francesca, Jason, Jared, Brandon,
Guy, Roberta, and Leland

Abstract

Despite the fact that germanium played a significant role in the advent of modern electronics, silicon-germanium alloys have not been used or studied nearly as extensively as silicon. However, a recent resurgence in industrial and research interest in silicon-germanium ensures that it will have an increasingly important role in nano- and opto-electronics. It is unavoidable that a sound understanding of the oxidation of silicon-germanium will be required as processes are developed for using the material in electronic applications. In fact, a profound appreciation for the oxidation kinetics of silicon-germanium could itself create new applications for the material.

The present work investigates the use of thermal oxidation in nanostructuring of epitaxially grown silicon-germanium by examining the kinetics of oxidation and the redistribution of germanium at the oxidation interface. This is done for oxidations in dry O_2 ambients with a particular focus on the influence of temperature and crystalline orientation on the post-oxidation germanium distribution. Physical characterization by x-ray diffraction and variable angle spectroscopic ellipsometry is used along with diffusion and oxidation modeling to derive a series of relations to describe the germanium content and layer thicknesses for the multiple layers created by oxidation. Both modeling and experimental results reveal that the germanium content at the oxidation front is strongly dependent on the oxidation temperature and only weakly dependent on the germanium content in the as-grown silicon-germanium layer. Evidence is presented showing that a decrease, rather than an increase, in the germanium content at the oxidation front may be achieved under certain conditions. The germanium content at the oxidation interface is used to discuss the potential for germanium to act as a catalyst or inhibitor for oxidation of silicon-germanium alloys. Taken together, germanium redistribution by thermal oxidation and the empiric relations presented here may be used to design process recipes for fabrication of nanostructures for nano- and opto-electronic applications.

Acknowledgments

The author gratefully acknowledges: the NSE-IM2NP team and NanoTecMat platform for providing MBE grown SiGe samples, Henry Radamson of KTH for providing CVD grown SiGe samples, Alexander Azarov and Frode Kløw at the University of Oslo for performing RBS measurements and associated simulations, Spyridon Diplas at the University of Oslo and SINTEF for assistance with XPS measurements and analysis, Augustinas Galeckas and Andrej Yu Kuznetsov for critical reviews of the publications, and the Norwegian Research Council for financial support through the FRINAT program.

Ethan Schuyler Long
February 2013

Table of Contents

Abstract **v**

Acknowledgments **vii**

Content **ix**

1 Introduction **1**
References 4

2 Materials properties **11**
2.1 Silicon-Germanium (SiGe) 11
2.1.1 Lattice constant 11
2.1.2 Phase diagram 12
2.1.3 Complex index of refraction 12
2.1.4 Bandgap 13
2.1.5 Critical thickness 14
2.1.6 Diffusion of Si and Ge 15
2.1.7 Gibbs free energies 16
2.1.8 Long range order and alternative morphologies 16
References 17

3 Physical analysis methods **21**
3.1 Variable angle spectroscopic ellipsometry (VASE) 21
3.2 X-ray diffraction (XRD) 27
3.3 X-ray photo-electron spectroscopy (XPS) 33
3.4 Rutherford backscattering spectroscopy (RBS) 36
References 38

4 Results and discussion **41**
4.1 Oxidation rate modeling 41
4.2 Diffusion modeling 42
4.3 Modeling of the pile-up region 42
4.4 Layer thicknesses: measurement and calculation 44

4.5 Ge content in the pile-up: measurement and calculation 51
4.6 Manipulating the Ge content in the pile-up region 54
4.7 Oxidation rate ratios 55
4.8 Ambient chemistry 58
4.9 Bond energies and electronegativity 60
4.10 Electric potential 61
4.11 Point defects 62
4.12 Strain and crystallographic orientation 64
4.13 Summary of results 68
References 69

5 Future work and potential applications **77**
5.1 Benefits of using low Ge contents in as-grown layers 77
5.2 Variable temperature, vacuum-UV, pressure, and ambient chemistry 78
5.3 SiSn and SiGeSn oxidation 79
5.4 Dopant and alloy gradients by differential diffusion 80
References 80

6 Overview of articles **83**
6.1 Article I 83
6.2 Article II 83
6.3 Article III 84
6.4 Article IV 84

Article I:
"A comparative analysis of oxidation rates for thin films of SiGe *versus* Si,"
E. Long, A. Galeckas, and A. Yu. Kuznetsov
Physica Status Solidi A **209**(10), 1934-1939 (2012) **85**

Article II:
"Ge redistribution in SiO_2/SiGe structures under thermal oxidation: Dynamics and predictions," E. Long, A. Azarov, F. Kløw, A. Galeckas, A. Yu. Kuznetsov, and S. Diplas
Journal of Applied Physics **111**, 024308 (2012) **93**

Article III:
"Ge concentrations in pile-up layers of sub-100-nm SiGe films for nano-structuring by thermal oxidation," E. Long, A. Galeckas, and A. Yu. Kuznetsov
Journal of Vacuum Science and Technology B **30**(4), 041212 (2012) **105**

Article IV:
"Nano-structuring in SiGe by oxidation induced anisotropic Ge self-organization,"
E. Long, A. Galeckas, A. Kuznetsov, A. Ronda, L. Favre, I. Berbezier, and H. Radamson
Journal of Applied Physics **113**, 104310 (2013) **115**

Chapter 1

Introduction

Among the great scientific and technological revolutions of the twentieth century were advances in semiconductor physics and the inventions of the transistor and the integrated circuit. Although compounds of sulphur and copper were cited by the earliest patents on field effect transistors by Lilienfeld, substantial uncertainty exists regarding whether these compounds were actually used to produced working transistors [1]. The research into semiconductor devices during and in the years following the second world war that led to transistors, integrated circuits, and modern solid state electronics focused on silicon and germanium [1–4]. In fact, both the first functioning transistor and integrated circuit were built with germanium [1, 2, 4, 5]. These were homojunction devices, but the earliest proposals for heterojunction devices were based on abrupt junction and alloyed silicon and germanium [6, 7]. Furthermore, even though solar cells and the photovoltaic effect were discovered using selenium crystals in the latter half of the nineteenth century, it wasn't until 1953 that research into silicon based electronics at Bell labs lead to the discovery of the utility of silicon in producing solar cells [8].

The semiconductor industry quickly came to be dominated by silicon; this was despite the fact that research into silicon and germanium was conducted concurrently, and both the first functioning transistor and integrated circuit were made of germanium. Among the reasons why silicon eclipsed germanium in the electronics industry is the use of oxide layers in diffusion masking and the reduction of surface states at the silicon to oxide interface [4, 9]. Oxidation processes in silicon-germanium alloys are also distinguished from those in silicon by two complicating phenomena; firstly, the potential for germanium to act as a catalyst or inhibitor for oxidation, and secondly, the formation of a germanium rich layer between the oxide and the underlying silicon-germanium, commonly referred to as germanium condensation, a pile-up layer, or snow plowing [10–13]. As a result, the oxidation of silicon-germanium has not received the same attention as the oxidation of silicon. It is perhaps something of a self fulfilling prophecy that the superiority of the oxide on silicon and the subsequent industrial dominance of silicon has led to oxidation of silicon being substantially more profoundly understood than oxidation of silicon-germanium.

Still, Kroemer and Shockley's descriptions of silicon-germanium heterostructure devices [6, 7] were prescient, and the use of germanium in standard digital and analog processes is becoming common. Silicon-germanium has enormous potential for applications in the fields of nano-electronics and opto-electronics, including applications in RF, BiCMOS, CMOS, waveguides, photodetectors, and lasers [6, 9, 14–18]. Among the numerous examples of how silicon-germanium in general, and germanium condensation by oxidation of silicon-germanium in particular, shows promise for construction of nanoscale devices are: monolithically integrated optical interconnects and waveguides [19, 20], nano-antennas [21], bolometers for uncooled infrared photodetectors [22–25], nanocrystals for use in high density non-volatile memories [26–30], multiple gate field effect transistors (including FinFETs) [31–35], and nanowires [36–46].

Direct bandgaps in silicon-germanium super-lattices and core-shell nanowires [47–50] might allow creation of novel opto-electronic devices or find use in optical interconnects. The possibility to create direct bandgaps in core-shell nanowires could also have profound implications for solar cell or energy harvesting applications. The obvious utility of a direct bandgap is in addition to the geometric advantages of core-shell nanowires; such a construction allows for a long absorption path for incident photons along the length of the wire, while taking advantage of the small radius of the wire to minimize the collection distance of the carriers. So, combination of the geometric advantages of core-shell nanowires with the physical and electronic properties of SiGe could lead to substantial improvements in solar-cell efficiencies [51–55].

Germanium has been incorporated into the source, drain, and channel of CMOS transistors as a method of reducing parasitic effects like drain induced barrier lowering (DIBL) and subthreshold leakage, and of enhancing beneficial transistor characteristics by strain manipulation [56–58]. Localized oxidation of silicon-germanium has been proposed as a method to manipulate the germanium content in the channel or source and drain regions of transistors [59–62], which, in addition to the performance benefits, may help reduce manufacturing costs and cycle times by removing steps from silicon-germanium CMOS process flows [61, 62].

Silicon-germanium-on-insulator (SGOI) has been suggested as a replacement for bulk silicon in deep sub-micron CMOS applications [57], and the fabrication of SGOI wafers using germanium condensation by thermal oxidation [63–66] as well as by thermally induced germanium dilution [67] has been suggested. Use of thermal oxidation for SGOI fabrication may also allow for endotaxial growth of high germanium content layers and germanium nanocrystals at the interface between a buried silicon dioxide and a silicon-germanium layer [68, 69]. Silicon dioxide is a common insulator for SGOI applications, but silicon-germanium-on-sapphire [70–73] is a variant of SGOI that has potential for uniquely high performance RF, analog, image sensor, or photovoltaic based energy harvesting applications.

Despite the fact that germanium played a significant role in the advent of modern electronics, silicon-germanium alloys have not been used or studied nearly as extensively as silicon. There has been a recent resurgence in industrial and academic interest in silicon-germanium and other group IV alloys due to their potential for direct and tunable bandgaps and their compatibility

with the existing silicon based infrastructure and research. As processes are developed for using silicon-germanium in new electronic applications, it is unavoidable that a sound understanding of the oxidation of silicon-germanium will be required. Indeed, a profound appreciation for the oxidation kinetics of silicon-germanium could itself create new applications for the use of silicon-germanium in nano-electronics and opto-electronics.

The present work uses physical characterization along with diffusion and oxidation modeling to examine the kinetics of oxidation of epitaxially grown silicon-germanium and the redistribution of germanium at the oxidation interface. This is done with a particular focus on oxidations in dry O_2 ambients and the influence of oxidation temperature and crystalline orientation on the post-oxidation germanium distribution. Physical characterization relies on measurements made by x-ray diffraction (XRD), variable angle spectroscopic ellipsometry (VASE), x-ray photo-electron spectroscopy (XPS), and Rutherford backscattering spectroscopy (RBS). The experimental work was conducted with layers of silicon-germanium grown epitaxially on silicon substrates to a thickness of $\sim$80 nm and germanium contents of 15 to 20%. The oxidations were conducted at temperatures between 750 and 1150 °C in a dry O_2 ambient to grow oxides up to 100 nm thick.

The present work systematically characterizes and models the formation of the region of high germanium content adjacent to the oxidation front (*i.e.* the pile-up layer.) Both modeling and experimental results reveal that the germanium content at the oxidation front is strongly dependent on the oxidation temperature and only weakly dependent on the germanium content in the as-grown silicon-germanium layer. Evidence is presented showing that a decrease, rather than an increase, in the germanium content at the oxidation front may be achieved under certain conditions. The germanium content at the oxidation interface is used to discuss the potential for germanium to act as a catalyst or inhibitor for oxidation of silicon-germanium alloys. An empiric relation for the germanium content at the oxidation interface is derived and supported by experimental data. The relation for the germanium content at the oxidation interface may also be used to determine the diffusivity of silicon in silicon-germanium under oxidation, which is done here for the (100), (110), (111) orientations. Additional relations are presented describing the thicknesses of the silicon-germanium layers that result from oxidation induced germanium condensation. Taken together, germanium redistribution by thermal oxidation and the empiric relations presented here may be used to design process recipes for fabrication of nanostructures for nano- and opto-electronic applications.

References

[1] R. G. Arns, "The other transistor: early history of the metal-oxide semiconductor field-effect transistor," *Engineering Science and Education Journal*, vol. 7, no. 5, pp. 233–240, Oct 1998.

[2] W. S. Gorton, "The genesis of the transistor," *Proc. IEEE*, vol. 86, no. 1, pp. 50–52, Jan 1998.

[3] W. H. Brattain, "Nobel lecture - surface properties of semiconductors," Dec 1956.

[4] M. Riordan, "the road to silicon was paved with germanium," *Proc. Electrochem. Soc.*, vol. 1, pp. 134–142, 1998.

[5] J. S. Kilby, "Nobel lecture - turning potential into realities: The invention of the integrated circuit," Dec 2000.

[6] D. Harame, M. Oprysko, and R. Singh, *Silicon Germanium: Technology, Modeling, and Design*. New Jersey: Wiley-IEEE Press, 2004.

[7] H. Kroemer, "Nobel lecture - quasi-electric fields and band offsets: teaching electrons new tricks," Dec 2000.

[8] J. Perlin, *From space to earth: The story of solar electricity*. Ann Arbor, Michigan: Aatec publications, 1999.

[9] D. J. Paul, "Silicon-germanium strained layer materials in microelectronics," *Advanced Materials*, vol. 11, no. 3, pp. 191–204, Apr 1999.

[10] F. K. LeGoues, R. Rosenberg, T. Nguyen, F. Himpsel, and B. S. Meyerson, "Oxidation studies of SiGe," *J. Appl. Phys.*, vol. 65, no. 4, pp. 1724–1728, Feb 1989.

[11] M. Spadafora, G. Privitera, A. Terrasi, S. Scalese, C. Bongiorno, A. Carnera, M. Di Marino, and E. Napolitani, "Oxidation rate enhancement of SiGe epitaxial films oxidized in dry ambient," *Appl. Phys. Lett.*, vol. 83, no. 18, pp. 3713–3715, Nov 2003.

[12] M. A. Rabie, Y. M. Haddara, and J. Carette, "A kinetic model for the oxidation of silicon germanium alloys," *J. Appl. Phys.*, vol. 98, no. 7, p. 074904, Oct 2005.

[13] S. J. Kilpatrick, R. J. Jaccodine, and P. E. Thompson, "A diffusional model for the oxidation behavior of $Si_{1-x}Ge_x$ alloys," *J. Appl. Phys.*, vol. 81, no. 12, pp. 8018–8028, Jun 1997.

[14] D. J. Paul, "Si/SiGe heterostructures: from material and physics to devices and circuits," *Semicond. Sci. Technol.*, vol. 19, no. 10, pp. R75–R108, Sep 2004.

[15] D. L. Harame, S. J. Koester, G. Freeman, P. Cottrel, K. Rim, G. Dehlinger, D. Ahlgren, J. S. Dunn, D. Greenberg, A. Joseph, F. Anderson, J. S. Rieh, S. A. S. T. Onge, D. Coolbaugh, V. Ramachandran, J. D. Cressler, and S. Subbanna, "The revolution in sige: impact on device electronics," *Applied Surface Science*, vol. 224, no. 1-4, pp. 9–17, 2004.

[16] R. A. Soref, "Silicon-based optoelectronics," *Proc. IEEE*, vol. 81, no. 12, pp. 1687–1706, Dec 1993.

[17] J. C. Bean, "Silicon-based semiconductor heterostructures: column IV bandgap engineering," *Proc. IEEE*, vol. 80, no. 4, pp. 571–587, Apr 1992.

[18] J. N. Aqua, I. Berbezier, L. Favre, T. Frisch, and A. Ronda, "Growth and self-organization of SiGe nanostructures," *Physics Reports*, vol. 522, no. 2, pp. 59–189, Jan 2013.

[19] R. Soref, "Mid-infrared photonics in silicon and germanium," *Nat. Photonics*, vol. 4, pp. 495–497, Aug 2010.

[20] Y. Kim, M. Yokoyama, N. Taoka, M. Takenaka, and S. Takagi, "Fabrication of Ge-rich SiGe-on-insulator waveguide for optical modulator," in *IEEE Photonics Conf.*, Oct 2011, pp. 465–466.

[21] L. Cao, J.-S. Park, P. Fan, B. Clemens, and M. L. Brongersma, "Resonant germanium nanoantenna photodetectors," *Nano Lett.*, vol. 10, no. 4, pp. 1229–1233, Mar 2010.

[22] A. H. Z. Ahmed and R. N. Tait, "Characterization of amorphous $Ge_xSi_{1-x}O_y$ for micromachined uncooled bolometer applications," *J. Appl. Phys.*, vol. 94, no. 8, pp. 5326–5332, Oct 2003.

[23] M. M. Rana and D. P. Butler, "Radio frequency sputtered $Si_{1-x}Ge_x$ and $Si_{1-x}Ge_xO_y$ thin films for uncooled infrared detectors," *Thin Solid Films*, vol. 514, no. 1-2, pp. 355–360, Aug 2006.

[24] E. Iborra, M. Clement, L. V. Herrero, and J. Sangrador, "IR uncooled bolometers based on amorphous $Ge_xSi_{1-x}O_y$ on silicon micromachined structures," *J. Microelectromech. S.*, vol. 11, no. 4, pp. 322–329, Aug 2002.

[25] M. Kolahdouz, A. A. Farniya, M. Östling, and H. H. Radamson, "The performance improvement evaluation for SiGe-based IR detectors," *Solid-State Electron.*, vol. 62, no. 1, pp. 72–76, Aug 2011.

[26] T. Stoica and E. Sutter, "Ge dots embedded in SiO_2 obtained by oxidation of Si/Ge/Si nanostructures," *Nanotechnology*, vol. 17, no. 19, pp. 4912–4916, Oct 2006.

[27] A. G. Novikau and P. I. Gaiduk, "Germanium segregation in CVD grown SiGe layers," *Cent. Eur. J. Phys.*, vol. 8, no. 1, pp. 57–60, 2010.

[28] D. Tsoukalas, P. Dimitrakis, S. Kolliopoulou, and P. Normand, "Recent advances in nanoparticle memories," *Mater. Sci. Eng. B-Solid*, vol. 124-125, pp. 93–101, Dec 2005.

[29] E. S. Marstein, A. E. Gunnæs, A. Olsen, T. G. Finstad, R. Turan, and U. Serincan, "Introduction of Si/SiO_2 interface states by annealing Ge-implanted films," *J. Appl. Phys.*, vol. 96, no. 8, pp. 4308–4312, Oct 2004.

[30] M. Kanoun, A. Souifi, S. Decossas, C. Dubois, G. Bremond, F. Bassani, Y. Lim, A. Ronda, I. Berbezier, O. Kermarrec, and D. Bensahel, "Oxidation of Si / nc-Ge / Si heterostructures for non volatile memory applications," *MRS Proc.*, vol. 776, p. Q11.34, 2003.

[31] N. Singh, K. D. Buddharaju, S. K. Manhas, A. Agarwal, S. C. Rustagi, G. Q. Lo, N. Balasubramanian, and D.-L. Kwong, "Si, SiGe nanowire devices by top-down technology and their applications," *IEEE Trans. Electron Devices*, vol. 55, no. 11, pp. 3107–3118, Nov 2008.

[32] S. Balakumar, K. D. Buddharaju, B. Tan, S. C. Rustagi, N. Singh, R. Kumar, G. Q. Lo, S. Tripathy, and D. L. Kwong, "Germanium-rich SiGe nanowires formed through oxidation of patterned SiGe FINs on insulator," *J. Electron. Mater.*, vol. 38, no. 3, pp. 443–448, 2009.

[33] T.-Y. Liow, K.-M. Tan, Y.-C. Yeo, A. Agarwal, A. Du, C.-H. Tung, and N. Balasubramanian, "Investigation of silicon-germanium fins fabricated using germanium condensation on vertical compliant structures," *Appl. Phys. Lett.*, vol. 87, no. 26, p. 262104, Dec 2005.

[34] K.-M. Tan, T.-Y. Liow, R. T. P. Lee, K.-J. Chui, C.-H. Tung, N. Balasubramanian, G. S. Samudra, W.-J. Yoo, and Y.-C. Yeo, "Sub-30 nm strained p-channel fin-type field-effect transistors with condensed SiGe source/drain stressors," *Japan. J. Appl. Phys.*, vol. 46, no. 4B, pp. 2058–2061, Apr 2007.

[35] J. Hållstedt, P. E. Hellström, and H. H. Radamson, "Sidewall transfer lithography for reliable fabrication of nanowires and deca-nanometer mosfets," *Thin Solid Films*, vol. 517, no. 1, pp. 117–120, Nov 2008.

[36] S.-Y. Kim, H.-J. Lee, and D.-H. Ko, "Agglomeration of cylindrically condensed cores in $Si_{1-x}Ge_x$ nanowires by oxidation," *Electrochemical and Solid-State Letters*, vol. 13, no. 6, pp. k57–k59, Mar 2010.

[37] E. Sutter, F. Camino, and P. Sutter, "One-step synthesis of $Ge\text{-}SiO_2$ core-shell nanowires," *Appl. Phys. Lett.*, vol. 94, no. 8, p. 083109, Feb 2009.

[38] S.-Y. Kim, S.-W. Kim, H.-J. Chang, H.-K. Seong, H.-J. Choi, and D.-H. Ko, "Oxidation characteristics of $Si_{0.85}Ge_{0.15}$ nanowires," *Mater. Sci. Semicond. Process.*, vol. 11, no. 5-6, pp. 182–186, Oct 2008.

[39] S.-Y. Kim, H.-J. Chang, H.-K. Seong, H.-J. Choi, and D.-H. Ko, "Comparison of growth rate at oxidation of $Si_{1-x}Ge_x$ nanowires," *ECS Trans.*, vol. 13, no. 18, pp. 7–12, May 2008.

[40] H. S. P. Wong, P. Peumans, M. Brongersma, and Y. Nishi, "Lateral nanoconcentrator nanowire multijunction photovoltaic cells," Stanford University, Tech. Rep., Apr 2009, global Climate and Energy Project, GCEP Progress Report.

[41] F.-J. Ma, B. S. Chia, S. C. Rustagi, and G. C. Samudra, "Study on SiGe nanowire shape engineering and Ge condensation," in *ESciNano*, ser. Int. Conf. on Enabling Sci. and Nanotechnology, Dec 2010, pp. 1–2.

[42] H.-K. Chang and S.-C. Lee, "The growth and radial analysis of Si/Ge core-shell nanowires," *Appl. Phys. Lett.*, vol. 97, no. 25, p. 251912, Dec 2010.

[43] E. C. Garnett, M. L. Brongersma, Y. Cui, and M. D. McGehee, "Nanowire solar cells," *Annu. Rev. Mater. Res.*, vol. 41, pp. 269–295, Aug 2011.

[44] R. N. Musin and X.-Q. Wang, "Structural and electronic properties of epitaxial core-shell nanowire heterostructures," *Phys. Rev. B*, vol. 71, no. 15, p. 155318, Apr 2005.

[45] M. Amato, S. Ossicini, and R. Rurali, "Band-offset driven efficiency of the doping of SiGe core-shell nanowires," *Nano Lett.*, vol. 11, no. 2, pp. 594–598, Dec 2011.

[46] M. Amato, R. Rurali, and S. Ossicini, "Doping of SiGe core-shell nanowires," *J. Comput. Electron.*, Feb 2012.

[47] L. Zhang, M. d'Avezac, J.-W. Luo, and A. Zunger, "Genomic design of strong direct-gap optical transition in Si/Ge core/multishell nanowires," *Nano Lett.*, vol. 12, no. 2, pp. 984–991, Jan 2012.

[48] S. Froyen, D. M. Wood, and A. Zunger, "Electronic structure of ultrathin Si_nGe_n strained superlattices: The possibility of direct band gaps," *Thin Solid Films*, vol. 183, no. 1-2, pp. 33–48, Dec 1989.

[49] M. Palummo, M. Amato, and S. Ossicini, "*Ab initio* optoelectronic properties of SiGe nanowires: Role of many-body effects," *Phys. Rev. B*, vol. 82, no. 7, p. 073305, Aug 2010.

[50] X. Peng, F. Tang, and P. Logan, "Band structure of Si/Ge core-shell nanowires along the [110] direction modulated by external uniaxial strain," *J. Phys.: Condens. Matter*, vol. 23, no. 11, p. 115502, Jan 2011.

[51] B. Tian, X. Zheng, T. J. Kempa, Y. Fang, N. Yu, G. Yu, J. Huang, and C. M. Lieber, "Coaxial silicon nanowires as solar cells and nanoelectronic power sources," *Nature*, vol. 449, pp. 885–889, Oct 2007.

[52] Y. Zhang, L.-W. Wang, and A. Mascarenhas, "Quantum coaxial cables for solar energy harvesting," *Nano Lett.*, vol. 7, no. 5, pp. 1264–1269, Apr 2007.

[53] C. Pan, Z. Luo, C. Xu, J. Luo, R. Liang, G. Zhu, W. Wu, W. Guo, X. Yan, J. Xu, Z. L. Wang, and J. Zhu, "Wafer-scale high-throughput ordered arrays of Si and coaxial $Si/Si_{1-x}Ge_x$ wires: Fabrication, characterization, and photovoltaic application," *ACS Nano*, vol. 5, no. 8, pp. 6629–6636, 2011.

[54] R. Peköz, O. B. Malcıoğlu, and J.-Y. Raty, "First-principles design of efficient solar cells using two-dimensional arrays of core-shell and layered SiGe nanowires," *Phys. Rev. B*, vol. 83, no. 3, p. 035317, Jan 2011.

[55] R. Yan, D. Gargas, and P. Yang, "Nanowire photonics," *Nature Photonics*, vol. 3, no. 10, pp. 569–576, Oct 2009.

[56] K. J. Kuhn, A. Murthy, R. Kotlyar, and M. Kuhn, "Past, present and future: SiGe and CMOS transistor scaling," *ECS Trans.*, vol. 33, no. 6, pp. 3–17, 2010.

[57] C. Le Royer, "Interfaces and performance: What future for nanoscale Ge and SiGe based CMOS?" *Microelectron. Eng.*, vol. 88, no. 7, pp. 1541–1548, Jul 2011.

[58] A. G. O'Neill and D. A. Antoniadis, "Deep submicron cmos based on silicon germanium technology," *IEEE Trans. Electron Devices*, vol. 43, no. 6, pp. 911–918, Jun 1996.

[59] T. Tezuka, N. Sugiyama, T. Mizuno, M. Suzuki, and S. ichi Takagi, "A novel fabrication technique of ultrathin and relaxed SiGe buffer layers with high Ge fraction for sub-100 nm strained silicon-on-insulator MOSFETs," *Japan. J. Appl. Phys.*, vol. 40, no. Part 1 No 4B, pp. 2866–2874, Apr 2001.

[60] S.-W. Kim, J.-H. Yoo, S. mo Koo, D.-H. Ko, and H.-J. Lee, "Enhancement of a channel strain via dry oxidation of recessed source/drain $Si_{1-x}Ge_x$ structures," *ECS Trans.*, vol. 41, no. 7, pp. 175–180, Oct 2011.

[61] K.-W. Ang, K.-J. Chui, A. Madan, L.-Y. Wong, C.-H. Tung, N. Balasubramanian, M.-F. Li, G. S. Samudra, and Y.-C. Yeo, "Strained thin-body p-MOSFET with condensed silicon-germanium source/drain for enhanced drive current performance," *IEEE Electr. Device L.*, vol. 28, no. 6, pp. 509–512, Jun 2007.

[62] K.-J. Chui, K.-W. Ang, A. Madan, H. Wang, C.-H. Tung, L.-Y. Wong, Y. Wang, S.-F. Choy, N. Balasubramanian, M. F. Li, G. Samudra, and Y.-C. Yeo, "Source/drain germanium condensation for p-channel strained ultra-thin body transistors," in *IEEE Int. Electron Devices Meeting*, ser. IEDM Technical Digest, Dec 2005, pp. 493–496.

[63] D. Wang and H. Nakashima, "Optical and electrical evaluations of SiGe layers on insulator fabricated using Ge condensation by dry oxidation," *Solid-State Electron.*, vol. 53, no. 8, pp. 841–849, Aug 2009.

[64] S. Nakaharai, T. Tezuka, N. Hirashita, E. Toyoda, Y. Moriyama, N. Sugiyama, and S. Takagi, "Formation process of high-purity Ge-on-insulator layers by Ge-condensation technique," *J. Appl. Phys.*, vol. 105, no. 2, p. 024515, Jan 2009.

[65] L. Souriau, V. Terzieva, W. Vandervorst, F. Clemente, B. Brijs, A. Moussa, M. Meuris, R. Loo, and M. Caymax, "High Ge content SGOI substrates obtained by the Ge condensation technique: A template for growth of strained epitaxial Ge," *Thin Solid Films*, vol. 517, no. 1, pp. 23–26, Nov 2008.

[66] L. Souriau, G. Wang, R. Loo, M. Caymax, M. Meuris, M. M. Heyns, and W. Vandervorst, "Comprehensive study of the fabrication of SGOI substrates by the Ge condensation technique: Oxidation kinetics and relaxation mechanism," *ECS Trans.*, vol. 25, no. 7, pp. 363–375, 2009.

[67] K. Kutsukake, N. Usami, K. Fujiwara, T. Ujihara, G. Sazaki, B. Zhang, Y. Segawa, and K. Nakajima, "Fabrication of SiGe-on-insulator through thermal diffusion of Ge on Si-on-insulator substrate," *Japan. J. Appl. Phys.*, vol. 42, no. Part 2 No. 3A, pp. L232–L234, Mar 2003.

[68] I. E. Tyschenko, M. Voelskow, A. G. Cherkov, and V. P. Popov, "Growth and electrical properties of the (Si/Ge)-on-insulator structures formed by ion implantation and subsequent hydrogen-assisted transfer," *Semiconductors*, vol. 43, no. 1, pp. 52–56, 2009.

[69] Z. Di, P. K. Chu, M. Zhang, W. Liu, Z. Song, and C. Lin, "Germanium movement mechanism in SiGe-on-insulator fabricated by modified Ge condensation," *J. Appl. Phys.*, vol. 97, no. 6, p. 064504, Mar 2005.

[70] Y. Park, G. C. King, and S. H. Choi, "Rhombohedral epitaxy of cubic SiGe on trigonal c-plane sapphire," *J. Cryst. Growth*, vol. 310, no. 11, pp. 2724–2731, May 2008.

[71] I. Lagnado and P. R. de la Houssaye, "Integration of Si and SiGe with Al_2O_3 (sapphire)," *Microelectron. Eng.*, vol. 59, no. 1-4, pp. 455–459, Nov 2001.

[72] H. S. Gamble, B. M. Armstrong, P. T. Baine, Y. H. Low, P. V. Rainey, Y. W. Low, D. W. McNeill, S. J. N. Mitchell, J. H. Montgomery, and F. H. Ruddell, "Germanium on sapphire substrates for system on a chip," *Mater. Sci. Semicond. Process.*, vol. 11, no. 5-6, pp. 195–198, Oct 2008.

[73] P. T. Baine, H. S. Gamble, B. M. Armstrong, D. W. McNeill, S. J. N. Mitchell, Y. H. Low, and P. V. Rainey, "Germanium on sapphire by wafer bonding," *Solid-State Electron.*, vol. 52, no. 12, pp. 1840–1844, Dec 2008.

Chapter 2

Materials properties

This chapter presents the electronic and optical characteristics of silicon-germanium alloys that are most pertinent to the research presented herein. An emphasis is placed on the way in which various properties change as a function of the germanium content in the alloy.

2.1 Silicon-Germanium (SiGe)

2.1.1 Lattice constant

Silicon-germanium (SiGe) is a miscible binary alloy that takes a diamond crystal structure [1]. The random placement of silicon and germanium atoms in the alloy result in a lattice constant that varies continuously between those of silicon and germanium [1, 2]. Figure 2.1 shows how the lattice constant of $Si_{1-X}Ge_X$ varies as a function of the Ge content, X, and reveals a slight deviation from what is predicted by Vegard's law.

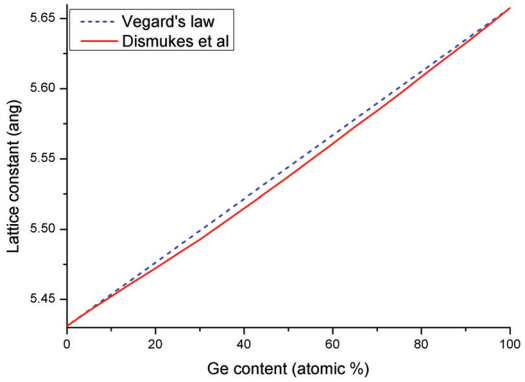

Figure 2.1: *Lattice constant for $Si_{1-X}Ge_X$ as a function of X [2].*

2.1.2 Phase diagram

The melting point of $Si_{1-X}Ge_X$ is also a continuous function of X and varies continuously between ~940 °C for Ge to ~1412 °C for Si. The phase diagram for $Si_{1-X}Ge_X$ is shown in figure 2.2.

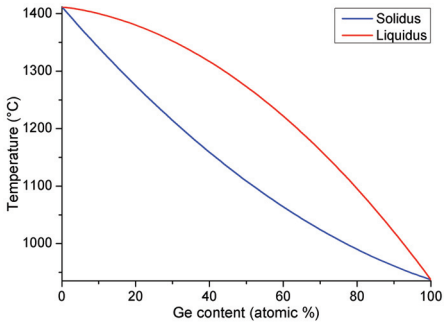

Figure 2.2: *Phase diagram for $Si_{1-X}Ge_X$ [1].*

2.1.3 Complex index of refraction

As shown in figure 2.3, the complex index of refraction, $n^* = n + ik$, for $Si_{1-X}Ge_X$ is also a function of X. The real part of the index of refraction, n, varies between ~3.9 for Si and ~5.5 for Ge for an incident beam with $\lambda = 632.8$ nm. The complex index of refraction is a function of both the morphology and the band structure of the material.

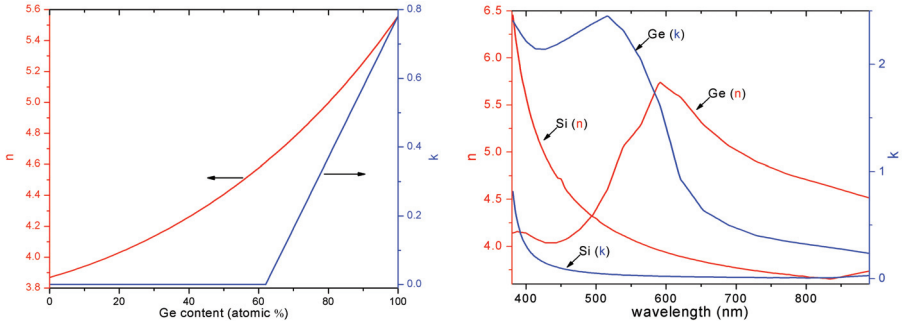

(a) (b)

Figure 2.3: *Real, n, and imaginary, k, parts of the complex index of refraction for $Si_{1-X}Ge_X$. (a) n and k versus Ge content, X, for 632.8 nm (1.96 eV) light. (b) n and k versus wavelength for Si ($X = 0$) and Ge ($X = 1$). [3]*

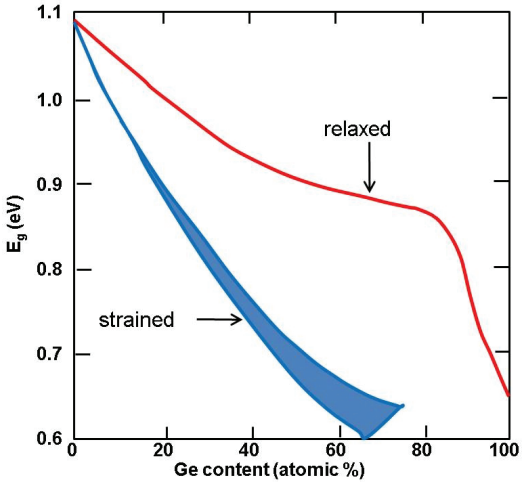

Figure 2.4: *Minimum energy band gap for $Si_{1-X}Ge_X$ as a function of X [7, 8]. Curves are shown for both relaxed $Si_{1-X}Ge_X$ and strained layers of $Si_{1-X}Ge_X$ on a Si(100) substrate.*

2.1.4 Bandgap

As seen in figure 2.4, the bandgap of bulk (*i.e.* relaxed) $Si_{1-X}Ge_X$ is indirect and shows a kink at $\sim$80% Ge content. This kink indicates where the conduction band minima that define the minimum energy gap shift from the δ valleys (that are characteristic of Si) to the L valleys (that are characteristic of Ge) [4, 5]. The possibility to use strain and Ge content to manipulate the bandgap of SiGe (*i.e.* bandgap engineering) is at the heart of the alloy's utility in modern electronics. This sort of bandgap engineering can also be extended to binary, ternary, and quaternary alloys of various group IV elements, allowing manipulation of the bandgap between $\sim$5.5 eV for diamond and 0 eV for tin. The broad range of bandgaps, as well as the possibility of direct gaps, make group IV alloys suitable for a large number of applications within opto-electronics [6].

Modern SiGe based applications are based on epitaxially grown layers, rather than bulk material, and the two most common methods for SiGe epitaxy are molecular beam epitaxy (MBE) and chemical vapor deposition (CVD) [9]. Epitaxial growth of SiGe is particularly apt for an industry dominated by Si based processes and gives the additional benefit of allowing use of strain effects in device design. The strain in heteroepitaxial thin films of SiGe arises as a direct consequence of the 4% difference in the lattice constants of Si and Ge. Noting the close correlation between the lattice constant and Ge content shown in figure 2.1, whether the strain is compressive or tensile depends on whether the lattice constant in the film is greater than or less than the lattice constant in the substrate, respectively. It follows that the valence and conduction band offsets, and thus the bandgap, of strained layers of SiGe will depend on the Ge content

of both the substrate and the epitaxial layer [4, 5, 8, 10–12]. Though, the compressive strain in pseudomorphically strained $Si_{1-X}Ge_X$ on Si will tend to reduce the bandgap from the value for relaxed $Si_{1-X}Ge_X$. Figure 2.4 shows a clear tendency for higher degrees of strain, that are associated with higher Ge contents, to exaggerate the reduction in the bandgap.

2.1.5 Critical thickness

A fundamental limitation associated with using strain to alter the bandgap is the tendency for strain energy to be relieved by formation of threading defects and misfit dislocations. Epitaxial growth methods have been shown to be capable of producing thin films of $Si_{1-X}Ge_X$ with low defect densities up to a critical thickness that is a function of X [4, 9, 13–15]. As the growth process proceeds the increase in strain energy due to the misfit between the heteroepitaxial layers will induce defects as well as an increase in surface roughness (also called islanding or 3D growth) [4, 13, 14]. Figure 2.5 shows the critical thickness as predicted by Matthews and Blakeslee [13] as well as that predicted by People and Bean [14]. Defect free films grown to thicknesses greater than the critical thickness may exist in a metastable region wherein defects will develop over time. Although People and Bean [14] relied on data from studies of SiGe epilayers on Si substrates, it has been suggested that their predictions may sit in a region of metastability [4]. The development of defects over time would make such layers unsuitable for applications in electronics due to compromised reliability.

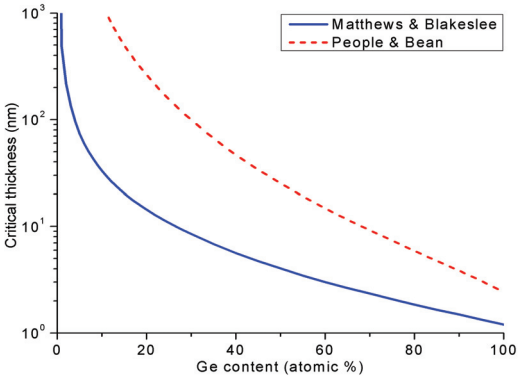

Figure 2.5: *Critical layer thickness for epitaxial $Si_{1-X}Ge_X$ on a Si substrate as a function of X. Curves shown follow predictions by Matthews and Blakeslee [13] and People and Bean [14]. The predictions by People and Bean may fall within a region of metastability such that defects and relaxation will develop over time [4].*

2.1.6 Diffusion of Si and Ge

Kube *et al* [16] used time of flight secondary ion mass spectrometry (TOF-SIMS) to measure the diffusivity of Si and Ge in $Si_{1-X}Ge_X$ for a range of X and reviewed data published elsewhere in the literature. The diffusivity of Si and Ge in $Si_{1-X}Ge_X$ follows a standard Arrhenius relation, $D = D_0 \exp\left[-E_a/(kT)\right]$, where D is the diffusivity in cm^2/s, D_0 is a pre-exponential constant in cm^2/s, E_a is the activation energy for diffusion in eV, k is Boltzmann's constant, and T is the temperature in K. Figures 2.6(a) and 2.6(b) show the activation energies and pre-exponential constants for diffusion of Si and Ge in $Si_{1-X}Ge_X$. Figure 2.6(c) plots the diffusivity of Si in $Si_{1-X}Ge_X$ for several temperatures typical of thermal oxidation. The diffusivities in figure 2.6(c) indicate that Si diffuses between four and six orders of magnitude faster in Si than in Ge.

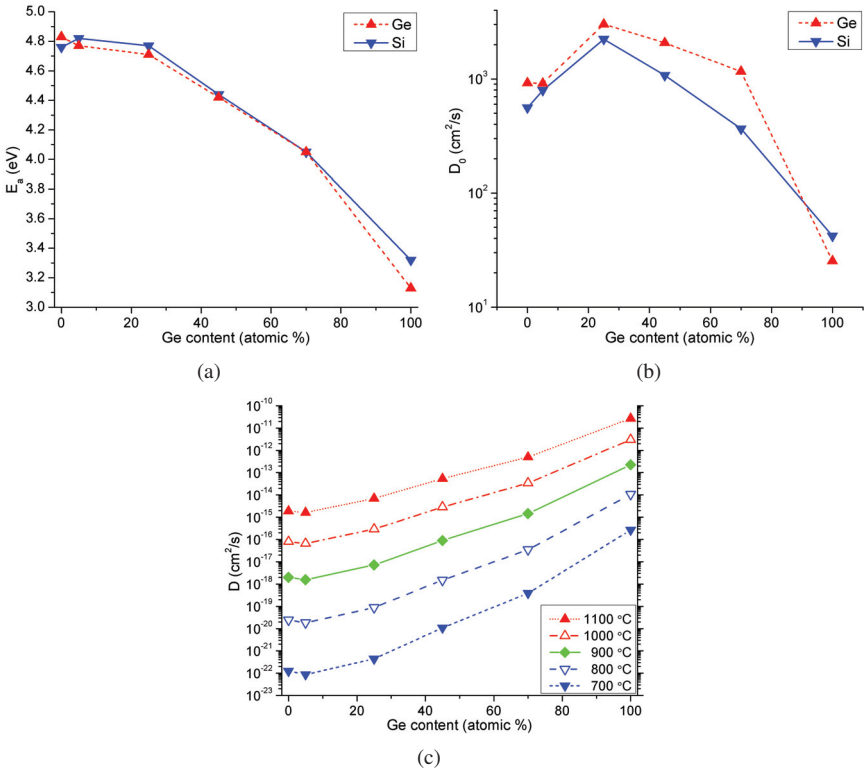

Figure 2.6: *Diffusivity of Si and Ge in $Si_{1-X}Ge_X$ as a function of X and modeled following an Arrhenius relation, $D = D_0 \exp\left[-E_a/(kT)\right]$. (a) Activation energies, E_a, for Si and Ge measured in eV. (b) Pre-exponential constant, D_0, for Si and Ge measured in cm^2/s. (c) Diffusivity of Si in $Si_{1-X}Ge_X$ for temperatures between 700 and 1100 °C. The data is as tabulated by Kube et al [16].*

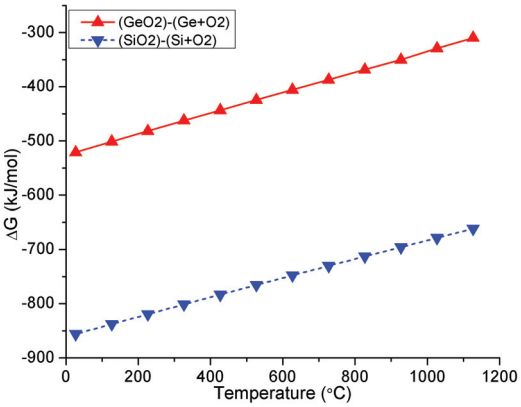

Figure 2.7: *Gibbs energies for oxidation of Si and Ge [20].*

2.1.7 Gibbs free energies

In studies of the oxidation of SiGe, the preferential oxidation of Si is commonly explained by citing the Gibbs free energies for silicon, germanium, oxygen, and oxidized silicon and germanium [17, 18]. The change in Gibbs free energies for the formation of Si and Ge dioxides from their constituent components are shown in figure 2.7. It has been reported that, in contrast to amorphous SiO_2, thermal oxidation of Ge produces a polycrystalline oxide, and that SiO_2 is differentiated from GeO_2 by higher electronic and lower ionic conduction [19].

2.1.8 Long range order and alternative morphologies

As stated above, SiGe forms in the diamond structure wherein the Ge and Si atoms are randomly placed in the crystal lattice. However, it has been demonstrated that long range order of the Ge and Si atoms may occur under certain conditions. This is significant because, although SiGe is typically described as having an indirect bandgap, strain and long range ordering may allow creation of SiGe based structures that exhibit a direct bandgap [21]. Additionally, alternative crystalline structures could prove useful in producing devices with SiGe-on-sapphire technologies [22]. Ordering has been shown in strained super-lattice structures [23], and although it is presumed that strain plays a critical role in establishing or stabilizing long range order, ordering has also been observed in relaxed or bulk like films [24]. LeGoues *et al* [24] postulate that the presence of long range order in bulk like $Si_{0.5}Ge_{0.5}$ films may be associated with a peculiarity of the deposition method creating super-latices or residual strain in the thick films. Long range ordering represents a phase change from the diamond structure to either a zinc-blende or a rhombohedral structure and depends on both chemical and mechanical energies [25, 26]. It is argued that the relative weakness of Si-Ge bonds, as compared to the average of the Si-Si and Ge-Ge

bonds, will influence the ratio of the number of Si-Ge to Si-Si and Ge-Ge bonds in a SiGe crystal, which would in turn result in the rhombohedral structure being more stable than the zinc-blende structure [24, 25]. The Ge-Ge and Si-Si binding energies are occasionally reported as being between about 1.6 and 2 eV [27–31], though, more recent studies report the dissociation energies for Ge-Ge, Si-Ge, and Si-Si bonds as approximately 2.7, 3.0, and 3.2 eV, respectively [32–35]. These more recent values are consistent with Pauling's [27] estimation for the relationship between bond energies of diatomic molecules and the electronegativities of the constituent atoms (reported as 1.9 and 2.0 for Si and Ge, respectively [36].) The wide variations in reported values for diatomic bonds and the strong dependence of electronegativities on bonds with tertiary elements make it difficult to form definitive conclusions about the validity of arguments based on bond energies.

References

[1] H. Stöhr and W. Klemm, "Über zweistoffsysteme mit germanium. I. germanium/aluminium, germanium/zinn und germanium/silicium," *Z. Anorg. Allg. Chem.*, vol. 241, no. 4, pp. 305–323, Jun 1939.

[2] J. P. Dismukes, L. Ekstrom, and R. J. Paff, "Lattice parameter and density in germanium-silicon alloys," *J. Phys. Chem.*, vol. 68, no. 10, pp. 3021–3027, Oct 1964.

[3] J. Humlíček, M. Garriga, M. I. Alonso, and M. Cardona, "Optical spectra of Si_xGe_{1-x} alloys," *J. Appl. Phys.*, vol. 65, no. 7, pp. 2827–2832, 1989.

[4] D. J. Paul, "Si/SiGe heterostructures: from material and physics to devices and circuits," *Semicond. Sci. Technol.*, vol. 19, no. 10, pp. R75–R108, Sep 2004.

[5] C. G. Van de Walle and R. M. Martin, "Theoretical calculations of heterojunction discontinuities in the Si/Ge system," *Phys. Rev. B*, vol. 34, no. 8, pp. 5621–5634, Oct 1986.

[6] R. A. Soref, "Silicon-based optoelectronics," *Proc. IEEE*, vol. 81, no. 12, pp. 1687–1706, Dec 1993.

[7] R. Braunstein, A. R. Moore, and F. Herman, "Intrinsic optical absorption in germanium-silicon alloys," *Phys. Rev.*, vol. 109, no. 3, pp. 695–710, Feb 1958.

[8] R. People, "Indirect band gap of coherently strained Ge_xSi_{1-x} bulk alloys on $<001>$ silicon substrates," *Phys. Rev. B*, vol. 32, no. 2, pp. 1405–1408, Jul 1985.

[9] A. Nylandsted Larsen, "Epitaxial growth of Ge and SiGe on Si substrates," *Mater. Sci. Semicond. Process.*, vol. 9, no. 4-5, pp. 454–459, Nov 2006.

[10] M. M. Rieger and P. Vogl, "Electronic-band parameters in strained $Si_{1-x}Ge_x$ alloys on $Si_{1-y}Ge_y$ substrates," *Phys. Rev. B*, vol. 48, no. 19, pp. 14 276–14 287, Nov 1993.

[11] M. V. Fischetti and S. E. Laux, "Band structure, deformation potentials, and carrier mobility in strained Si, Ge, and SiGe alloys," *J. Appl. Phys.*, vol. 80, no. 4, pp. 2234–2252, Aug 1996.

[12] J. C. Bean, "Silicon-based semiconductor heterostructures: column IV bandgap engineering," *Proc. IEEE*, vol. 80, no. 4, pp. 571–587, Apr 1992.

[13] J. W. Matthews and A. E. Blakeslee, "Defects in epitaxialmultilayers: I. misfit dislocations," *J. Cryst. Growth*, vol. 27, pp. 118–125, Dec 1974.

[14] R. People and J. C. Bean, "Calculation of critical layer thickness versus lattice mismatch for Ge_xSi_{1-x}/Si strained-layer heterostructures," *Appl. Phys. Lett.*, vol. 47, no. 3, pp. 322–324, Aug 1985.

[15] J. C. Bean, L. C. Feldman, A. T. Fiory, S. Nakahara, and I. K. Robinson, "Ge_xSi_{1-x}/Si strained-layer superlattice grown by molecular beam epitaxy," *J. Vac. Sci. Technol. A*, vol. 2, no. 2, pp. 436–440, Apr 1984.

[16] R. Kube, H. Bracht, J. Lundsgaard Hansen, A. Nylandsted Larsen, E. E. Haller, S. Paul, and W. Lerch, "Composition dependence of Si and Ge diffusion in relaxed $Si_{1-x}Ge_x$ alloys," *J. Appl. Phys.*, vol. 107, no. 7, p. 073520, Apr 2010.

[17] D. C. Paine, C. Caragianis, and A. F. Schwartzman, "Oxidation of $Si_{1-x}Ge_x$ alloys at atmospheric and elevated pressure," *J. Appl. Phys.*, vol. 70, no. 9, pp. 5076–5084, Nov 1991.

[18] M. K. Bera, S. Chakraborty, R. Das, G. K. Dalapati, S. Chattopadhyay, S. K. Samanta, W. J. Yoo, A. K. Chakraborty, Y. Butenko, L. Šiller, M. R. C. Hunt, S. Saha, and C. K. Maiti, "Rapid thermal oxidation of Ge-rich $Si_{1-x}Ge_x$ heterolayers," *J. Vac. Sci. Technol. A*, vol. 24, no. 1, p. 84, Dec 2006.

[19] A. G. Revesz, "Noncrystalline structure and electronic conduction of silicon dioxide films," *Phys. Status Solidi B*, vol. 24, no. 1, pp. 115–126, 1967.

[20] I. Barin, *Thermochemical Data of Pure Substances*, 2nd ed. Weinheim: VCH, 1993.

[21] S. Froyen, D. M. Wood, and A. Zunger, "Electronic structure of ultrathin Si_nGe_n strained superlattices: The possibility of direct band gaps," *Thin Solid Films*, vol. 183, no. 1-2, pp. 33–48, Dec 1989.

[22] Y. Park, G. C. King, and S. H. Choi, "Rhombohedral epitaxy of cubic SiGe on trigonal c-plane sapphire," *J. Cryst. Growth*, vol. 310, no. 11, pp. 2724–2731, May 2008.

[23] A. Ourmazd and J. C. Bean, "Observation of order-disorder transitions in strained-semiconductor systems," *Phys. Rev. Lett.*, vol. 55, no. 7, pp. 765–768, Aug 1985.

[24] F. K. LeGoues, V. P. Kesan, and S. S. Iyer, "Long-range order in thick, unstrained $\mathrm{si}_{0.5}\mathrm{ge}_{0.5}$ epitaxial layers," *Phys. Rev. Lett.*, vol. 64, no. 1, pp. 40–43, Jan 1990.

[25] J. L. Martins and A. Zunger, "Stability of ordered bulk and epitaxial semiconductor alloys," *Phys. Rev. Lett.*, vol. 56, no. 13, pp. 1400–1403, Mar 1986.

[26] P. B. Littlewood, "Strain-induced ordering in silicon-germanium alloys," *Phys. Rev. B*, vol. 34, no. 2, pp. 1363–1366, Jul 1986.

[27] L. Pauling, *The nature of the chemical bond*, 3rd ed. Ithaca, New York: Cornell University Press, 1960.

[28] R. J. Jaccodine, "Surface energy of germanium and silicon," *J. Electrochem. Soc.*, vol. 110, no. 6, pp. 524–527, 1963.

[29] E. H. Nicollian and J. R. Brews, *MOS (Metal Oxide Semiconductor) Physics and Technology*, ser. Wiley Classics Library. Wiley-Interscience, 2002.

[30] T. Shimura, Y. Okamoto, D. Shimokawa, T. Inoue, T. Hosoi, and H. Watanabe, "Interface reaction and rate enhancement of SiGe thermal oxidation," *ECS Trans.*, vol. 33, no. 6, pp. 893–899, 2010.

[31] O. W. Holland, C. W. White, and D. Fathy, "Novel oxidation process in Ge+-implanted Si and its effect on oxidation kinetics," *Appl. Phys. Lett.*, vol. 51, no. 7, pp. 520–522, Aug 1987.

[32] J. Drowart, G. De Maria, A. J. H. Boerboom, and M. G. Inghram, "Mass spectrometric study of inter-group IVB molecules," *J. Phys. Chem.*, vol. 30, no. 1, pp. 308–313, Jan 1959.

[33] J. Drowart and R. E. Honig, "A mass spectrometric method for the determination of dissociation energies of diatomic molecules," *J. Phys. Chem.*, vol. 61, no. 7, pp. 980–985, Jul 1957.

[34] R. Viswanathan, R. W. S. Jr., and K. A. Gingerich, "Molar atomization enthalpies and molar enthalpies of formation of GeSi, $GeSi_2$, Ge_2Si, and Ge_2Si_2 by Knudsen-effusion mass spectrometry," *J. Chem. Thermodyn.*, vol. 27, no. 7, pp. 763–770, Jul 1995.

[35] P. Wielgus, S. Roszak, D. Majumdar, J. Saloni, and J. Leszczynski, "Theoretical studies on the bonding and thermodynamic properties of Ge_nSi_m $(m+n=5)$ clusters: The precursors of germanium/silicon nanomaterials," *J. Chem. Phys.*, vol. 128, no. 14, p. 144305, 2008.

[36] A. L. Allred and E. G. Rochow, "Electronegativities of carbon, silicon, germanium, tin and lead," *J. Inorg. Nucl. Chem.*, vol. 5, no. 4, pp. 269–288, Jun 1958.

Chapter 3

Physical analysis methods

The physical characterization methods employed in the current study are variable angle spectroscopic ellipsometry (VASE), x-ray diffraction (XRD), x-ray photo-electron spectroscopy (XPS), and Rutherford backscattering spectroscopy (RBS). This chapter presents a brief introduction to these techniques as they were used to characterize the silicon-germanium and oxide thin films in the present work.

3.1 Variable angle spectroscopic ellipsometry (VASE)

Ellipsometry is a non-destructive optical method for characterizing both thin and thick layers of either amorphous or crystalline material. It is well suited for measuring films with thicknesses of a few angstroms up to several microns, particularly for those materials that have well established values for the indices of refraction. Although the method may use wavelengths from the extreme ultra-violet to the far infrared, the wavelengths of light used in this study are between 380 and 900 nm.

Ellipsometry relies on measuring the polarization of light which has been reflected and refracted by one or more layers in a sample. The polarization of light may be described by two time variant vector components of the electric field which are perpendicular to the direction of propagation of the light, call them the X and Y vectors. The oscillation of the electric field will form an elliptical shape in the XY plane (hence the name ellipsometry) and the polarization can be described by the two angles, Δ and Ψ. The ratio of the maximum magnitudes of the X and Y vectors is the relative amplitude, $X/Y = \tan\Psi$, while the angle between the directions of the electric field vector when the X and Y components are at their maximums is the relative phase, Δ [1, 2].

Both of the ellipsometers used in the present study, the *AutoEL-II* by Rudolph Research and the *alpha-SE* by J.A. Woollam Co., operate by measuring the values of Δ and Ψ for one or more wavelengths of incident light, λ, and one or more angles of incidence, θ. The essential

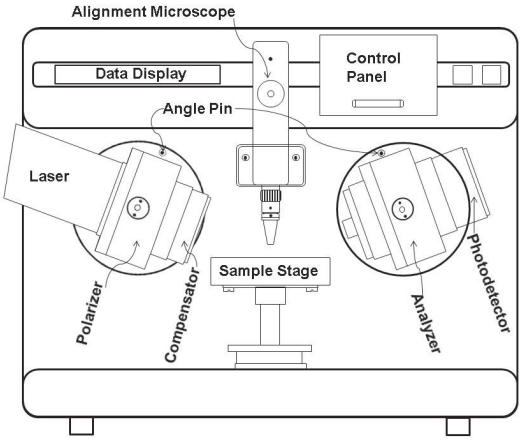

Figure 3.1: *A schematic of the AutoEL-II ellipsometer by Rudolph Research showing basic functional components. After drawing number D7905-8 of [3].*

components of the *AutoEL-II* are shown in figure 3.1. The laser is used as a light source that produces a monochromatic beam of light that is directed at an angle, $90° - \theta$, to the plain of the surface of the sample. The value of θ is manually set to one of three discreet values (65°, 70°, or 75°) by rotating the primary and secondary side components and fixing their position using a pin. The polarizers on the primary and secondary sides are labeled "Polarizer" and "Analyzer", respectively, and are used to condition the light prior to measurement by the photodetector.

The so called null ellipsometry method used by the *AutoEL-II* is succinctly described by the instrument's manual,

> "The AutoEL is a microprocessor-controlled automatic-nulling ellipsometer which measures changes in the state of polarization of a laser beam reflected from sample surfaces, by determining the azimuth P of a rotatable polarizer prism in the incident beam and the azimuth A of a rotatable analyzer prism in the reflected beam for which the intensity of the reflected beam (after passage through the analyzer) is a minimum. From the measured azimuths P and A at 'extinction', the instrument computes two intermediate parameters Δ (DELTA) and Ψ (PSI) which can be used to calculate the optical constants of bare surfaces, and the thickness and refractive index of thin films on those surfaces." [3]

The *alpha-SE* has a similar principle of operation, but instead of relying on rotation of the polarizer and analyzer, it uses rotation of an additional component on the primary side, called a compensator, to manipulate the phase of the polarized light and to change the incident beam from linear to elliptical polarization. There are advantages and disadvantages to both methods but these are not critical to the present application [2, 4].

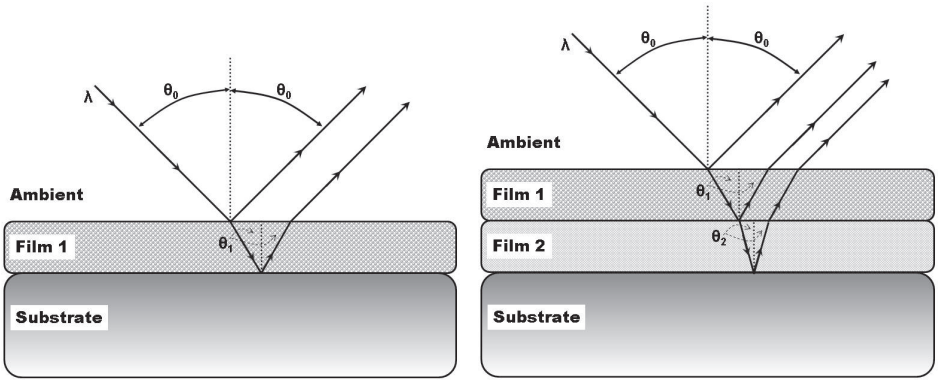

(a) single layer model (b) double layer model

Figure 3.2: *Ellipsometry models using (a) a single layer and (b) two layers. After figure 5-24 of [3].*

The way in which light is refracted by various materials is determined by the permitivity, ε, of the material which is closely related to the electron density of the material. In the context of ellipsometry, the permitivity is commonly described in terms of the complex index of refraction, N, where $N = n + \mathrm{i}k = \sqrt{\varepsilon}$. The extinction coefficient, k, is indicative of the absorptivity of the material, and is close to zero for those wavelengths where the material is transparent. Figure 3.2(a) shows the basic geometry for the reflection and refraction of a beam of light with wavelength λ that is incident upon a sample with a single film at an angle θ_0. The way in which the light beam is refracted and reflected when passing between the ambient and the top layer of the sample is described by Snell's law, $N_0 \sin\theta_0 = N_1 \sin\theta_1$. Furthermore, if the plane that contains both the incident and reflected beam is the plane of incidence, the polarization may be separated into the component that is parallel to the plane of incidence (p-polarization) and that which is perpendicular to the plane of incidence (s-polarization.) The parallel and perpendicular Fresnel coefficients may be written as,

$$r_p = \frac{N_0 \cos\theta_1 - N_1 \cos\theta_0}{N_0 \cos\theta_1 + N_1 \cos\theta_0} \quad \text{and} \quad r_s = \frac{N_0 \cos\theta_0 - N_1 \cos\theta_1}{N_0 \cos\theta_0 + N_1 \cos\theta_1}. \tag{3.1}$$

The ratio of the Fresnel coefficients is related to the values of Δ and Ψ as $r_p/r_s = \tan\Psi \exp \mathrm{i}\Delta$ [1, 2].

In the event that the sample is composed of more than one layer of different materials, each with its own N, these equations may be extended to models with multiple layers. This is demonstrated in figure 3.2(b), where the relationship between layers 1 and 2 is synonymous to that between layers 0 and 1. By considering the relationships between Δ, Ψ, N, and θ, a known value for θ_0, and using basic trigonometry, the thickness and complex index of refraction of the

various layers may be determined using the method of least squares. This involves calculating Δ and Ψ using a variety of values of N for a number of samples. The difference between the measured and calculated values is expressed by the mean squared error, χ^2, and is written as,

$$\chi^2 = \sum_{i=1}^{j} \left[\left(\frac{\Delta_i^m - \Delta_i^c}{\sigma_\Delta} \right)^2 + \left(\frac{\Psi_i^m - \Psi_i^c}{\sigma_\Psi} \right)^2 \right], \tag{3.2}$$

where j is the total number of measurements and the superscripts m and c indicate measured and calculated values, respectively, for Δ and Ψ. The values of σ_Δ and σ_Ψ may be neglected if they are determined to be equal to one another and constant for all samples measured on the same instrument. This is a standard form for calculating χ^2 [5], but there is some variation in the details of the way in which χ^2 is calculated. The *CompleteEASE* software that is associated with the *alpha-SE* ellipsometer defines χ^2 as [4],

$$\chi^2 = \frac{1}{3j - l} \sum_{i=1}^{j} \left[(A_i^m - A_i^c)^2 + (B_i^m - B_i^c)^2 + (C_i^m - C_i^c)^2 \right], \tag{3.3}$$

where l is the number of unknowns being solved for, $A = \cos 2\Psi$, $B = \sin 2\Psi \cos \Delta$, and $C = \sin 2\Psi \sin \Delta$. This definition assumes that the standard deviations for A, B, and C are the same. The combination of values of n, k, and layer thicknesses that produce the minimum value of χ^2 represent the most probable true values of these variables.

The computational complexity of determining the minimum value of χ^2 will depend strongly on the number of unknowns in the system and the range and precision with which these unknowns are being determined. For example, for a sample with three layers wherein the thicknesses and values of n and k for the layers and substrate are unknown, there will be 12 unknowns. If each unknown is considered to have 1000 possible values, the number of possible combinations of variables that must be considered will be 1000^{12}. Using a 2.5 petaflop computer, this would take longer than the age of the universe to complete the calculations, and would require about 7×10^{24} TB of storage; this is clearly not a practical approach. If the number of unknown variables is reduced to three with each variable being limited to 100 possible values, the storage space required could be reduced to less than 2 MB, and the computation time would be on the order of seconds using the 1980's technology that was used to build the *AutoEL-II*. There are a variety of ways in which the problem may be simplified, including: using the simplest model that is appropriate for the samples being measured, minimizing the number of unknowns and the ranges of possible values for those unknowns, measuring multiple similar samples, using multiple values of λ and θ for measurements, using algorithmic searches for the minimum χ^2 rather than a brute force method, and using an understanding of the physics associated with N to limit the possible values for that variable.

In fact, using a brute force method to find χ^2 for all possible combinations of all of the

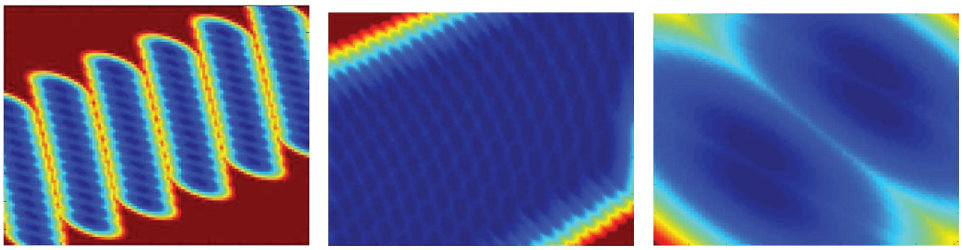

(a) (b) (c)

Figure 3.3: *Color maps for χ^2 values calculated with a two layer model and a range of values for two unknowns. Red areas represent combinations of the two unknowns with large χ^2 values, while blue areas represent lower χ^2 values. The color maps demonstrate that a large number of minima can be generated for various combinations of values for the two unknowns without producing a unique minimum χ^2 value during analysis of ellipsometry data.*

unknowns is not a common or efficient method for analyzing ellipsometry data. Levenberg-Marquardt, Monte Carlo, and Genetic algorithms are examples of more sophisticated search routines for finding the minimum value of χ^2. The Levenberg-Marquardt method is common in ellipsometry analyses, but suffers from the tendency to produce results for χ^2 from local minima, rather than the global minimum for the range of unknowns being considered [1, 4]. Figure 3.3 shows color maps of the χ^2 values calculated with a two layer model and a range of values for two unknowns. The color maps demonstrate that a large number of local minima can be generated for various combinations of values for the two unknowns, without producing a unique minimum χ^2 value. The problem of multiple local minima is aggravated with larger numbers of unknowns.

Rather than varying independently of one another, the values of n and k should be related by a Kramer-Kronig relation, and should be physically realistic [1]. Linking n and k by such a physical relation allows them to be considered as a single variable. Furthermore, some materials have been well characterized in the literature, and SiO_2, for example, is recognized as having $k = 0$ in the range of wavelengths considered here. For the present work, measurements were made of thermal SiO_2 grown from SiGe films on Si substrates and from bare Si substrates. Published values of the optical constants of Si, SiO_2 [6], and SiGe [7] have either been used outright or used to minimize the range in which to search for n and k. In the case of SiGe, where the value of N is a function of the Ge content (seen in figure 3.4), N may either be fixed for a known Ge content, or the Ge content may be measured by determining N. Furthermore, as seen in figure 3.4(a), the values of n for SiGe and Si begin to approach one another at a λ of about 600 nm and become increasingly similar as the wavelength is increased. Figure 3.4(b) shows that the value of k for Si and SiGe quickly approaches zero as λ increases towards 600 nm and beyond. The similarity of the optical constants between Si and SiGe at longer wavelengths

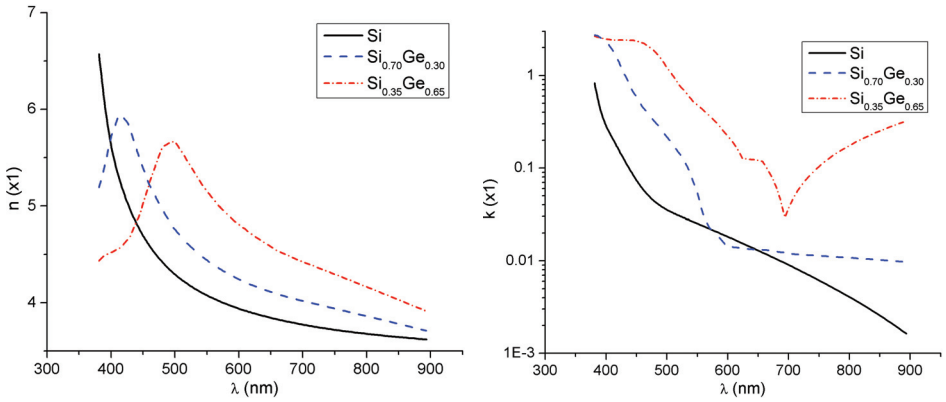

(a) index of refraction (b) extinction coefficient

Figure 3.4: *The (a) real and (b) imaginary components of the indices of refraction for Si, $Si_{0.70}Ge_{0.30}$, and $Si_{0.35}Ge_{0.65}$. The data is extracted from the CompleteEASE software by J.A. Woollam Co. [4] following data presented in [6] and [7].*

makes it possible to simplify the model used for data analysis by considering the SiGe as a part of the Si substrate. An alternative view is that, when measuring the thickness of SiO_2 on top of SiGe and Si, any error introduced by uncertainty in the Ge content of the SiGe layers is minimized at longer wavelengths. On the other hand, due to the difficulty distinguishing SiGe from Si at longer wavelengths, there will be a higher degree of uncertainty when measuring the SiGe layer thicknesses. This is contrasted to shorter wavelengths, where the values of n and k differ substantially between Si and SiGe, which facilitates characterization of SiGe layers but adds to the complexity of the analysis.

It should be clear that measuring each sample with a series of wavelengths (referred to as spectroscopic ellipsometry) can add substantially to the certainty with which various sample characteristics are determined. This approach has the obvious disadvantage of increasing the number of unknowns that must be determined due to the dependence of N on λ. However, aside from the option of using published data for given materials, N can be parameterized as a function of λ using an appropriate relation, *e.g.* a Cauchy or B-Spline function [1, 4]. The method referred to as variable angle spectroscopic ellipsometry (VASE) takes this one step further by making spectroscopic ellipsometry measurements at a variety of angles of incidence. This has the advantage of increasing the number of measurements for each sample, and measuring various path lengths within the sample without altering λ or N. VASE will act to minimize both random and systematic measurement error and to maximize the contrast in χ^2 for the range of unknowns being considered.

As some of the characteristics of the materials and layers for the different samples in an

experiment are bound to be similar or the same, a number of samples may be analyzed simultaneously to minimize the uncertainty in the solutions. For example, a number of samples of Si and SiGe that have been oxidized for various times and temperatures will have a range of oxide and SiGe film thicknesses, but, the values of N for the SiO_2 and Si will be the same for all of the samples. Analyzing all of the samples simultaneously and using a common value for N will produce a substantial improvement in the certainty of the solutions. The analyses done for the present work made use such simultaneous analyses of groups of samples in combination with data produced by both spectroscopic ellipsometry and VASE. Data measured using the *AutoEL-II* used wavelengths of 632.8 and 830.0 nm and an angle of incidence of 70°. VASE measurements were done with the *alpha-SE* ellipsometer by stepping λ in intervals of 0.01 eV between 1.39 and 3.25 eV (between 382 and 900 nm) and with angles of incidence of 65°, 70°, and 75°. Use of the measured data to determine N for SiO_2 and Si produced results that were essentially the same as published values [6, 7] as implemented by the *CompleteEASE* software [4].

3.2 X-ray diffraction (XRD)

X-ray Diffraction (XRD) is an analysis method that relies on diffraction of monochromatic x-rays to characterize the structure of the crystalline material being analyzed. Although XRD may be applied to powders, large single crystals, or polycrystalline samples, this work uses the method exclusively for analysis of thin films.

The present work used a *Bruker AXS Discover* diffractometer. Figure 3.5 shows the basic components of such an instrument. A copper based x-ray tube is used to generate Cu-Kα_1 (0.154057 nm), Cu-Kα_2 (0.154440 nm), and Cu-Kβ (0.139223 nm) radiation [8–10]. The Göbel mirror removes the Cu-Kβ radiation and reflects the Cu-Kα x-rays as a parallel beam. The beam then passes through an asymmetric (220) Ge two bounce monochromator which filters out the Cu-Kα_2 radiation and only passes the Cu-Kα_1 radiation. The slit on the primary side defines the beam width, while the slit on the secondary side helps to confine the detected signal

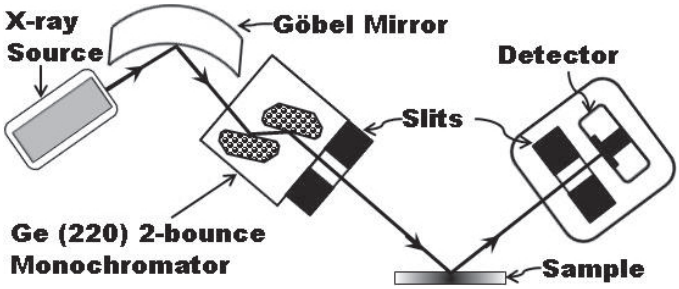

Figure 3.5: *A schematic of an x-ray diffraction (XRD) instrument.*

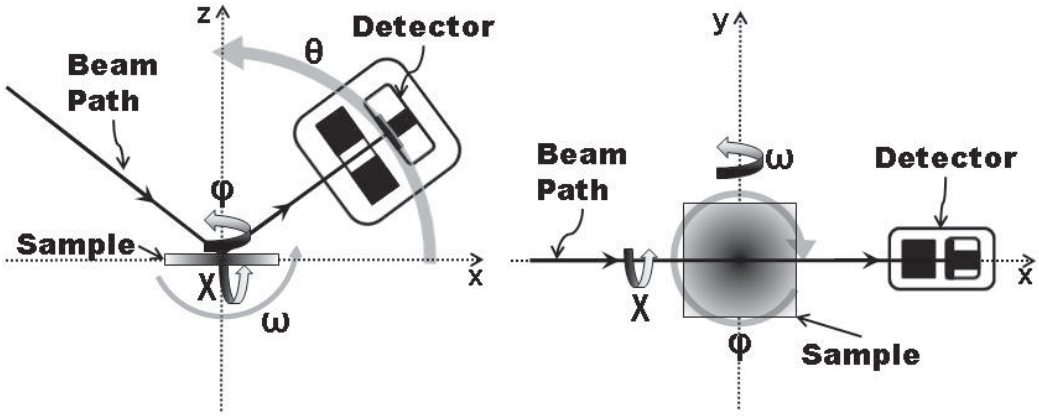

Figure 3.6: *Angular rotations of a sample in an Eulerian cradle.*

to diffracted radiation by removing scattered radiation. The detector is a one dimensional point source detector. It is also possible to use a Ge analyzer crystal on the secondary side with a scintillation detector to increase the angular resolution, however, the cost of the higher resolution is a substantially reduced detected beam intensity. The reduction in the detected beam intensity with the analyzer crystal and scintillation detector precludes use of such a high resolution setup for detecting weak peaks or Kiessig fringes, or for generating reciprocal space maps.

The sample is placed on a vacuum chuck at the center of an Eulerian cradle which allows the sample to be rotated to any position. If, as shown in figure 3.6, the Cartesian coordinate system, (x,y,z), is used to define the reference axes, the angles of rotation for the sample are χ, ϕ, and ω. The sample surface sits in the xy plane and χ is the rotation about the x axis. Rotation in χ is used primarily to align the sample such that the preferred crystallographic plane (i.e. (100), (110), or (111)) is perpendicular to the plane containing the x-ray beam. This alignment is only done prior to measurement and will adjust for deviations between the (100), (110), or (111) planes from the sample surface (often referred to as sample offcut) or for samples that are, for some reason, tilted with respect to the chuck surface. Rotation in ϕ is about the z axis and is used to align the sample prior to measurement of asymmetric peaks. Rotation in ω is about the y axis and is used to align the sample for measurement of both symmetric and asymmetric Bragg peaks. Both 2θ-ω scans and reciprocal space mapping rely on manipulation of ω to tilt the sample relative to the incident beam path and detector during data collection. The beam path and the detector sit in the xz plane with the detector and Eulerian cradle held by a goniometer. The detector may be moved in an arc about the y axis; this is the same direction as ω but instrument is built to allow movement of the detector, independent of rotation of the sample.

The defining equation for XRD is Bragg's law, $n\lambda = 2d\sin\theta$, which describes the relationship between the wavelength of incident x-rays, λ, the spacing between planes of atoms in a

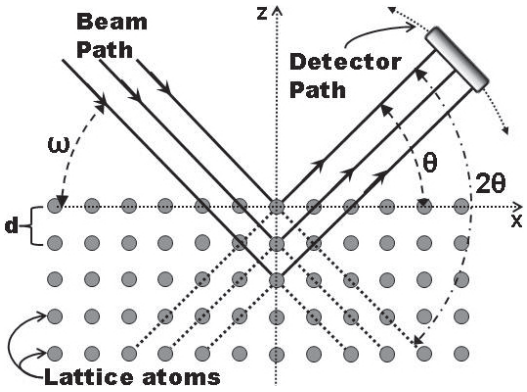

Figure 3.7: *A schematic describing the diffraction of x-rays by a crystal lattice.*

crystal lattice, d, and the angle of incidence and diffraction, θ [10]. Figure 3.7 presents a graphical representation of XRD as described by Bragg's law. Considering the wave nature of x-rays, if an incident beam of x-rays strikes a crystal structure at an angle, ω, the x-rays that are diffracted by multiple planes of the crystal will undergo constructive or destructive interference. Constructive interference will only occur in the event that d is related to an integer multiple, n, of λ such that Bragg's law is satisfied. A 2θ-ω XRD scan measures d for a crystalline structure by simultaneously sweeping the detector and the sample through a range of angles while maintaining $\omega = \theta$. The peaks in intensity of the diffracted x-rays that are caused by constructive interference will be detected at values of 2θ where Bragg's law is satisfied.

It is evident from Bragg's law that, for a given λ and d, there will be multiple values of θ for which intensity peaks occur. For a simple cubic structure with a (001) oriented surface, peaks will occur for integer values of n and will be referred to by the miller indices of the planes of reflection, (001), (002), (003), (004), and so forth. Although silicon, germanium, and their alloys are cubic in nature, they form crystals that have a diamond structure. The diamond lattice structure may be described as being composed of two interlaced face centered cubic (fcc) cells, and is critically different from the simple cubic and fcc structures, in that it will lead to destructive interference for a number of reflections, sometimes referred to as forbidden reflections [10]. In addition to those reflections that are forbidden by the nature of the lattice structure, there are a number of reflections that can not be measured due to the geometry of the instrument and the sample. This is best illustrated by considering the space drawn by the scattering vector, Q, which is also referred to as the reciprocal space. The x and z components of the vector Q are defined

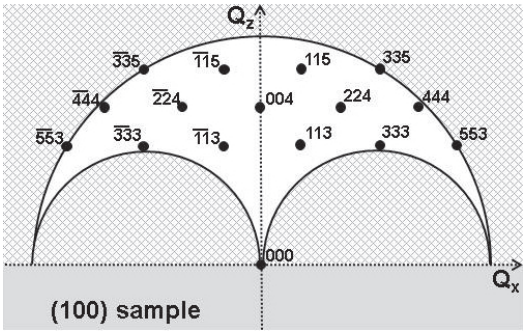

Figure 3.8: *Bragg diffraction peaks for a crystal with a diamond structure that has a (100) oriented surface plotted in Q space. The peaks that are forbidden due to instrument or sample geometry and due to the sample's crystal structure are excluded. After figure 7.16 in [10].*

as

$$Q_x = K\left[\cos\left(\theta - \omega\right) - \cos\left(\theta + \omega\right)\right] \tag{3.4a}$$

and

$$Q_z = K\left[\sin\left(\theta - \omega\right) - \sin\left(\theta + \omega\right)\right], \tag{3.4b}$$

where $K = 2\pi/\lambda$ [10]. As shown in figure 3.8, the diffraction peaks that are permitted and that can be measured are confined within an arc in the Q_xQ_z plane. However, there are two symmetric hemispheres within this arc that represent the space in which the incident or diffracted beams are below the surface of the sample, thus preventing measurement of the peaks that fall within these two smaller hemispheres.

Figure 3.8 is drawn for a sample with a (100) oriented surface, for which the (004) peak is the most commonly measured symmetric peak. For a sample with any given surface orientation, the peaks that occur along the Q_z axis are referred to as symmetric and can be measured with a 2θ-ω scan where $\omega = \theta$. Those peaks that occur to the left or right of the Q_z axis are asymmetric peaks and can be measured with a 2θ-ω scan wherein an offset is added to ω. The map of the reciprocal space and the symmetry of the Bragg peaks depend on the surface orientation of the sample being measured.

For a single crystalline Si wafer with a (100) surface orientation, the primary symmetric Bragg peak is the (004) peak. Using a 2θ-ω scan and Cu-Kα_1 radiation, the (004) peak from a (100) oriented single crystalline Si wafer will occur at 69.128°. Similarly, the (333) peak for (111) oriented Si will occur at about 94.949°. Whereas Si has a lattice constant of 0.54310 nm, Ge has a lattice constant of 0.56575 nm and the lattice constant of relaxed $Si_{1-X}Ge_X$ varies according to X in a way that is similar to Vegard's law [11]. This difference in lattice constant

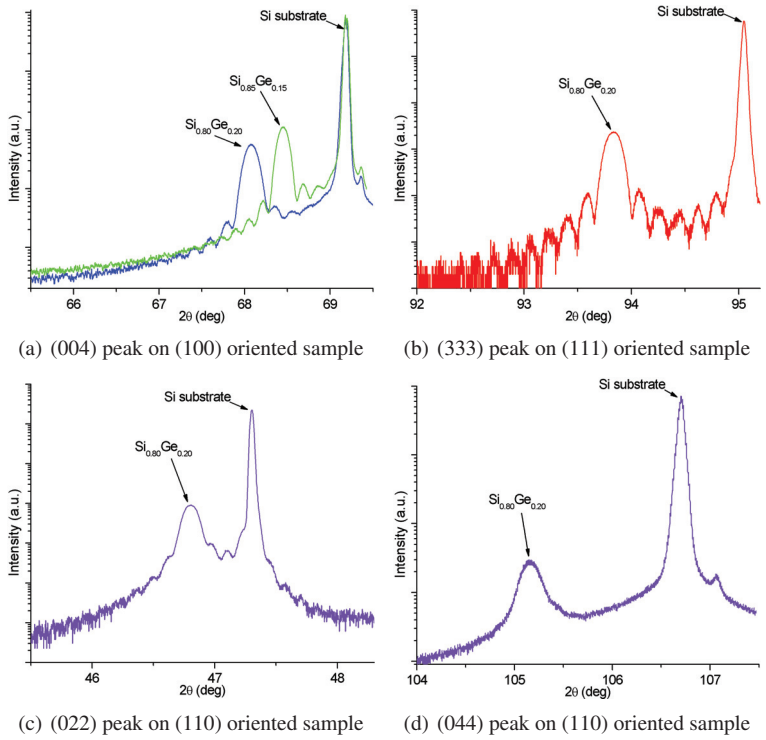

(a) (004) peak on (100) oriented sample (b) (333) peak on (111) oriented sample

(c) (022) peak on (110) oriented sample (d) (044) peak on (110) oriented sample

Figure 3.9: *XRD 2θ-ω scans of samples with 80 nm epitaxial layers of $Si_{1-X}Ge_X$ on a Si substrate. The (004) peak is measured for (100) oriented material, the (333) peak for (111) material, and the (022) and (044) peaks for (110) material.*

for $Si_{1-X}Ge_X$ will shift the (004) peak on (100) material towards 65.996° (the 2θ value for Ge.) The samples in the present work are composed of an 80 nm epitaxial layer of $Si_{1-X}Ge_X$ on a Si substrate. Figure 3.9 shows the results of 2θ-ω scans of the symmetric (004), (333), (022), and (044) peaks for $Si_{0.8}Ge_{0.2}$ on variously oriented Si substrates. It is clear that the substrates produce the strongest peaks, while the thinner SiGe layers produce less intense peaks that are shifted according the Ge content in the layer. Both the intensity of the thin film peak and the periodicity of the Kiessig fringes are indications of the layers' thickness. The tendency of an increase in Ge content in the epitaxial layer to shift a peak to lower 2θ values is clear in figure 3.9(a), which shows a samples with $Si_{0.85}Ge_{0.15}$ contrasted with a sample with $Si_{0.80}Ge_{0.20}$.

It is frequently difficult to fully evaluate an epitaxially grown thin film using a single 2θ-ω scan. A reciprocal space map is a scan of an area of the Q_xQ_z space that is typically focused around one or more peaks and can be used to evaluate epitaxial layer characteristics, like layer tilt,

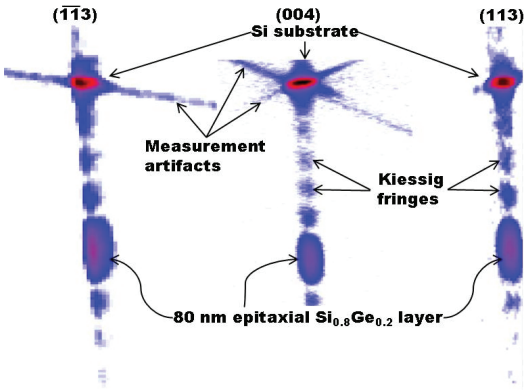

Figure 3.10: *XRD reciprocal space maps of the (-1-13), (004), and (113) peaks of a (100) oriented sample with an 80 nm epitaxial layer of $Si_{0.8}Ge_{0.2}$ on a Si substrate. The epitaxial layer of SiGe has a slight tilt with respect to the substrate.*

strain and relaxation, lattice mismatch, and defectivity. Any measurements of asymmetric peaks will require alignment of the sample in ϕ. Figure 3.10 shows an example of the reciprocal space mapping of the negative and positive asymmetric (113) peaks and the symmetric (004) peak of a (100) oriented sample with an 80 nm epitaxial layer of $Si_{0.8}Ge_{0.2}$ on a Si substrate. The slight tilt in the lines linking the substrate and epitaxial layer peaks is an indication that the epitaxial layer is physically tilted with respect to the substrate. A fully relaxed epitaxial layer would be indicated by the lines linking the substrate and epitaxial layer peaks being directed towards the origin in Q_xQ_z space. Fully pseudomorphically strained epitaxial layers would show the epitaxial layer and substrate peaks aligned vertically along Q_z as a consequence of pseudomorphically strained material having a face centered tetragonal crystal structure, rather than the face centered cubic structure of relaxed material.

In the present work, reciprocal space maps were measured on a limited number of samples to evaluate the strain in the thin films of SiGe before and after oxidation. All samples were fully pseudomorphically strained prior to oxidation. After oxidation, the reciprocal space maps of both symmetric and asymmetric reflections showed that the substrate and SiGe layer peaks were aligned vertically along Q_z. This vertical alignment along Q_z indicates that the peak position in a symmetric 2θ-ω scan is a reflection of the lattice constant (*i.e.* the Ge content) of the layer. Relaxation due to an increase in the lattice mismatch in the plane of the layer would cause the relaxed SiGe layer peak to shift towards the line connecting the Q_xQ_z origin to the substrate peak, this was not observed in the RSM measurements done in the present work. The oxidation process may also cause relaxation by formation of dislocations and other defects (such as those shown in figure 3.11), but defectivity will contribute to broadening of the XRD peak for the layer, rather than shifting of the peak in the reciprocal space. Although both peak broadening and

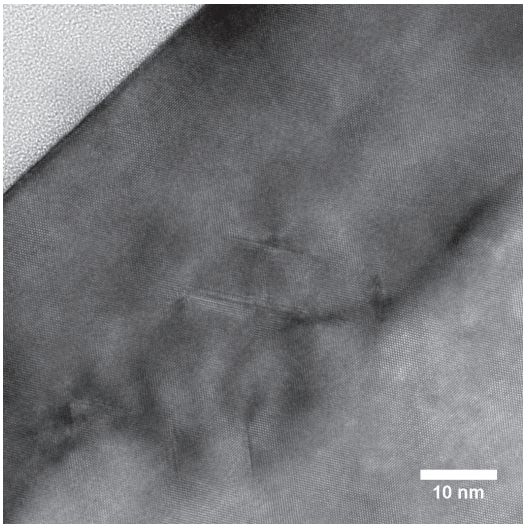

Figure 3.11: *Transmition Electron Microscopy (TEM) image showing extended defects in the crystalline lattice of a thin film of SiGe on Si which has been subjected to oxidation at 1000 °C.*

intensity reductions may occur due to both thinning of layers and relaxation, layer thickness can also be estimated based on the spacing of the fringes around the main layer peak. Assumption of the SiGe layers as having the same lattice constant as the substrate allows measurement of the Ge content in the SiGe layers using only 2θ-ω scans of symmetric peaks, but without the confounding influence of strain or relaxation induced variations in the lattice constant.

All samples in the present work were measured using 2θ-ω scans of one or more symmetric peaks. The results of these scans were analyzed using the *Leptos* software in order to determine the Ge content and layer thicknesses of the SiGe layers. The software allows construction of multilayered models for which specific model characteristics (*i.e.* Ge content and layer thickness) may be set as variables. The 2θ-ω scan is simulated for the model and matched to the measured scan using a genetic algorithm and the MSE method.

3.3 X-ray photo-electron spectroscopy (XPS)

X-ray photo-electron spectroscopy (XPS) is a non-destructive method for both chemical and elemental surface analysis. The method depends on analysis of the kinetic energy and flux of photo-electrons that are ejected from the core energy levels of chemically bound atoms in a sample that is illuminated by x-ray radiation [2]. The instrument used in the present study was a *Kratos Axis Ultra DLD*, and figure 3.12 shows a schematic of the essential components of such a

system. A monochromatic x-ray source illuminates a sample within a high vacuum environment. The electrons emitted from the sample surface are propelled through an electrostatic lens and an electron analyzer towards a detector. The electron current and kinetic energy are measured by the detector, and form the basis for the analysis.

Although photo-electrons can be generated from various materials with a wide range of photon energies, XPS uses an x-ray source because x-rays are high enough in energy to excite core level electrons to the vacuum level. It is this excitation of core level electrons that makes XPS unique among analysis techniques and allows for the identification of chemical states as well as elements. Figure 3.13 shows a schematic of the vacuum, conduction, valence, and core energy levels in an atom, and illustrates how the energy from an incident x-ray can excite a core level electron to the vacuum level. The energy of the ejected electron as measured by the XPS instrument, E_{XPS}, is related to the binding energy of the electron, E_{b}, as

$$E_{\mathrm{XPS}} = \mathrm{h}\nu - E_{\mathrm{b}} - \mathrm{q}\phi_{\mathrm{XPS}}, \tag{3.5}$$

where ϕ_{XPS} is the work function of the XPS instrument and $\mathrm{h}\nu$ is the energy of the incident x-ray.

Although Auger emissions may also occur during XPS measurements, XPS is distinct from Auger Electron Spectroscopy (AES). Auger analysis relies on excitation of core level electrons by an incident electron beam, rather than an x-ray source. Excitation of Auger electrons is illustrated in figure 3.13. An incident electron ejects a K level core electron, allowing an L1 level core electron to fall into the K level. The energy from the electron transition from L1 to K is transferred to another core level electron which is ejected and becomes an Auger electron. The Auger electron in figure 3.13 would be referred to as a KLL emission to highlight the multiple energy level transitions that distinguish it as an Auger electron. The core level transitions in Auger will produce both emitted electrons and x-rays, with the electron emissions dominating for elements with low atomic numbers ($\lesssim$30) and x-ray emissions dominating for elements with

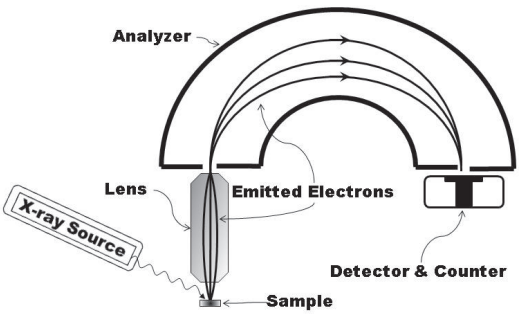

Figure 3.12: *A schematic of an x-ray photo-electron spectroscopy (XPS) instrument.*

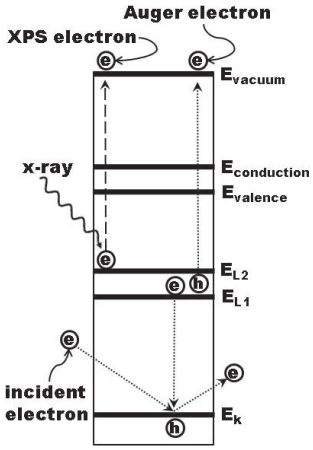

Figure 3.13: *XPS and Auger transitions between energy levels. After figures 10.8 and 10.33 of [2].*

high atomic numbers ($\gtrsim$30.) Though, as a practical matter, neither hydrogen nor helium is measurable by either AES or XPS [2].

The end result is the same in both Auger and XPS, that is, electrons are emitted and subsequently collected to measure their kinetic energy and current at the detector. Figure 3.14 shows an example of the results of an XPS measurement of a sample of oxidized SiGe with Ge incorporated into the oxide. Both XPS and Auger emissions from oxygen, germanium, and silicon are visible and plotted as a function of their binding energies. Changes in the binding energies for the various elements are indicative of the chemical states of the atoms in the sample. The translation of the binding energy to a chemical or elemental identification is done through tabulated or collected references that are published in both books and XPS system software. There are varying degrees of complexity to the analysis of the binding energies, including, but not limited to, atomic models, chemical shifts, Koopman's theorem, spin orbit coupling, and sample charging induced shifts.

The x-ray source in an XPS system is typically made of Al or Mg in order to take advantage of their Kα x-ray emissions [2]. The Al Kα radiation (h$\nu = 1486.6$eV) used in the present work offers a relatively small bandwidth of x-rays leading to reduced full-width-half-max (FWHM) values for the measured peaks and thus clearer discrimination between peaks during analysis.

The detection depth for an XPS measurement is related to the penetration depth of the incident x-rays and the inelastic mean free path of the photo-electrons, as described by the Beer-Lambert law. For the oxidized SiGe sample in figure 3.14, if the detection depth is written as $d = 3\Lambda\cos\theta$, where Λ is the inelastic mean free path of photo-electrons and $\theta = 0^\circ$ is the angle at which photo-electrons are emitted, Ge2p and Ge3d photo-electrons will give detection depths of 3.5 and 11.7 nm, respectively. These detection depth values were derived assuming that the

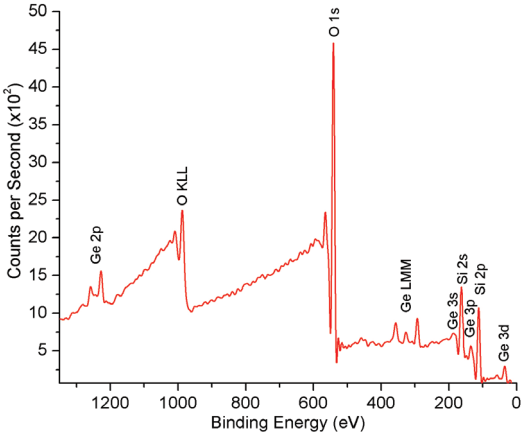

Figure 3.14: *XPS spectrum of oxidized SiGe with Ge incorporated into the oxide. The spectrum shows the binding energies of emitted electrons for silicon (Si), germanium (Ge), and oxygen (O.) The peaks due to photo-electrons are marked by the core energy levels from which the electrons are emitted, while the Auger emission peaks are labeled according to the levels involved in the Auger transitions.*

photo-electrons are traveling through an SiO_2 layer, and by using data from the Tanuma, Powell, and Penn algorithm [12, 13]. Although XPS is fundamentally a surface analysis method, sample tilting or ion milling can be used in conjunction with XPS to create depth profiles for arbitrarily deep analyses [2].

3.4 Rutherford backscattering spectroscopy (RBS)

Rutherford backscattering spectroscopy (RBS) is based on measuring the intensity and energy of ions with small masses that have been scattered from the larger atoms in a sample. The instrument used for an RBS measurement may be described as a modification of an ion implantation system, and figure 3.15 shows a schematic such an instrument. The ion source produces ^{4}He+ cations (also commonly referred to as alpha particles) which are subsequently propelled towards a large magnet that acts as a beam path selector and mass separator. The beam path selector directs the ion beam towards the sample, where the ^{4}He+ cations will be elastically scattered by the more massive atoms in the sample. The detector is positioned to measure the backscattered He ions. The 100° angle between the incident ion beam path and the detector (in figure 3.15) is referred to as a glancing-angle detector geometry, and is used to provide enhanced depth resolution for accurate analysis of films near the sample surface; a typical detector geometry would use an angle closer to 170°. The 2 MeV energy of the incident ion beam should result in detection depth

on the order of 1×10^4 nm and a depth resolution of around 15 nm for a Si sample [2]. Given that the thicknesses of the SiGe and oxide films on the samples in the present study are frequently smaller than 20 nm, it is critical to use the instrument configuration that will give the highest possible resolution.

Even though RBS is not restricted to use of helium for the ion beam, since the method relies on the incident ions being significantly smaller in mass than the atoms that are to be detected, use of a more massive element, like carbon, is precluded by the need to measure the composition of the oxide layers on the samples in the present study. The measured spectrum will show a count rate or yield *versus* backscattering energy; the backscattering energy may be binned into discrete channels. Two examples of RBS spectra for samples with SiGe films on a silicon substrate are shown in figure 3.16; one of the two samples has been oxidized. The spectrum features for each of the elements in the sample will be shifted in energy according to the mass of the detected element. There will also be a width to the feature for each element that is characteristic of the distribution of the element in the sample; the broader the distribution of an element, the wider the feature will be. In figure 3.16, the silicon substrate has a signal that extends from beyond the lowest graphed channel to the surface position where the count rate drops precipitously (between channels 300 and 350.) There is a shelf at the surface of the silicon that represents the silicon in the oxide or the silicon in the SiGe. The germanium signal starts wide and becomes much thinner after oxidation, which is consistent with the increased concentration of germanium in the SiGe layer after oxidation of the sample. Similar to what is done to analyze XRD and Ellipsometry data, RBS relies on software to generate simulated curves for a user defined sample model and to match the simulated and measured spectra to find the most likely values for the given unknowns.

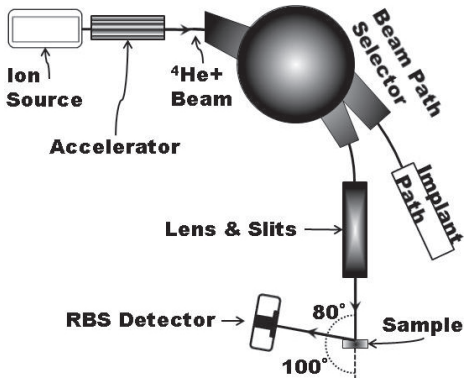

Figure 3.15: *A schematic of an ion beam implanter modified for Rutherford backscattering spectroscopy (RBS) measurements with a glancing-angle detector geometry.*

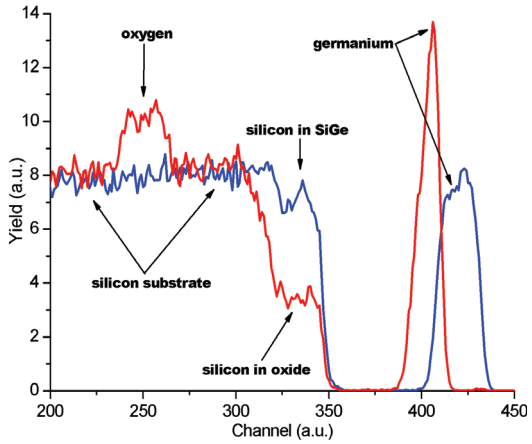

Figure 3.16: *Two example spectra measured by Rutherford backscattering spectroscopy (RBS). The samples were thin films of SiGe on a Si substrate, one of the samples was oxidized to enhance the Ge content of the SiGe layer.*

References

[1] H. G. Tompkins and E. A. Irene, *Handbook of Ellipsometry*. Heidelberg: Springer, 2005.

[2] D. K. Schroder, *Semiconductor Material and Device Characterization*, 2nd ed. New York: Wiley-Interscience, 1998.

[3] *AutoEL-II Automatic Ellipsometer Instruction Manual*, Rudolph Research, 1980.

[4] *CompleteEASE Data Analysis Manual*, J.A. Woollam Co., 2009.

[5] J. R. Taylor, *An introduction to error analysis: the study of uncertainties in physical measurements*, 2nd ed. Sausalito, California: University Science Books, 1997.

[6] C. M. Herzinger, B. Johs, W. A. McGahan, J. A. Woollam, and W. Paulson, "Ellipsometric determination of optical constants for silicon and thermally grown silicon dioxide via a multi-sample, multi-wavelength, multi-angle investigation," *J. Appl. Phys.*, vol. 83, no. 6, pp. 3323–3336, Mar 1998.

[7] J. Humlíček, M. Garriga, M. I. Alonso, and M. Cardona, "Optical spectra of Si_xGe_{1-x} alloys," *J. Appl. Phys.*, vol. 65, no. 7, pp. 2827–2832, 1989.

[8] J. A. Bearden, "X-ray wavelengths," *Rev. Mod. Phys.*, vol. 39, no. 1, pp. 78–124, Jan 1967.

[9] G. Hölzer, M. Fritsch, M. Deutsch, J. Härtwig, and E. Förster, "$K\alpha_{1,2}$ and $K\beta_{1,3}$ x-ray emission lines of the $3d$ transition metals," *Phys. Rev. A*, vol. 56, no. 6, pp. 4554–4568, Dec 1997.

[10] M. Birkholz, *Thin Film Analysis by x-ray scattering*. Weinheim: Wiley-VCH, 2006.

[11] J. P. Dismukes, L. Ekstrom, and R. J. Paff, "Lattice parameter and density in germanium-silicon alloys," *J. Phys. Chem.*, vol. 68, no. 10, pp. 3021–3027, Oct 1964.

[12] S. Tanuma, C. J. Powell, and D. R. Penn, "Calculations of electron inelastic mean free paths (IMFPS). IV. evaluation of calculated IMFPs and of the predictive IMFP formula TPP-2 for electron energies between 50 and 2000 eV," *Surf. Interface Anal.*, vol. 20, no. 1, pp. 77–89, Jan 1993.

[13] C. J. Powell and A. Jablonski, "NIST electron inelastic mean free path database, version 1.1," National Institute of Standards and Technology, Gaithersburg, MD, Tech. Rep. Version 1.1, 2000.

Chapter 4

Results and discussion

This chapter reviews the modeling and experimental results that are detailed in the attached articles. Additionally, supporting data is presented and discussed with an emphasis on the physical mechanisms and materials characteristics that are important for designing and constructing nanostructures by thermal oxidation of silicon-germanium.

4.1 Oxidation rate modeling

Early literature on the oxidation of metals was reviewed and explained by diffusion of ions and electrons in a space charge induced field in an oft-cited work by Cabrera and Mott [1]. In their analysis, they made a critical distinction between very thin oxides with high growth rates and thicker films characterized by slower growth rates. They describe the thickness of thin films with a logarithmic model, $1/z_{\mathrm{ox}} = A - B\ln(t)$, while thicker films are described by a parabolic model, $z_{\mathrm{ox}}^2 = 2At$. Here, z_{ox} is the oxide thickness and t is the oxidation time, while A and B are rate constants that show Arrhenius like behaviour and that are determined by the materials and oxidation conditions. They also briefly mention that growth of thick oxides can be described by linear, $z_{\mathrm{ox}} = At$, or cubic, $z_{\mathrm{ox}}^3 = 3At$, models and that A may take on various definitions. Oxidation of silicon has been explained by both linear [2, 3] and parabolic [4] models. Deal [5] suggested that oxidation of silicon can be modeled by the combination of linear and parabolic regions, and along with Grove [6], established the frequently cited model $z_{\mathrm{ox}}^2 + Az_{\mathrm{ox}} = B(t + \tau)$, where B is the parabolic rate constant, B/A is the linear rate constant, and τ is a factor which adjusts the oxidation time to account for any pre-existing oxide. For thick oxides or long oxidation times, the Deal and Grove model reduces to the previously mentioned parabolic form, $z_{\mathrm{ox}}^2 \cong Bt$, and for very short oxidation times it reduces to a linear form, $z_{\mathrm{ox}} \cong (B/A)(t+\tau)$. An alternative model, presented by Massoud *et al* [7, 8], does a better job of modeling the earliest stages of oxidation as well as oxidations in the linear and parabolic regions. The Massoud model defines the oxidation rate as $\mathrm{d}z_{\mathrm{ox}}/\mathrm{d}t = B/(2z_{\mathrm{ox}} + A) + C_1\exp(-z_{\mathrm{ox}}/L_1) + C_2\exp(-z_{\mathrm{ox}}/L_2)$,

where C_1, L_1, C_2, and L_2 are additional oxidation constants. The values used for any given model's coefficients depend critically on such variables as the oxidant partial pressure [3, 6, 9], crystalline orientation [2, 7, 9–12], water content in the ambient [4–6, 9, 11], and impurities in both the ambient and the material being oxidized [9].

Despite the wide variety of models for oxidation of silicon, a simple Arrhenius model is adequate for describing the growth of oxides with thicknesses between a few tens of angstroms and about a hundred nanometers. So, in the context of the present study, it is a reasonable approximation to describe the oxidation rate as $\mathrm{d}z_{ox}/\mathrm{d}t = A_0 \exp[-E_{\mathrm{ox}}/(\mathrm{k}T)]$, where E_{ox} is the activation energy for the oxidation process and A_0 is a pre-exponential constant, T is the oxidation temperature, k is the Boltzmann constant.

4.2 Diffusion modeling

The concentration of a diffusing substance at any given place within a system, at any given time is characterized by the diffusivity of the substance and the dimensions of the system in which the substance is diffusing. The fundamental relation describing diffusion is Fick's law, $J = -D\partial N/\partial x$, where J is the flux of diffusing substance in the direction x, $N(x,t)$ is the concentration of the diffusing substance, and D is the diffusivity of the diffusing substance in the medium. The dose, Q, is defined as the amount of diffusing substance to pass $x = 0$ over a given period of time and may be found by solving Fick's law for N and integrating this over time, t.

While Crank [13] discusses solutions to Fick's law for a wide variety of boundary conditions and system geometries, there is one solution that is of particular import to the present work. This solution is referred to as a semi-infinite medium by Crank [13] and as pre-deposition diffusion by Campbell [14] and involves diffusion in a planar structure with an infinite diffusion source. The boundary conditions for this solution are $N(0,t) = N_0$, $N(x,0) = 0$, and $N(\infty,t) = 0$, while the concentration and dose are written as

$$N(x,t) = N_0 \mathrm{erfc}\left(\frac{x}{2\sqrt{Dt}}\right) \quad \text{for} \quad t > 0, \tag{4.1a}$$

and

$$Q = 2N_0\sqrt{\frac{Dt}{\pi}}\,. \tag{4.1b}$$

4.3 Modeling of the pile-up region

The pre-deposition model may be used to analyze the formation of the pile-up region in oxidizing silicon-germanium by considering the initial silicon-germanium layer to be an infinite source of silicon and the pile-up region to be an arbitrary medium in which the silicon is diffusing. This

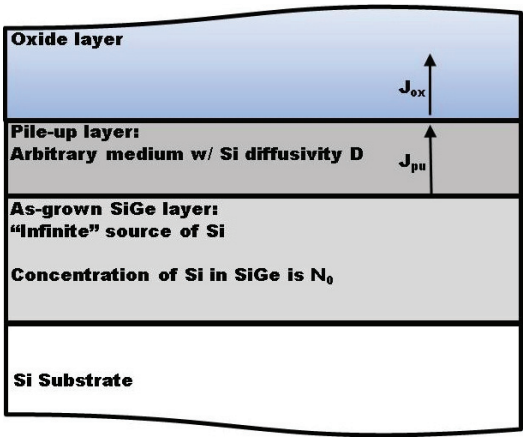

Figure 4.1: *diffusion model*

structure is sketched in figure 4.1. The width of the pile-up region may be considered to be very small such that the flux of silicon exiting the initial silicon-germanium layer, J_{pu}, is exactly equal to the flux of Si entering the oxide, J_{ox}, *i.e.* $J_{\mathrm{pu}} = J_{\mathrm{ox}}$. The flux of silicon atoms into the oxide, J_{ox}, is defined by the rate at which silicon atoms are removed from the surface of the crystalline silicon-germanium and bonded to oxygen atoms to form the growing oxide, *i.e.* the oxidation rate. The requirement that $J_{\mathrm{pu}} = J_{\mathrm{ox}}$ is then equivalent to requiring that the dose from silicon diffusion through the pile-up is equal to the dose of silicon incorporated into the oxide, $Q_{\mathrm{pu}} = Q_{\mathrm{ox}}$. The dose of silicon incorporated into the oxide, Q_{ox}, can be determined directly from the oxidation rate and the atomic density of silicon in silicon dioxide.

Considering the pile-up region to be an arbitrary medium is a means of accommodating for the fact that the Ge content in the pile-up region is unknown. It has been established that the diffusivity of Si in $\mathrm{Si}_{1-X}\mathrm{Ge}_X$ is a function of X and can be modeled by an Arrhenius relation, $D = D_0 \exp\left[-E_{\mathrm{a}}/(\mathrm{k}T)\right]$ [15]. Furthermore, if the Ge content in the pile-up region is written as X_{pu}, then $D(X_{\mathrm{pu}})$ can be reasonably approximated by considering D_0 to be constant and $E_{\mathrm{a}} = E_{\mathrm{m}} X_{\mathrm{pu}} + E_{\mathrm{Si}}$, where E_{Si} is the activation energy for Si self-diffusion and E_{m} is a coefficient to account for the Ge content.

By adopting an Arrhenius relation to describe both the oxidation rate and the diffusivity of Si, and by assuming a linear function for $E_{\mathrm{a}}(X_{\mathrm{pu}})$, while keeping D_0 independent of X_{pu}, the relation between the doses of silicon due to the diffusion and oxidation fluxes, $Q_{\mathrm{pu}} = Q_{\mathrm{ox}}$, may be solved for X_{pu}:

$$X_{\mathrm{pu}} = \frac{\mathrm{k}T \ln\left(\frac{4N_0^2 D_0}{\pi t N_{\mathrm{ox}}^2 A_0^2}\right) - E_{\mathrm{Si}} + 2E_{\mathrm{ox}}}{E_{\mathrm{m}}}, \tag{4.2}$$

where N_{ox} is the atomic density of Si in SiO_2 and N_0 is the atomic density of Si in the initial or as-grown layer of SiGe.

In the event that E_{ox} and A_0 are not well characterized (*e.g.* due to complications from germanium's tendency to induce oxidation rate enhancement in some ambients), considering that $Q_{\mathrm{ox}} = N_{\mathrm{ox}} z_{\mathrm{ox}}$ allows the relationship between doses to be written as

$$Q_{\mathrm{pu}} = 2N_0\sqrt{\frac{Dt}{\pi}} = Q_{\mathrm{ox}} = N_{\mathrm{ox}} z_{\mathrm{ox}}, \tag{4.3}$$

which, if the oxide thickness is directly measured, allows X_{pu} to be determined following

$$X_{\mathrm{pu}} = \frac{\mathrm{k}T \ln\left(\frac{4tN_0^2 D_0}{\pi N_{\mathrm{ox}}^2 z_{\mathrm{ox}}^2}\right) - E_{\mathrm{Si}}}{E_{\mathrm{m}}}. \tag{4.4}$$

Once X_{pu} has been determined by either measurement or calculation, the thickness of the pile-up region may be determined following the empirical relation,

$$z_{\mathrm{pu}} = \frac{X z_{\mathrm{ox}} N_{\mathrm{ox}}}{(1-X) X_{\mathrm{pu}} N_{\mathrm{pu}}}, \tag{4.5}$$

where X is the Ge content in the initial or as-grown SiGe layer and N_{pu} is the atomic density of the pile-up layer. The density of the pile-up layer, N_{pu}, is a function of the Ge content and may be determined either by Vegard's law or following the data presented by Dismukes *et al* [16].

4.4 Layer thicknesses: measurement and calculation

The measurement methods used in the present work each rely on different physical phenomena but are capable of measuring some of the same sample characteristics. X-ray diffraction (XRD) is adept at measuring layer thicknesses, *e.g.* z_{pu}, and Ge content, X_{pu} and X, in crystalline material. However, XRD is not suited to making direct measurements of the thickness of amorphous oxides, *i.e.* z_{ox}. Variable angle spectroscopic ellipsometry (VASE) is best suited to measuring z_{ox}, but can also measure z_{pu}, X_{pu}, and X. Although the VASE measurement scheme used herein provides robust values for z_{ox}, its estimation of z_{pu} is less robust due to uncertainty in the values for X_{pu} and X, as well as, the high degree of sensitivity of the complex index of refraction to Ge content at short wavelengths (as shown in figure 3.4). Rutherford backscattering spectroscopy (RBS) can also be used to measure these values and is convenient as a means of confirming z_{ox}, but its utility in estimating z_{pu} and X_{pu} is limited.

Figures 4.2, 4.3, and 4.4 compare different measurement methods by plotting results for (100) oriented, MBE grown $Si_{0.8}Ge_{0.2}$ and $Si_{0.85}Ge_{0.15}$ samples that have been oxidized for various times at temperatures between 775 and 1000 °C. These figures also show several statistics

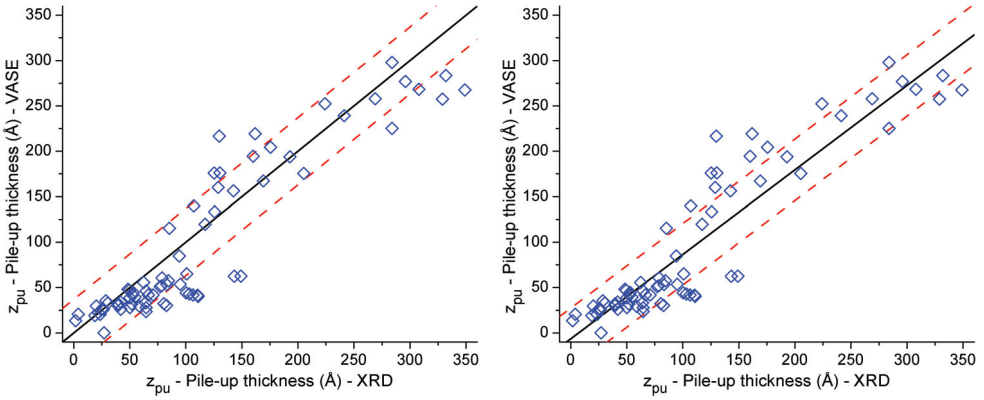

(a) (b)

Figure 4.2: *The pile-up layer thickness, z_{pu}, as measured by XRD compared to the values measured by VASE. (a) The solid diagonal line is drawn as a visual guide to indicate where $x = y$. The dashed lines represent $\pm\sigma = 37\,\text{Å}$. (b) The solid line is the linear regression to the data ($b_{\mathrm{R}} = -6\,\text{Å}$, $m_{\mathrm{R}} = 0.93$, $r_{\mathrm{R}} = 0.92$) and the dashed lines represent $\pm\sigma_{\mathrm{SE}} = 34\,\text{Å}$*

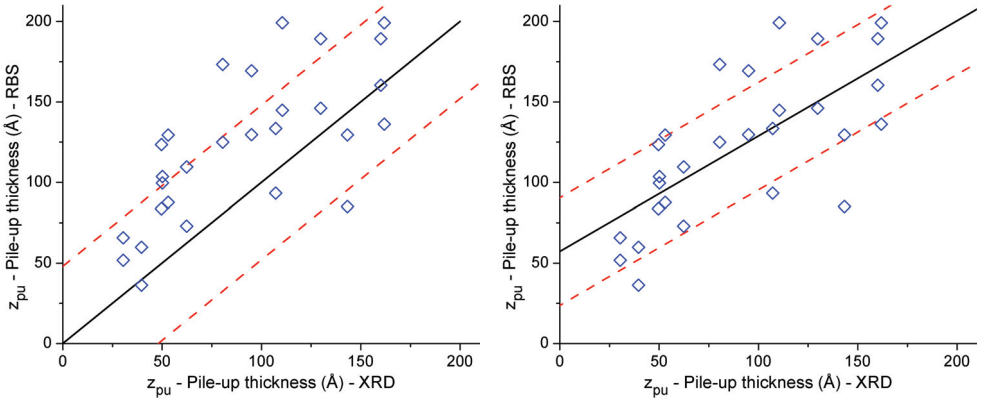

(a) (b)

Figure 4.3: *The pile-up layer thickness, z_{pu}, as measured by XRD compared to the values measured by RBS. (a) The solid diagonal line is drawn as a visual guide to indicate where $x = y$. The dashed lines represent $\pm\sigma = 48\,\text{Å}$. (b) The solid line is the linear regression to the data ($b_{\mathrm{R}} = 57\,\text{Å}$, $m_{\mathrm{R}} = 0.72$, $r_{\mathrm{R}} = 0.70$) and the dashed lines represent $\pm\sigma_{\mathrm{SE}} = 33\,\text{Å}$*

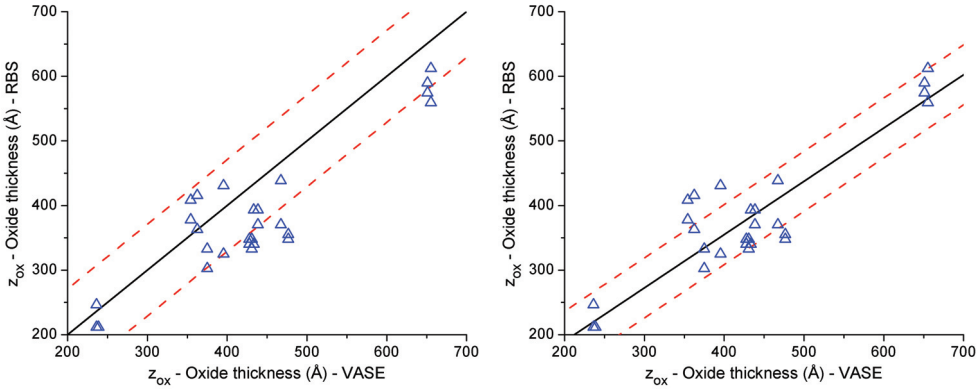

Figure 4.4: *The oxide layer thickness, z_{ox}, as measured by RBS compared to the values measured by VASE. (a) The solid diagonal line is drawn as a visual guide to indicate where $x = y$. The dashed lines represent $\pm\sigma = 71$ Å. (b) The solid line is the linear regression to the data ($b_{\mathrm{R}} = 25$ Å, $m_{\mathrm{R}} = 0.82$, $r_{\mathrm{R}} = 0.91$) and the dashed lines represent $\pm\sigma_{\mathrm{SE}} = 46$ Å*

to demonstrate the uncertainty in the plotted values; these statistics include: 1) the sample standard deviation, σ, comparing results from the two measurement methods, 2) linear least squares regression, where b_{R} is the intercept and m_{R} is the slope, 3) the standard error of the linear regression, σ_{SE}, and 4) the linear correlation coefficient, r_{R}. While one method might be more or less accurate than the others for measuring a particular sample aspect, the methods are complimentary and give results that are in reasonable agreement with one another.

The difficulty in using RBS to measure z_{pu} and X_{pu} for very thin pile-up layers (0 to 20 nm) arises from the fact that RBS is adept at measuring the quantity of atoms within the depth resolution of the measurement, but does not explicitly measure how the atoms are distributed within that depth. During simulation, as long as the dose of Ge in the pile-up layer remains constant, the operator has some freedom to make compensating changes to z_{pu} and X_{pu} without altering the quality of the match between the simulated and measured spectra. This is a particular problem when the depth resolution is large compared to the thickness of the layer being measured. This difficulty in using RBS to differentiate between z_{pu} and X_{pu} is evident in the conclusion of Article II [17] wherein it is written, "For a given oxide thickness, the redistribution of Ge and the formation of a pile-up region was shown by RBS data to be independent of temperature in the range between 800 °C and 1000 °C. Simulations using common models for the oxidation of Si and diffusion of Si in SiGe indicate that temperature does have an influence on the composition of the pile-up layer ..." This conclusion is based on the similarity of the RBS profiles presented in figure 7 of Article II and was made without the benefit of XRD results. Subsequent studies using XRD data confirm the validity of the simulation results and show that the pile-up layers

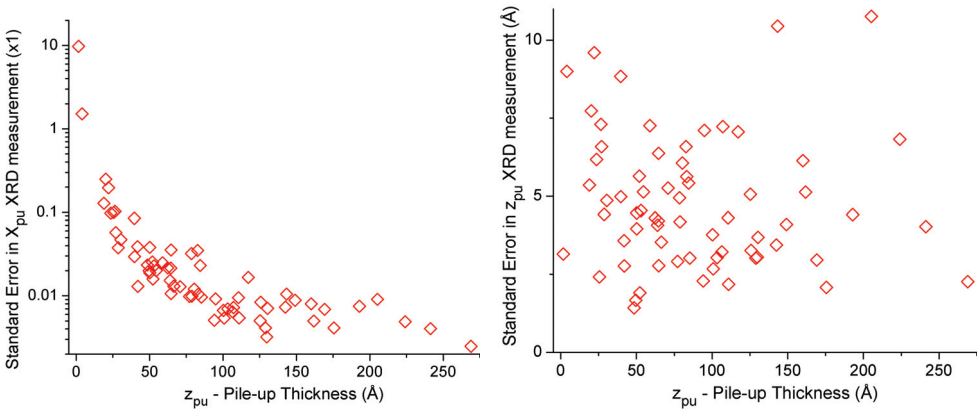

Figure 4.5: *The standard error (as reported by the Leptos software) for XRD measurements of (a)* X_{pu} *and (b)* z_{pu}.

for the samples presented in figure 7 of Article II are between 5 and 11 nm thick. Considering that the channel data for the RBS measurements in figure 7 of Article II was converted to a depth scale by assuming 2.4 nm/channel, the depth resolution of the RBS measurement may be considered to be large with respect to the thickness of the pile-up layers that were being measured. The uncertainty in the RBS measurements that is introduced by the large depth resolution (with respect to the thin pile-up layers) and the difficulty in differentiating between z_{pu} and X_{pu} during simulation is evident in figure 4.3(b); the non-zero intercept and the non-unity slope of the linear regression comparing RBS and XRD measurements of z_{pu} indicate a systematic error in the measurements which is aggravated as z_{pu} approaches zero. However, given that the samples presented in figure 7 of Article II have similar oxide thicknesses as well as pile-up thickness between 5 and 11 nm, the total quantity of Ge in the 15 nm of SiGe nearest to the oxide should be the same for all of the samples. Put another way, since all of the samples had the same dose of Si removed from the surface of the initial SiGe layer (*i.e.* similar oxide thicknesses) and have pile-up layers that are smaller than 15 nm, all of the samples will have the same dose of Ge remaining in the upper 15 nm of the SiGe after oxidation (regardless of oxidation temperature). So, although the profiles presented in figure 7 of Article II do not accurately indicate the influence of oxidation temperature on z_{pu}, they do support the notion that Ge is rejected from the oxide to form a pile-up region wherein the Ge is distributed according to equation 4.5 (*i.e.* $Q_{\mathrm{pu}} = Q_{\mathrm{ox}}$).

XRD is better suited to measuring both z_{pu} and X_{pu} than RBS because z_{pu} appears in the XRD spectrum as peak intensity and Kiessig fringes, while X_{pu} appears as the 2θ position of the pile-up layer peak in an XRD scan. That is, z_{pu} and X_{pu} are manifest in different and independent aspects of the XRD spectrum. Examples showing pile-up layer peaks in XRD 2θ-ω scans may

be seen in figure 4 of Article IV [18] and figure 1 of Article III [19]. The intensity of the pile-up layer's XRD peak will be determined by the thickness of the pile-up layer, and so, the uncertainty in the measurement of X_{pu} increases as the thickness of the pile-up layer approaches zero. This is made clear in figure 4.5(a), which shows the standard error (as reported by the *Leptos* software) in X_{pu} increasing drastically for pile-up layers thinner than about 3 nm. The standard errors in figure 4.5(a) that are greater than 1 simply indicate that X_{pu} can not be measured, which is sensible given that these values are for pile-up layers that are thin enough to be considered non-existent. For pile-up layers thicker than 10 nm, the standard error in the X_{pu} measurement is less than $\sim$1%. The standard error in the XRD measurement of z_{pu} (shown in figure 4.5(b)) is independent of the pile-up thickness, consistently less than 10 Å, and is on average 5 Å.

Although XRD can not measure z_{ox} directly, XRD measurements of z_{pu}, X_{pu}, and X can be used with equation 4.5 to generate an estimate of the oxide thickness. Figure 4.6(a) compares the oxide thickness as measured by VASE to that determined by equation 4.5 with XRD measurements of z_{pu}, X_{pu}, and X. Similarly, figure 4.6(c) compares the pile-up layer thickness as measured by XRD to z_{pu} determined by equation 4.5. The calculated values of z_{pu} use values of z_{ox} from VASE, while X_{pu} and X are measured by XRD. The data in figure 4.6 would ideally lie along the straight diagonal, indicating that equation 4.5 produces a robust prediction of the measured values, but a non-unity slope is clearly present. This slope amounts to a systematic error in the values presented in figure 4.6. The accuracy of the calculated values can be significantly improved either by using the linear regression to adjust the calculated values or by identifying a correction to the model used for the calculations.

The calculated values in figure 4.6 use $N_{\mathrm{ox}} = 2.21 \times 10^{22}\ \mathrm{Si\ atoms/cm^3}$ which is consistent with the density of thermally grown silicon oxide as is commonly reported in the literature [9, 14, 20–22]. An oxide density of $\sim 2.2\ \mathrm{g/cm^3}$ was used to interpret the RBS results which gave good correlation to results from VASE. Furthermore, although there are multiple polymorphs of silica with densities as high as $\sim 2.9\ \mathrm{g/cm^3}$, it is expected that a higher density will coincide with a higher index of refraction [23]. However, the ellipsometry analyses done in the present study show a very good agreement between the index of refraction for the thermal oxides grown on SiGe and the values reported in literature [24]. So, even though the mismatch between measured and calculated values in figure 4.6 can be reduced by altering N_{ox} to $2.95 \times 10^{22}\ \mathrm{Si\ atoms/cm^3}$, it is unlikely that the oxide density can account for the deviation of the slope from unity.

The atomic density of the pile-up layer, N_{pu}, follows data presented by Dismukes *et al* [16] which is based on relaxed material, while the samples in the present study are pseudomorphically strained SiGe on Si substrates. Using the density of relaxed SiGe, instead of the density of pseudomorphically strained SiGe, can underestimate N_{pu} by a maximum of $\sim 8\%$, but this underestimation would only exacerbate the deviation between the calculated and measured data.

The most likely source of the deviant slope is the measurement of X. For practical reasons, the values of X used to generate the calculated data in figure 4.6 were taken from measurements done after the sample was oxidized. Equation 4.5 does not account for the diffusion of silicon

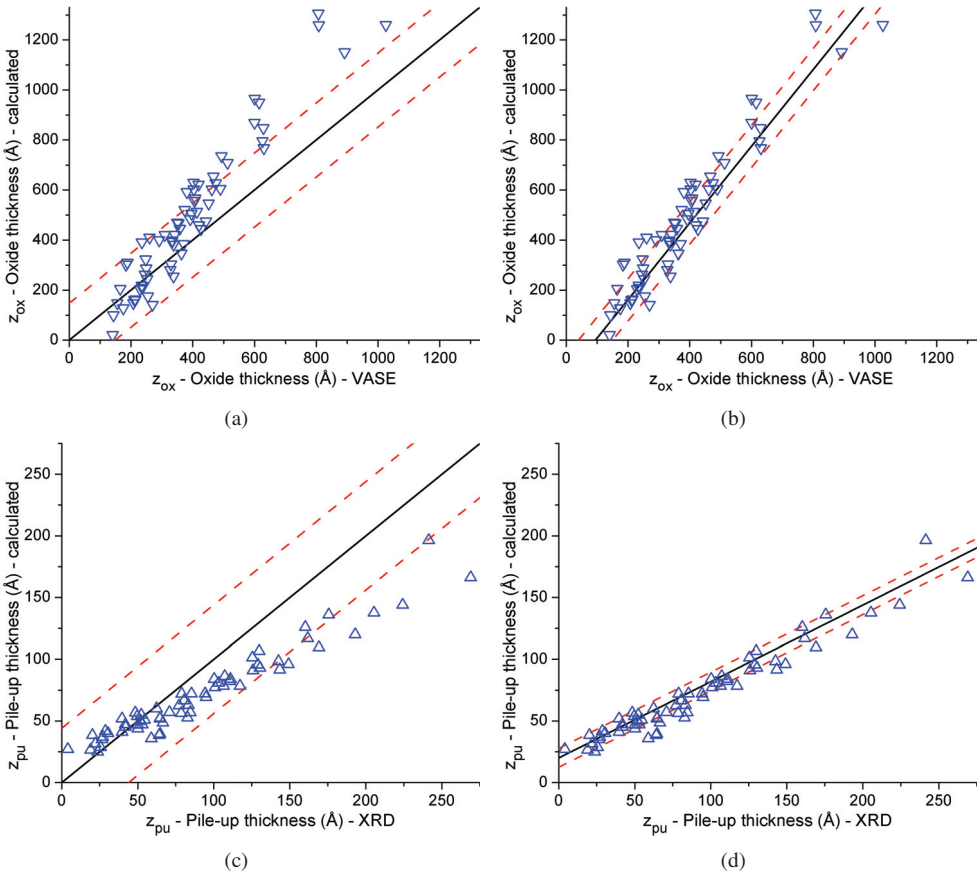

Figure 4.6: *Oxide and pile-up layer thicknesses; comparison of calculated and measured values.*
(a) & (b) Oxide thickness, z_{ox}, calculated with equation 4.5 versus VASE measurements. The calculated values use z_{pu}, X_{pu}, and X as measured by XRD.
(c) & (d) Pile-up layer thickness, z_{pu}, calculated with equation 4.5 versus XRD measurements. The calculated values use z_{ox} measured by VASE while X_{pu} and X are measured by XRD. The atomic density of the pile-up layer, N_{pu}, follows data presented by Dismukes et al [16].
(a) & (c) The solid line is a visual guide showing where $x = y$. The dashed lines represent $\pm\sigma$.
(b) & (d) The solid line is the linear regression to the data and the dashed lines represent $\pm\sigma_{\mathrm{SE}}$.
(a) & (b) $\sigma = 148\,\text{Å}$, $b_{\mathrm{R}} = -145\,\text{Å}$, $m_{\mathrm{R}} = 1.53$, $r_{\mathrm{R}} = 0.96$, $\sigma_{\mathrm{SE}} = 85\,\text{Å}$
(c) & (d) $\sigma = 44\,\text{Å}$, $b_{\mathrm{R}} = 20\,\text{Å}$, $m_{\mathrm{R}} = 0.62$, $r_{\mathrm{R}} = 0.98$, $\sigma_{\mathrm{SE}} = 8\,\text{Å}$

from the substrate into the initial SiGe layer that is inevitable during oxidation. Although the diffusion of Si from the substrate should have a nominal effect on X, underestimation of X will have a profound influence on the calculated values of z_{pu} and z_{ox}. The deviation between X measured post oxidation and the actual pre-oxidation value will be aggravated by longer oxidations (*i.e.* thicker oxides) and variation in X between samples. The same deviation will be minimized by lower values of X due to the steep drop in Si diffusivity in SiGe as the Ge content is reduced.

Critical thickness is of fundamental importance to nanostructure design for opto-electronic applications. So, it is useful to have an appreciation for the relative magnitudes of the pile-up thickness and critical thickness. Figure 4.7(a) shows the same plots of critical thickness as shown in chapter 2. Calculated values of $z_{\mathrm{pu}}\,(X_{\mathrm{pu}})$ for several values of X and assuming a 50 nm thick oxide are also plotted in figure 4.7(a). The supplemental axis showing oxidation temperature is directly correlated to the Ge content axis and reflects the temperature dependence of X_{pu} that is apparent in equation 4.2. The data for z_{pu} in the figure is limited to temperatures above 700 °C because all of the oxidations in the present study were done at temperatures above this and because lower temperatures may lead to oxidation of Ge as well as Si. It is clear that z_{pu} can be manipulated by changing a variety of variables, however, lower initial Ge contents produce generally thinner pile-up layers. Also, for any given X, a decrease in temperature (and thus an increase in X_{pu}) will result in z_{pu} decreasing in roughly the same way as the critical thickness. The similar shape of the $z_{\mathrm{pu}}\,(X_{\mathrm{pu}})$ and critical thickness curves is an indication that oxidation temperature manipulation may function well in nanostructuring without high defectivities.

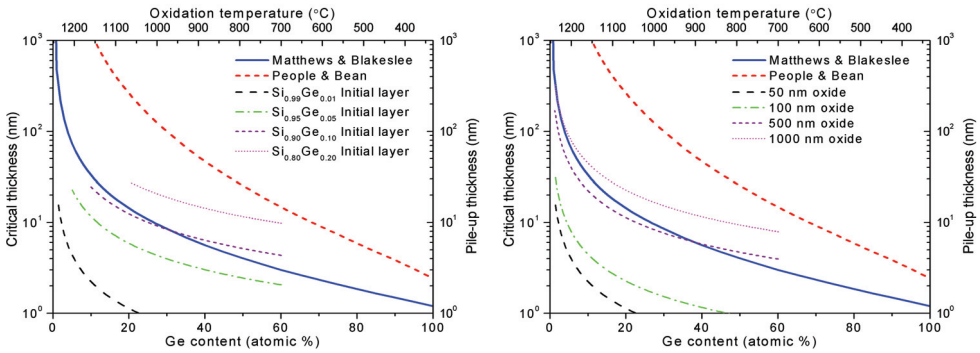

Figure 4.7: *Critical layer thickness for epitaxial $Si_{1-X}Ge_X$ on a Si substrate as a function of X. Curves shown follow predictions by Matthews and Blakeslee [25] and People and Bean [26]. Pile-up thicknesses (calculated with equation 4.5) as a function of Ge content in the pile-up layer for (a) a 50 nm oxide and different initial layer Ge contents, and (b) for a $Si_{0.99}Ge_{0.01}$ initial layer and different oxide thicknesses. The axis showing Ge content in the pile-up corresponds directly to the oxidation temperature axis ($X_{\mathrm{pu}} = 1.361 - \left(1.087 \times 10^{-3} \times T\right)/°C$). Data shown is for the (100) orientation.*

Figure 4.7(b) presents a similar analysis comparing critical thickness to z_{pu} for a 1% initial Ge content and a variety of oxide thicknesses. By starting with a sufficiently low initial Ge content, thin pile-up layers may be grown without adverse effects from variations in the oxidation rate. This is particularly important when oxidizing SiGe, where the oxidation rate is relatively poorly characterized and strongly dependent on the oxidizing ambient.

4.5 Ge content in the pile-up: measurement and calculation

In order to understand the diffusivity of Si in SiGe, values of E_{m} and D_0 were determined using a mean squared error analysis to compare values of X_{pu} from XRD to those calculated with equation 4.4. The resulting correlation between calculated and measured values of X_{pu} is shown in figure 6 of Article IV [18]. The values for E_{m} and D_0 for (100), (110), and (111) oriented material are shown in table 4.1.

As shown in figure 4.8, the activation energies and diffusivities for diffusion of Si in SiGe calculated from the data in table 4.1 generally agree with data presented by Kube *et al* [15].

It is obvious from equation 4.4 that X_{pu} is a function of oxidation temperature, T. This is illustrated by figure 4.9, wherein the calculated values of X_{pu} are plotted against T. Figure 4.9 also shows linear fits to the data for each orientation. The linearity of $X_{\mathrm{pu}}(T)$ becomes clear if one considers equation 4.2. Qualitative confirmation of the relationship between temperature and Ge content at the oxidation interface is presented in figure 4.10, which shows Ge concentrations from Energy Filtered Transmission Electron Microscopy (EFTEM). The sample oxidized at 900 °C (figure 4.10(a)) shows a brighter band than the sample oxidized at 1000 °C (figure 4.10(b)), indicating a higher Ge content in the 900 °C sample than in the 1000 °C sample.

It is important to note the negative slope of $X_{\mathrm{pu}}(T)$; the fact that the melting point of SiGe decreases as Ge content increases might seem to suggest that conducting high temperature oxidations to increase the Ge content at the oxidation interface might result in melting of the pile-up layer. However, as is shown in figure 4.11, X_{pu} happens to decrease as the oxidation temperature increases, which will have the effect of keeping the Ge content low enough to avoid melting. Melting of the pile-up layer might occur if the slope and intercept of $X_{\mathrm{pu}}(T)$ are altered substantially by changing either the diffusivity of Si in SiGe or the oxidation rate.

Table 4.1: *Coefficients for the diffusivity of Si in SiGe for different orientations. The activation energy is* $E_{\mathrm{a}} = E_{\mathrm{m}} X_{\mathrm{pu}} + E_{\mathrm{Si}}$, *where* $E_{\mathrm{Si}} = 4.76$ eV, *and* D_0 *is the pre-exponential constant.*

orientation	E_{m} (eV)	D_0 (cm^2/s)
111	-1.81	199
110	-1.89	219
100	-1.70	239

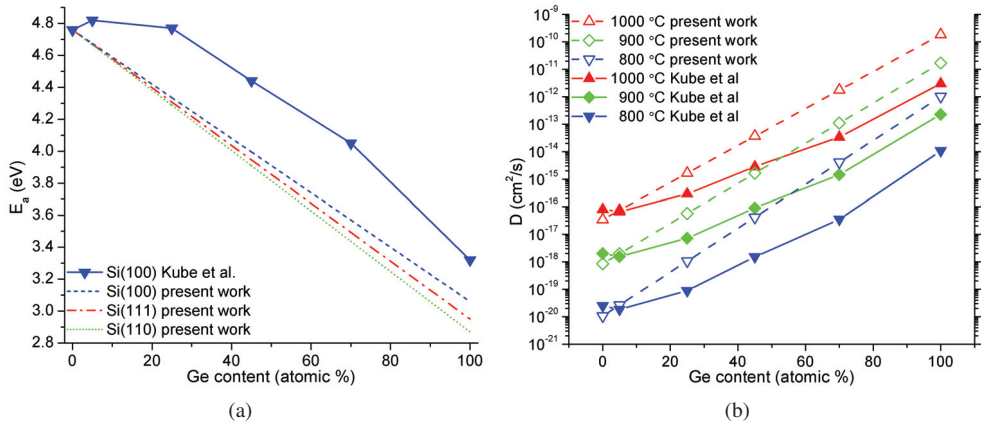

Figure 4.8: *(a) Activation energies, E_a, for diffusion of Si in SiGe for the (100), (110), and (111) orientations. (b) Diffusivities, $D = D_0 \exp\left[-E_\mathrm{a}/(\mathrm{k}T)\right]$, for Si diffusion in SiGe for three different temperatures. Results from the present work are calculated using $E_\mathrm{a} = E_\mathrm{m} X_\mathrm{pu} + E_\mathrm{Si}$, where $E_\mathrm{Si} = 4.76$ eV, and E_m and D_0 from table 4.1. Results tabulated by Kube et al [15] are also shown.*

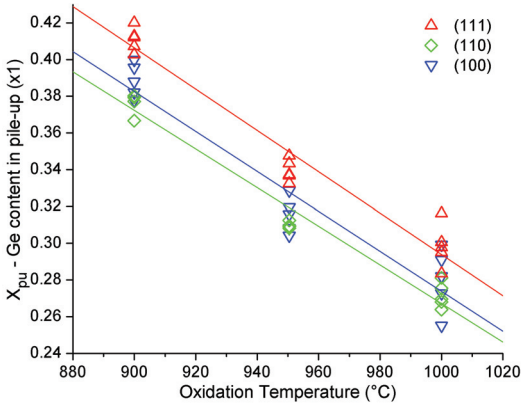

Figure 4.9: *The Ge content in the pile-up layer, X_pu, versus oxidation temperature, T. Values of X_pu were calculated by equation 4.4 using values of z_ox measured by VASE and values for E_m and D_0 from table 4.1. Samples include (111), (110), and (100) oriented, MBE grown $Si_{0.8}Ge_{0.2}$ that have been oxidized at various times, targeting oxide thicknesses of 20, 40, 60, 80, and 100 nm. The data is labeled according to the sample orientation. The lines are linear fits to the data and have intercepts of 1.418, 1.318, 1.361 and slopes of -0.001124, -0.001051, and -0.001087 /°C for the orientations (111), (110), and (100), respectively.*

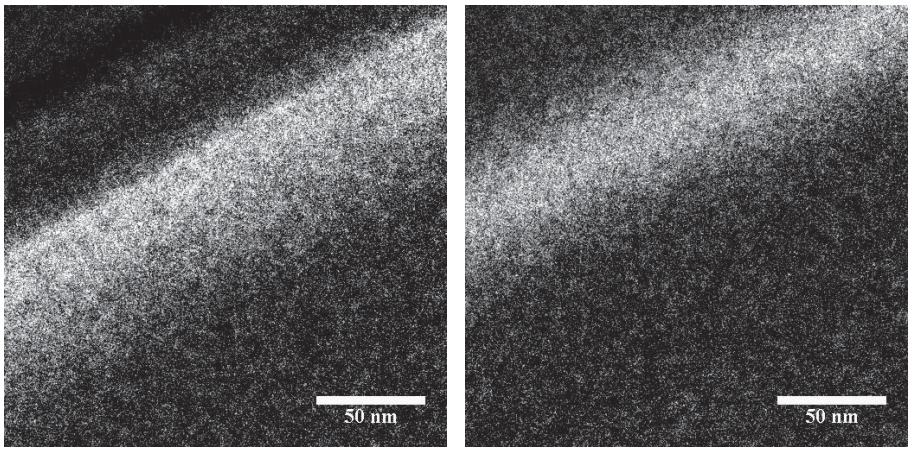

(a) (b)

Figure 4.10: *Energy Filtered Transmission Electron Microscopy (EFTEM) mapping of the Ge content in samples subjected to multiple oxidations. (a) $Si_{0.8}Ge_{0.2}$ oxidized at 1000 °C and then at 900 °C. (b) $Si_{0.8}Ge_{0.2}$ oxidized at 1000 °C and then again at 1000 °C. Discussion and analysis of the XRD data for these samples is presented in chapter 6.4.*

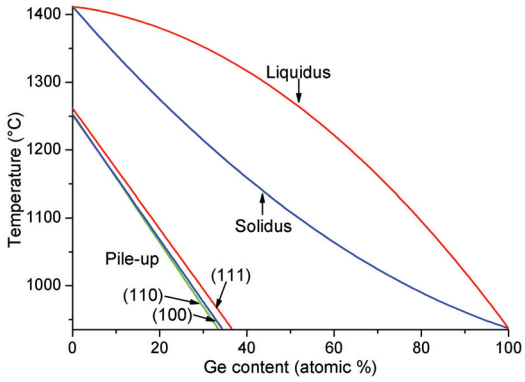

Figure 4.11: *Phase diagram for $Si_{1-X}Ge_X$ as a function of X [27]. The Ge content in the pile-up as a function of oxidation temperature for the (111), (110), and (100) orientations is also shown. For any given oxidation temperature the Ge content in the pile-up will be limited such that the pile-up layer remains solid (i.e. the SiGe will not melt during oxidation).*

4.6 Manipulating the Ge content in the pile-up region

The factors that contribute to establishing $X_{\mathrm{pu}}(T)$ become apparent by considering equation 4.2. The logarithmic dependence on time is consistent with the observation that, for any given temperature and orientation, the values of X_{pu} remain nearly constant for a variety of oxide thicknesses; this is shown in figure 4.12. The Ge content in the as-grown layer, as reflected by N_0, also has a very small influence on X_{pu}, particularly given the limited range for this variable. Aside from T, the variables that have the largest potential for modifying X_{pu}, by manipulation of the oxidation conditions, are A_0 and E_{ox}. Their values are primarily a function of factors that are determined by the oxidant partial pressure, oxidant chemistry, crystalline orientation, and the presence of Ge at the oxidation front.

The oxidation rate is defined as being directly proportional to the oxidant partial pressure in the region where oxidation is limited by the concentration of oxidant at the oxidizing interface [9], as well as in models that do not distinguish between linear and parabolic oxidation regimes [2–4]. This direct proportionality is reflected by the magnitude of A_0. The possibility to increase or decrease oxidant partial pressure by orders of magnitude should ensure that, for any given temperature, it may be used to make substantial changes to X_{pu}. Lower oxidant pressures should lead to lower values of X_{pu}, as well as reducing the temperature at which formation of mixed oxides transitions to formation of an oxide composed exclusively of SiO_2. (A mixed oxide is composed of both SiO_x and GeO_x). This is consistent with experimental observations and

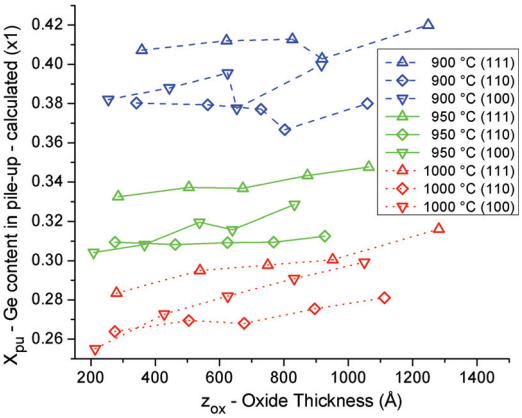

Figure 4.12: *The Ge content in the pile-up layer, X_{pu}, versus oxide thickness, z_{ox}. Values of X_{pu} were calculated by equation 4.4 using values of z_{ox} measured by VASE and values for E_{m} and D_0 from table 4.1. Samples include (111), (110), and (100) oriented, MBE grown $Si_{0.8}Ge_{0.2}$ that have been oxidized at 900, 950, and 1000 °C. The data is labeled according to the sample orientation and oxidation temperature. The lines connecting data points are for visual guidance only.*

associated modeling showing the tendency of high pressures to incite formation of mixed oxides [28–30]. Use of low oxidant pressures should also reduce the temperature required to avoid formation of a pile-up layer by steepening the slope of $X_{\mathrm{pu}}(T)$. The manipulation of oxidant pressure as a means of controlling X_{pu} is only applicable for those oxidations that are substantially controlled by the oxidant pressure, an exception being oxides with z_{ox} less than about 20 nm (where oxidation is faster than the linear oxidation rate model would predict).

Modifications to the chemistry of the oxidizing ambient can be used to increase or decrease the oxidation rate; an obvious example being dry *versus* wet oxidations. Any such chemically enhanced oxidation rate that does not also result in a concomitant increase in the diffusivity of Si in SiGe should result in higher values of X_{pu}. Remembering that low temperatures equate to high values of X_{pu} and that low enough temperatures will result in such high values of X_{pu} that a mixed oxide will form, the tendency of chemically enhanced oxidation rates to induce mixed oxides is evident in reports of wet and fluorinated oxidations [30] and of oxidations in ozone [31] which showed formation of mixed oxides at higher than expected temperatures.

Other modifications of the oxidation environment will alter both the oxidation rate and the diffusivity of Si in SiGe. Temperature is the obvious example of such an environmental control, but ultra-violet (UV) illumination will have a similar effect. Low temperature (<600 °C) dry oxidations wherein both the sample and oxidant are directly exposed to vacuum ultraviolet (V-UV) radiation show growth rate enhancement in both Si and SiGe [32–34]. A value of 0.27 eV is reported for E_{ox} for Si under V-UV irradiation, and it is argued that the enhanced oxidation rates of Si are due, not only to introduction of atomic oxygen and ozone to the ambient, but also to ionization of oxidants and injection of electrons into the oxide. Similarly grown oxides on SiGe samples are shown to be primarily or entirely SiO_2 despite the low oxidation temperatures and high oxidation rates, which gives a strong indication that direct illumination of the sample with V-UV radiation will increase the diffusivity of Si in SiGe. As no relaxation is observed in the samples, the increased diffusivity is attributed to point defect generation [32–34].

These observations are consistent with equation 4.2, where a drastic reduction in E_{ox} would lead to X_{pu} values greater than one, and thus formation of GeO_2, unless it is accompanied by a commensurate reduction in E_{Si}. This is important because it indicates that nanostructuring of SiGe by oxidation may be done without the high temperatures that are typically associated with relaxation and extended defects, and without the excessively long oxidation times of low temperature and low pressure oxidations.

4.7 Oxidation rate ratios

Figure 4.13 shows the oxide thickness *versus* time for both Si and SiGe samples of three different crystalline orientations that were oxidized at different temperatures. It is evident that both crystalline orientation and Ge have the potential to influence the oxidation rate; considering these

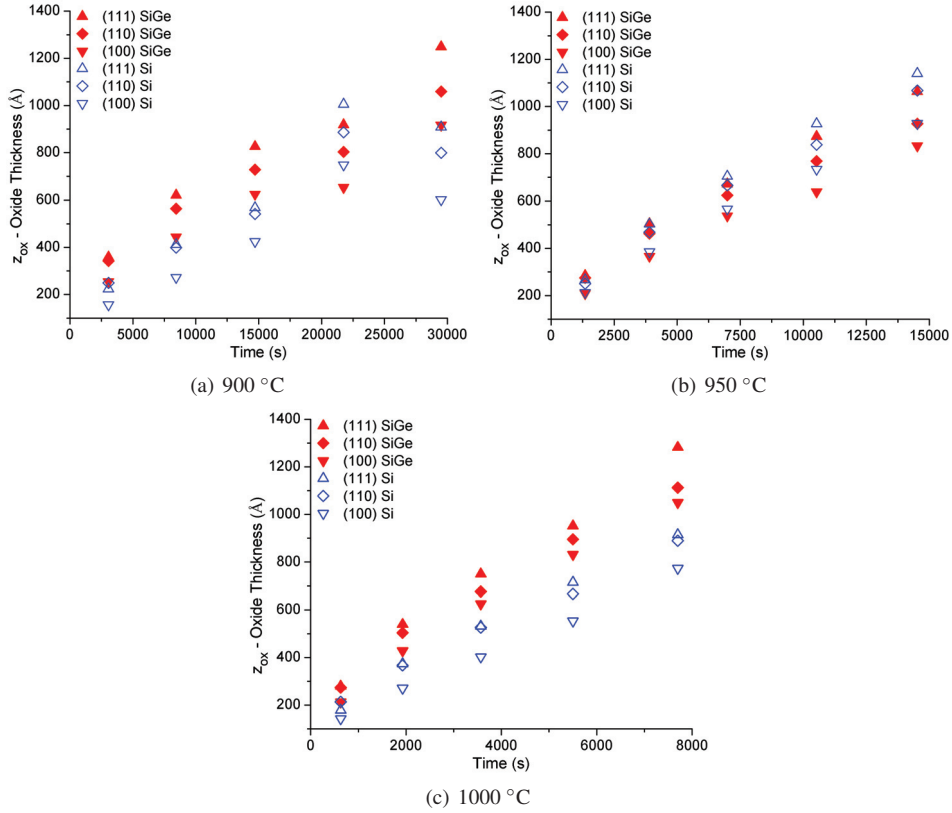

(a) 900 °C

(b) 950 °C

(c) 1000 °C

Figure 4.13: *Oxide thickness versus oxidation time for samples oxidized at (a) 900, (b) 950, and (c) 1000 °C. Data is presented for (111), (110), and (100) oriented, MBE grown $Si_{0.8}Ge_{0.2}$ and Si control samples. The data is labeled according to the sample type and orientation.*

factors separately will be useful in identifying the physical mechanisms involved in the oxidation of SiGe. The oxidation rate ratio, ρ, is a convenient measure for evaluating the degree to which the oxidation rate, ν, is enhanced or retarded due to variation in one aspect of a sample, *i.e.* the Ge content or orientation. The oxidation rate ratio is defined here as $\rho_{\mathrm{a/b}} = \nu_{\mathrm{a}}/\nu_{\mathrm{b}}$, where ν_{a} and ν_{b} are the oxidation rates for two samples with identical oxidation conditions and a single differentiating characteristic that is indicated by the subscript. The average values of the oxidation rate ratios comparing (111), (110), and (100) material are listed in table 4.2, while those comparing SiGe to Si are listed in table 4.3.

As the oxidations conducted in this study are in the linear or linear-parabolic regime, the oxidation rate can reasonably be described by an Arrhenius relation, $A_0\exp[-E_{\mathrm{ox}}/(\mathrm{k}T)]$. The vari-

Table 4.2: *Values for $\rho_{110/100}$, $\rho_{111/100}$ and $\rho_{111/110}$, where ρ is the ratio of oxidation rates for the given orientations. The values shown are the average values for Si or SiGe (as indicated) for the five oxidation times used at each oxidation temperature.*

	$\rho_{110/100}$	$\rho_{110/100}$	$\rho_{111/100}$	$\rho_{111/100}$	$\rho_{111/110}$	$\rho_{111/110}$
T (°C)	Si	SiGe	Si	SiGe	Si	SiGe
900	1.37	1.23	1.43	1.38	1.05	1.13
950	1.17	1.21	1.26	1.33	1.08	1.10
1000	1.30	1.14	1.28	1.23	0.99	1.09

Table 4.3: *Values for $\rho_{\mathrm{SiGe/Si}}$, where ρ is the ratio of oxidation rates of SiGe and Si samples. The values shown are the averages of values for all oxidation times for any given temperature (in °C) and orientation used in the present work.*

	orientation		
T (°C)	111	110	100
775			1.02
821			1.18
868			1.07
900	1.40	1.29	1.47
915			1.17
950	0.98	0.96	0.93
962			1.19
1000	1.46	1.33	1.55

ous influences of point defects, strain, steric hindrance, and Ge induced growth rate enhancement will be absorbed into the values of A_0 and $E_{\rm ox}$ and can be eliminated by considering the ratio of the oxidation rates of similar samples. By way of example, consider that the pre-exponential constant for Si(100) is A_0 while the pre-exponential for SiGe(111) is $A_0 * A_{\rm Ge} * A_{111}$, where $A_{\rm Ge}$ and A_{111} are factors to accommodate for the influence of Ge and orientation on the oxidation rate. If SiGe(111) is compared directly to Si(111), $\rho_{\rm SiGe/Si} = \nu^{111}_{\rm SiGe}/\nu^{111}_{\rm Si}$, the influence of orientation is eliminated, leaving only the influence of Ge. Similarly, comparing SiGe(111) to SiGe(100), $\rho_{111/100} = \nu^{111}_{\rm SiGe}/\nu^{100}_{\rm SiGe}$, will leave only the influence of orientation. If the influence of Ge and orientation on $E_{\rm ox}$ is presumed to be additive (*i.e.* $E_{\rm ox} + E_{\rm Ge} + E_{111}$), the activation energy may be treated in the same way as the pre-exponential constant. It follows that the ratio of oxidation rates for both Si and SiGe samples of two orientations, $P = (\nu^{111}_{\rm Si}\nu^{100}_{\rm SiGe})/(\nu^{100}_{\rm Si}\nu^{111}_{\rm SiGe})$, should be precisely equal to one. Using such oxidation rate ratios to compare oxidation rates is far more effective than making qualitative judgments based on viewing plots of oxide thickness *versus* oxidation time, as it is done in figure 4.13.

4.8 Ambient chemistry

The oxidation kinetics for Si and SiGe are similar in the sense that, the ambient chemistry will have an integral role in determining the oxidation rate. Comparison of dry and wet oxidations is perhaps the most obvious demonstration of the role of the oxidation ambient chemistry in determining the oxidation rate. It has been established that "dry" oxidations are typically not completely free of H_2O due to contamination from the room ambient by diffusion through the wall of a single walled furnace or by back-flow from the end of the furnace [9, 11, 35]. In a study of the influence of trace concentrations of H_2O on the oxidation rates of (111), (110), and (100) oriented Si at temperatures between 800 and 1000 °C, Irene [11] showed an increase of between 16% and 42% in the parabolic rate constant when 25 ppm of H_2O is added to an O_2 ambient. This is in contrast to the demonstration by Raider *et al* [35], showing that high temperature anneals in N_2 can slow the oxidation of (111) and (100) Si.

The introduction of H_2O to an oxidizing ambient will also accelerate the oxidation rate of SiGe (*i.e.* $\rho_{\rm wet/dry} > 1$ for both SiGe and Si). However, the introduction of H_2O to an oxidizing ambient may induce more growth rate enhancement in SiGe than in Si (*i.e.* $\rho^{\rm SiGe}_{\rm wet/dry} > \rho^{\rm Si}_{\rm wet/dry}$). It is common that the growth rate enhancement or reduction observed in dry, wet, or steam oxidations of SiGe is simply attributed to the influence of Ge [36–47], however, it may be more apt to attribute the growth rate enhancement or reduction that is observed in oxidation of SiGe to the combination of the presence of Ge and the chemistry of the oxidizing ambient.

In fact, LeGoues *et al* [48] demonstrated explicitly that, while steam oxidation induces growth rate enhancement in SiGe as compared to Si ($\rho_{\rm SiGe/Si} > 1$), a wet oxidation conducted with H_2O diluted by N_2 can result in SiGe oxidizing at the same rate as Si ($\rho_{\rm SiGe/Si} \approx 1$). Re-

ports of dry oxidation of SiGe have shown a wide variety of values for $\rho_{\mathrm{SiGe/Si}}$ [49], including reports of reduced oxidation rates in SiGe as compared to Si ($\rho_{\mathrm{SiGe/Si}} < 1$) [36, 50, 51]. While wet ambients induce growth rate enhancement ($\rho_{\mathrm{SiGe/Si}} > 1$), both wet ambients diluted with N_2 and dry ambients result in equivalent oxidation rates for SiGe and Si ($\rho_{\mathrm{SiGe/Si}} \approx 1$) [48]. Comparison of fluorinated and non-fluorinated dry oxidation to wet oxidations shows that fluorine induces higher values of $\rho_{\mathrm{SiGe/Si}}$ than seen with standard dry oxidation, but lower than in a wet oxidant [30]. Ambients composed of plasma generated atomic oxygen have also resulted in $\rho_{\mathrm{SiGe/Si}} > 1$ [52].

The oxidation ambient chemistry is only important insomuch as it will tend to control the various elements and molecules present at the interface between the oxide and the underlying Si or SiGe. Modifying the elements at the oxidation front by doping or alloying the Si or SiGe with other elements, or by depositing materials onto the surface of the Si or SiGe prior to oxidation will have a similar effect to modifying the oxidizing ambient. A common example of this is the addition of dopants like boron, phosphorus, arsenic, or antimony to the Si or SiGe [9, 53]. Jaquez *et al* [54] showed, for oxidations at 40 °C and up to 33 days long, that the catalytic effect of Cu on oxidation of Si is substantially larger than it is for SiGe, and that alloying SiGe with carbon eliminates oxidation. Other studies have also shown that inclusion of carbon has an influence on the oxidation rate of SiGe [51, 55].

Results from the present study show notable variation in the value of $\rho_{\mathrm{SiGe/Si}}$ for dry oxidations. The values of $\rho_{\mathrm{SiGe/Si}}$ listed in table 4.3 indicate growth rate enhancement ($\rho_{\mathrm{SiGe/Si}} > 1$) for 900 and 1000 °C, while 950 °C indicates growth rate reduction ($\rho_{\mathrm{SiGe/Si}} < 1$). Growth rate reduction ($\rho_{\mathrm{SiGe/Si}} < 1$) also appears at 900 °C and 21750 s in figure 4.13(a), while the (111) and (110) oriented samples oxidized at 950 °C for 1350 s, in figure 4.13(b), show $\rho_{\mathrm{SiGe/Si}} > 1$. Each oxidation run in the present study consisted of a single time and temperature and involved oxidizing SiGe and Si samples of each of the three orientations simultaneously and side by side in the oven to ensure identical oxidation conditions for all samples in a given oxidation run. Although the same dry O_2 source and flow rate was used for all of the oxidation runs, the flow rate may not have been high enough or stable enough to eliminate contamination by H_2O or N_2 from the room air.

It is also significant to note that (in table 4.3) the growth rate reduction ($\rho_{\mathrm{SiGe/Si}} < 1$) observed at 950 °C coincides with smaller than expected values of $\rho_{110/100}$ and $\rho_{111/100}$ for Si at 950 °C (in table 4.2) and a value of $\rho_{111/110}$ for Si that is larger than expected. If a change in the ambient caused the value of $\rho_{\mathrm{SiGe/Si}}$ to change from greater than one at 1000 and 900 °C to less than one at 950 °C, then the changes in $\rho_{110/100}$, $\rho_{111/100}$, and $\rho_{111/110}$ for Si may also have been caused by the same change in ambient. It is possible that this is associated with a difference in the effect of various ambient molecules (O_2 *versus* H_2O, for example) on steric hindrance or on the bond strength of Si in Si and in SiGe. So, even if the evidence is circumstantial, the most likely explanation for the aberrations in the relative oxidation rates of SiGe and Si shown in table 4.3 and figure 4.13 is contamination of the oxidizing ambient by some combination of H_2O and N_2.

This is a serendipitous observation in so much as it helps explain how the catalytic or inhibitive behaviour of Ge during the oxidation of SiGe is closely tied to the oxidizing ambient, and not due to the presence of Ge alone.

4.9 Bond energies and electronegativity

One of the more popular explanations for how Ge acts as a catalyst in oxidizing SiGe is that the dissociation energy for a Si-Ge bond is lower than for a Si-Si bond [36, 45, 56–58]. Some studies have either partially or entirely rejected this explanation based on the observation that if such a difference in bond energies were responsible for growth rate enhancement in SiGe, then growth rate enhancement would manifest itself in both dry and wet oxidations, which is not necessarily the case [37, 48, 59, 60].

The Ge-Ge and Si-Si binding energies are reported as being between about 1.6 and 2 eV [9, 45, 58, 61, 62], though, other studies report the dissociation energies for Ge-Ge, Si-Ge, and Si-Si bonds as approximately 2.7, 3.0, and 3.2 eV, respectively [63–66]. It might be tempting to cite that the activation energies for Si oxidation, being in the range between 1 and 2 eV [2–4, 6, 9, 11], are similar to the bonding energies of Si in SiGe, and so conclude that Si-Si and Si-Ge dissociation energies are a direct reflection of E_{ox}. However, if the oxidation rate is modified to take the difference in dissociation energies between Si-Ge and Si-Si into account by simply reducing E_{ox} by the difference in energies, then the oxidation rate could change by an order of magnitude or more. Such a simplistic explanation for the observed growth rate enhancement is clearly insufficient.

Given the random distribution of Ge in SiGe, the ratio of Si-Si to Si-Ge bonds will be determined by X_{pu}, independent of orientation. So, scaling E_{ox} by a factor, Γ, which represents the relative density of Si-Si and Si-Ge bonds, would help account for the fact that both Si-Ge and Si-Si bonds will be broken during oxidation. Defining this factor as, $\Gamma = \left[(1 - X_{\mathrm{pu}})\, H_{\mathrm{Si-Si}} + X_{\mathrm{pu}} H_{\mathrm{Si-Ge}}\right] / H_{\mathrm{Si-Si}}$, where $H_{\mathrm{Si-Si}}$ and $H_{\mathrm{Si-Ge}}$ are the dissociation energies for Si-Si and Si-Ge bonds, respectively, will increase the oxidation rate by a factor of about one to three which is approximately what has been observed empirically. A similar approach is taken by Rabie *et al* [60], who construct a model based on a two step oxidation process that includes oxidation of Ge and a compensating conversion of oxidized Ge to SiO_2. However, the idea that E_{ox} is a function of X_{pu} by virtue of its dependence on dissociation energies does not allow for a linear relationship between X_{pu} and T as is observed in the present study. Furthermore, dissociation energies for Si-Ge bonds *versus* those of Si-Si bonds fail to explain the growth rate reduction that appears in figures 4.13(a) and 4.13(b) and in table 4.3.

It is likely that growth rate enhancement and reduction in SiGe would be better explained by the concept of electronegativity. It is known that, despite it's position on the periodic table, Ge has a higher electronegativity than Si [67], and it follows from Pauling's definition of electroneg-

ativity [61] that an atom's tendency to attract electrons depends on which other atoms it is bound to. So, although the dissociation energy of Si-Ge may tend to be lower than for Si-Si, these bond energies, and the difference between them, will vary due to tertiary bonds with elements like hydrogen, fluorine, or chlorine. This may help explain how $\rho_{\mathrm{SiGe/Si}}$ can be both larger than and smaller than one, depending on the mix of atoms and bonds present at the oxidation interface.

4.10 Electric potential

The conclusion by Boyd *et al* [32] that V-UV induced ions in the oxide make a substantial contribution to the enhancement of the oxidation rate is important in light of the claim that ions diffuse faster in GeO_2 than in SiO_2 [68] and that the crystallinity of SiO_2 on SiGe is the same as that on Si [56]. These observations indicate that oxidations that involve ionized oxidants and that have fast enough oxidation rates (relative to the diffusivity of Si in SiGe) to form a mixed oxide may show higher $\rho_{\mathrm{SiGe/Si}}$ values than would be expected were the oxide to be composed entirely of SiO_2. That is, $\rho_{\mathrm{SiGe/Si}}$ would be larger for mixed oxides than for SiO_2 because of the higher diffusivity of ionic oxidants in mixed oxides. It has been suggested that ionized oxidants play a critical role in thermal oxidations that do not involve UV illumination. Jorgensen showed electric field assisted and retarded thermal oxidation for relatively thick oxides (where growth would be diffusion limited) and concluded that this must have been due to diffusion of ionized oxygen [69]. There is, however, some debate about how these results should be interpreted, and thus about the role of ions in dry thermal oxidations [9].

A widely cited model by Cabrera and Mott [1] claims that oxygen ions and built in fields can explain oxidation in the earliest stages of oxidation of metals. However, considering the small and changing SiGe layer thicknesses being oxidized here, the quickly changing Ge content in the pile-up layer at the earliest stages of oxidation, the dependence of the band structure on Ge content and strain [70–72], as well as the complex nature of surface states on Si or Ge with very thin oxide layers [73, 74], it would be exceptionally difficult to make any definitive conclusions about the applicability of the Cabrera and Mott model to growth rate enhancement or reduction in SiGe oxidation based on the empirical results presented here.

On the other hand, if one accepts that increasing values of X_{pu} will lead to weakened Si bonds, increased ion diffusion, or higher electron injection rates, then the qualitative observation that lower oxidation temperatures lead to higher values of X_{pu} (as shown in figure 4.9) should lead to the conclusion that lower oxidation temperatures also lead to larger values of $\rho_{\mathrm{SiGe/Si}}$. However, this is not supported by the data in table 4.3. Figure 4.14(a) is a plot of the data in table 4.3 and shows that $\rho_{\mathrm{SiGe/Si}}$ tends to decrease as temperature decreases. Contrary to what is commonly reported, the data in figure 4.14(a) and table 4.3 and the tendency of lower oxidation temperatures to induce higher values of X_{pu} (see figure 4.9) indicate that higher levels of Ge at the oxidation front are associated with smaller degrees of oxidation rate enhancement. If $\rho_{\mathrm{SiGe/Si}}$

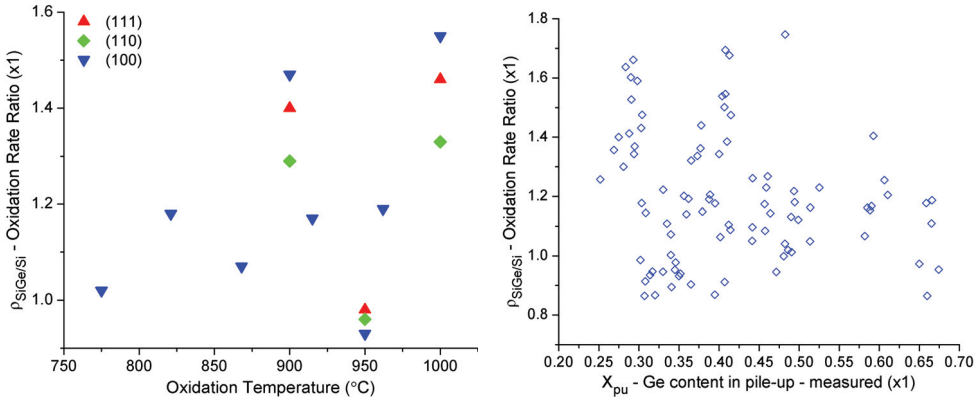

Figure 4.14: *(a) Average values of $\rho_{\mathrm{SiGe/Si}}$ from table 4.3 versus oxidation temperature. The data is separated by crystallographic orientation. (b) Values of $\rho_{\mathrm{SiGe/Si}}$ versus X_{pu} as measured by XRD.*

is compared directly to X_{pu}, as is done in figure 4.14(b), it becomes apparent that there is little or no correlation between the Ge content at the oxidation interface and the degree to which the oxidation rate is enhanced or reduced by the presence of Ge. This may lend credence to the notion that tertiary elements play an important role in determining the magnitude of $\rho_{\mathrm{SiGe/Si}}$.

4.11 Point defects

A number of studies have speculated that the generation of vacancies and interstitials in the SiGe layers plays a critical role in explaining Ge's role as a catalyst for oxidation [30, 37, 38, 48, 59, 60, 75]. This theory was nicely summarized by LeGoues *et al* [38] when they wrote, "A significant effect of Ge appears to be the elimination of the injection of interstitials. We propose that this mechanism is reversed and replaced by injection of vacancies which enhances rapid diffusion of Si through the Ge enriched layer." Furthermore, studies of Si and Ge self-diffusion suggest an interstitial mechanism for Si and a vacancy mechanism for Ge [76, 77].

If the presence of Ge does enhance oxidation by changing the diffusivity of Si in SiGe by point defect generation, then it will be reflected in X_{pu}, as described by equation 4.2. So, if the chemistry of the oxidizing ambient alters the extent of point defect generation, as suggested by Kilpatrick *et al* [30], then the X_{pu} to T correlation will shift in order to maintain a balance in the fluxes of Si, $J_{\mathrm{ox}}/J_{\mathrm{pu}} = 1$. The only condition in which no shift will occur is where the additional Si at the oxidation interface due to increased Si diffusion is exactly offset by an increase in the flux of Si into the oxide due to an increase in the oxidation rate.

The notion that point defects play an important role in the oxidation kinetics of SiGe is evi-

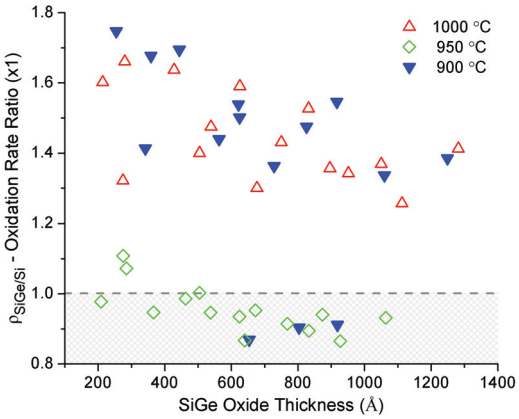

Figure 4.15: *Oxidation rate ratio, $\rho_{\mathrm{SiGe/Si}}$, versus the oxide thickness, z_{ox}, of the SiGe sample. The oxidation rate ratio is calculated as $\rho_{\mathrm{SiGe/Si}} = \nu^{hkl}_{\mathrm{SiGe}}/\nu^{hkl}_{\mathrm{Si}}$, where ν is the oxidation rate and hkl is one of the three crystallographic orientations in the present work, (111), (110), or (100). The data is labeled according to the oxidation temperature.*

dent in the data from the present study. It has been established that oxidation enhanced diffusion of dopants in Si is tied to both point defects and crystallographic orientation [78–80]. So, if point defects play a role in Si diffusion in SiGe, as argued by LeGoues *et al* [38, 75], then it is likely that any oxidation enhanced diffusion of Si in SiGe due to point defects is also orientation dependent. This is consistent with the orientation dependent shifts in X_{pu} in figure 4.9 and with the variation in the values for the diffusivity of Si in SiGe for various orientations listed in table 4.1. On the other hand, if point defects that are generated due to Ge play a dominant role in determining the diffusivity of Si in SiGe, and hence the growth rate enhancement, then the Ge induced growth rate enhancement will be reduced for thick oxides where the oxidation is limited by diffusion of oxidant in the oxide, that is, where the oxidation is not rate limited by point defect generation. This would suggest that, as the oxidation moves from the linear to the parabolic regime, growth rate enhancement, and thus X_{pu}, should decrease due to an abundance of Si at the oxidation interface resulting from enhanced Si diffusion without a commensurate removal of Si by oxidation.

As seen in figure 4.15, the data in this study does indicate that $\rho_{\mathrm{SiGe/Si}}$ is reduced as oxide thickness increases towards the parabolic regime, but, this effect is small and it is not clear if this is related to point defects or some other effect. Also, figure 4.12 shows that X_{pu} is nearly constant or slightly increasing as z_{ox} increases; a slight increase in X_{pu} with increasing z_{ox} is also supported by simulations [17].

4.12 Strain and crystallographic orientation

Both crystallographic orientation and strain between the oxide and the underlying SiGe have the potential to influence the oxidation of SiGe. These are particularly important considerations when oxidizing structures with multiple physical dimensions, not only because they are anisotropic effects, but also because, the way in which a structure oxidizes will depend on the structure's shape. Variation in the shape and aspect ratios of SiGe nanowires formed by thermal oxidation has been demonstrated and highlights the importance of both structure shape and the anisotropic nature of SiGe oxidation [81, 82]. The link between structure shape, orientation, and strain becomes clear if one considers that the strain induced in the oxide on planar surfaces is reported as being compressive [83–88] and due to the large volume of the SiO_2 molecule as compared to that of the Si atom [87].

Given that strain in the oxide is due to the change in volume between Si and SiO_2, the influence of strain on the oxidation of multi-dimensional structures will vary for purely geometric reasons; planar, cylindrical, spherical, and fin shaped structures all show different volume changes due to an increase in oxide thickness. Kao *et al* [86, 87] investigated the oxidation of concave and convex surfaces while using the radius of curvature of the rounded surfaces to examine the strain in the oxide. They found that the degree of strain increased as the radius of curvature decreased, and that the growth rate reduction associated with a decrease in the radius of curvature was more severe for concave surfaces (compressively strained) than for convex surfaces (tensilely strained). They also found that, for both tensile and compressive strain, the strain induced growth rate reduction increases as oxidation temperature is decreased. For any given temperature, higher degrees of strain in the oxide have been shown to induce lower oxidation rates [10, 84–87, 89, 90], which has been explained by the notion that strain in the oxide tends to hinder the diffusion of oxidant through the oxide [84–87, 89, 90]. Also, observations have shown that dry oxidation induces higher degrees of strain than wet oxidations [84, 86, 87].

Strain in the oxide is temperature dependent, with the degree of strain decreasing as temperature is increased, and with the oxide being fully relaxed after oxidations or anneals above about 965 °C. Explanations of this temperature dependence rely on the notion that there is a viscous flow in the oxide at high temperatures [83–87, 89]. More precisely, modeling has shown that the viscosity of the oxide has an Arrhenius like behaviour [85].

In addition to strain, the concept of steric hindrance is integral to explaining the orientation dependence of oxidation. The concept of steric hindrance evaluates the size of the oxidant molecule and the surface density of atoms in the crystal to calculate the number of surface bonds available for reaction with an oxidant molecule. While the number of surface bonds on differently oriented Si or SiGe follows the order $(110) > (111) > (100)$, the number of bonds available for an oxidation reaction due to steric hindrance, N, follows the order $(111) > (110) > (100)$ [2, 90].

Interestingly, while determining the Si-Si and Ge-Ge bond strength, Jaccodine [62] found

that the values for the surface energy of Si and Ge are ordered as $(111) < (110) < (100)$. The values for the surface energies, ε, are not the same for Si and Ge, but the ratio between Si and Ge is the same for the three orientations considered. It is also significant to point out that the ratios of ε between orientations, as determined by Jaccodine, are the same as the ratios of available surface bonds, N, as determined by Ligenza [2]: $\varepsilon_{100}/\varepsilon_{111} \approx N_{111}/N_{100} \approx 1.73$, $\varepsilon_{100}/\varepsilon_{110} \approx N_{110}/N_{100} \approx 1.41$, $\varepsilon_{100}/\varepsilon_{111} \approx N_{111}/N_{100} \approx 1.23$.

On its own, the steric hindrance model predicts that the oxidation rates will be ordered as $(110) > (111) > (100)$ [2, 84, 90, 91], but, the magnitude of strain due to oxidation has also been shown to be a function of orientation, following the order $(111) < (100) < (110)$ [84]. Taken together, the influence of steric hindrance and oxide strain result in orientation dependent oxidation rates being ordered as $(110) > (111) > (100)$ or $(111) > (110) > (100)$, depending on the oxide thickness and oxidation conditions [2, 10, 86, 87, 89–91]. So, oxidation rates for (110) oriented material may be either faster or slower than for (111) oriented material. For oxidations where the surface reaction rate is dominant, as with very thin oxides, the effects of steric hindrance prevail and (110) material oxidizes faster than (111). However, as the oxide thickens and more strain is introduced to the oxide, the oxidation rate of (110) material is hindered more substantially than that of (111) material, allowing faster oxidation for (111) than for (110). The oxide thickness where the coupling of the effects of steric hindrance and oxide strain result in the oxidation rate order switching from $(110) > (111)$ to $(111) > (110)$ (referred to herein as the crossover point) has been reported as being between 5 and 50 nm, while no crossover occurs for very high temperatures [84, 89, 90].

The data from the present study, as shown in table 4.2 and figures 4.13 and 4.16, show that the oxidation rates of the various orientations tend towards being ordered by orientation as $(111) > (110) > (100)$. This is the case for both Si and SiGe and the magnitudes of $\rho_{111/100}$ and $\rho_{110/100}$ reported here are comparable to what is reported in the literature [89, 90] for dry O_2 oxidations at temperatures between 900 and 1000 °C.

Nicollian and Brews [9] made an observation relating E_{ox} to the temperature dependence of the relative oxidation rates of various orientations. Putting their observation into the context of the present study: considering the values for ρ in table 4.2, the tendency of $\rho_{\mathrm{a/b}}$ to decrease as temperature increases is an indication that E_{ox} is larger for the orientation given by b than it is for the orientation given by a. This relation becomes clearer if one considers $\rho_{\mathrm{a/b}}$ as,

$$\rho_{\mathrm{a/b}} = \frac{A_0^{\mathrm{a}} \exp\left(\frac{-E_{\mathrm{ox}}^{\mathrm{a}}}{\mathrm{k}T}\right)}{A_0^{\mathrm{b}} \exp\left(\frac{-E_{\mathrm{ox}}^{\mathrm{b}}}{\mathrm{k}T}\right)} = \frac{A_0^{\mathrm{a}}}{A_0^{\mathrm{b}}} \exp\left(\frac{E_{\mathrm{ox}}^{\mathrm{b}} - E_{\mathrm{ox}}^{\mathrm{a}}}{\mathrm{k}T}\right). \tag{4.6}$$

As such, for the oxidation conditions in this study and for both Si and SiGe, the magnitudes of E_{ox} are ordered $(111) < (110) < (100)$, which is consistent with the oxidation rates for the different orientations. However, figure 4.16 shows data that supports the notion that a coupling

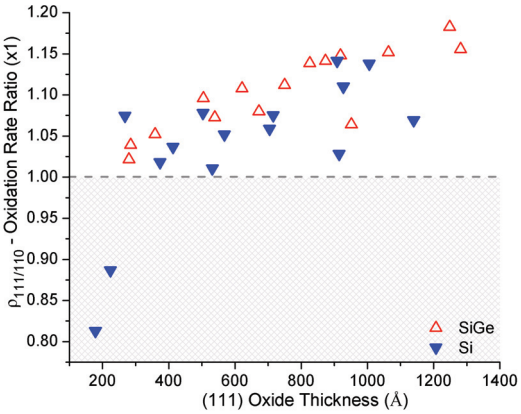

Figure 4.16: *Oxidation rate ratio, $\rho_{111/110}$, versus the oxide thickness, z_{ox}, of the (111) oriented sample. The oxidation rate ratio is calculated as $\rho_{111/110} = \nu_{111}/\nu_{110}$, where ν_{hkl} is the oxidation rate. The data is labeled according to the sample type, SiGe or Si.*

between oxide strain and steric hindrance creates a crossover point. The value of $\rho_{111/110}$ decreases towards one as z_{ox} decreases and is below one for the two points with $z_{\mathrm{ox}} < 23$ nm. A crossover point around 20 to 25 nm and a positive slope is an indication that the oxidation proceeds from being controlled by the surface reaction rate at very small values of z_{ox} to being increasingly influenced by strain and the diffusivity of oxidant in the oxide as z_{ox} increases. The strain due to the epitaxial growth of the SiGe layer for the samples in this study should add to the strain in the oxide. The additional strain due to the SiGe layer should shift the data to the left and result in a smaller crossover thickness for SiGe in figure 4.16. It is conceivable that, if electronegativities and bond energies only allow for the oxidation rate of SiGe to be greater than or the same as that of Si, the additional strain in the SiGe layers act to retard the oxidation of the SiGe samples enough to cause $\rho_{\mathrm{SiGe/Si}} < 1$, which would help to explain the data in figure 4.15. Though, the difference in the data for Si and SiGe in figure 4.16 is not profound, which would seem to indicate that the influence of the strain in the SiGe layer has a limited influence on the oxidation rate.

Due to the similarity in the influence of steric hindrance on Si and on fully strained SiGe, as well as the similarity between the oxides on the two materials, some portion of the influence of oxide strain on the oxidation rate will be divided out of the value of $\rho_{\mathrm{SiGe/Si}}$. However, recognizing that strain is a function of oxide thickness, and that, for a given oxidation time and temperature, z_{ox} for SiGe may be larger or smaller than for Si, oxide strain will have some influence on $\rho_{\mathrm{SiGe/Si}}$. Furthermore, the same difference in oxidizing ambient that was likely responsible for the variations in $\rho_{\mathrm{SiGe/Si}}$, shown in figure 4.15, is also likely to cause variations in the development of strain in the oxide and its effect on the oxidation rate. This is a critical point

in that, even though the strain in a fully strained SiGe layer may not have a profound influence on the oxidation rate, and that the influence of oxide strain on the oxidation rates of Si and SiGe are similar, the influence of oxide strain will, by virtue of its dependence on z_{ox}, obscure the degree to which Ge increases or decreases the oxidation rate of SiGe. That is, the tendency of strain to slow the oxidation rate for thicker oxides more than for thinner oxides will tend to reduce the difference between the oxide thicknesses on SiGe and Si from what they would be in the absence of oxide strain. The tendency of oxide strain to obscure the catalytic effect of Ge on oxidation, as measured by $\rho_{\mathrm{SiGe/Si}}$, will be aggravated by the fact that oxide strain is a function of the oxidizing ambient and the orientation of the material being oxidized.

The difference between the orientation dependence of the oxidation rate for Si and that of fully relaxed or tensilely strained SiGe layers may be more pronounced than the difference between the orientation dependence of the oxidation rate of Si as compared to fully compressively strained SiGe layers. The strain in the oxide is attributed to the difference in volume between an SiO_2 molecule and a Si atom, which, when translated to the distance between Si atoms, represents a 31% difference between the separation of Si atoms in SiO_2 compared to a Si crystal [87, 92]. Given that Ge has a lattice constant that is about 4% larger than Si [16], the distance between Si atoms is only 26% larger in SiO_2 than in a crystal with the lattice constant of Ge. The reduction in strain in the oxide due to the larger lattice constant in relaxed or tensilely strained SiGe, as compared to Si, would contribute to smaller values of $\rho_{111/110}$ and a larger crossover thickness. The reduction in strain should also lead to larger values of $\rho_{\mathrm{SiGe/Si}}$.

Uematsu *et al* [92] made clear that the oxidation rate of Si is dependent on the oxide strain induced generation of Si interstitials as well as viscous flow of the oxide. They also claim that the oxidation rate in dry oxidation of Si is dominated by the concentration of Si interstitials at the interface between the oxide and Si substrate, insinuating that the oxidant ambient also has a role in point defect generation. Furthermore, by inducing strain in Si substrates using stripes of oxide and measuring the oxidation rate adjacent to these stripes, Pliskin [10] showed that the influence of strain on the oxidation rate is not strictly due to changes in the diffusivity of oxidant in the oxide. LeGoues *et al* [38] recognized the possibility that variation in the lattice constant of relaxed SiGe could influence the oxidation rate of SiGe and suggested that Ge may induce vacancies in favor of the interstitials that would be expected in the case of Si oxidation; a surplus of vacancies should create misfit dislocations which would act to relieve oxide strain. The importance of interstitials and vacancies in determining the oxidation rate of SiGe has been repeated in several studies [37, 48, 59, 60]. Furthermore, the theory that vacancies are more readily created in the presence of Ge is supported by *ab initio* studies showing that the energy of formation of a vacancy is a function of the Ge content in SiGe, and is 1.5 eV lower in Ge than it is in Si [93].

The fact that point defect generation, oxide strain, SiGe layer strain, oxidant ambient, diffusivity of Si in SiGe, and other factors are so closely tied to one another makes it difficult to quantitatively differentiate between the various effects and their influence on Ge induced growth

rate enhancement or reduction. However, if Ge has a catalytic or inhibitive influence on the oxidation rate, it is certain that it is the Ge content at the oxidation front, and not the Ge content in the as-grown layer, that is the critical value. It is the Ge content in the pile-up region that will determine the degree to which strain, oxidant and impurity chemistry, *et cetera*, interact to increase or decrease the oxidation rate. Furthermore, the combination of temperature, oxidant partial pressure, oxidant and impurity chemistry, and UV illumination should provide a large degree of flexibility in determining both the Ge content at the oxidation interface and the oxidation rate.

4.13 Summary of results

It has been recognized that oxidizing crystalline SiGe will have the effect of leaching Si from the surface of the SiGe to form an oxide composed of SiO_2 and concentrating the remaining Ge at the interface between the oxide and the underlying SiGe. The present work provides a detailed analysis of the way in which Ge is redistributed during dry thermal oxidation. This analysis includes modeling based on balancing the diffusion of Si in SiGe with consumption of Si by oxidation. The modeling leads to equations describing the thickness of the pile-up region, z_{pu}, and the Ge concentration in the pile-up region, X_{pu}. Data from a series of experiments using XRD, VASE, and RBS are used to observe the redistribution of Ge and to support modeling predictions.

Both measurement and modeling results show that X_{pu} is controlled primarily by the oxidation temperature, T, while the Ge content in the initial SiGe layer plays a relatively minor role; a linear relationship between T and X_{pu} is demonstrated. As the formation of the pile-up layer is a consequence of the balance between the oxidation rate and the diffusivity of Si in SiGe, modifications of either the oxidation rate or the diffusivity of Si will alter $X_{\mathrm{pu}}(T)$. Both the oxidation rate and the diffusivity of Si in SiGe vary with crystallographic orientation, however, they vary in such a way that $X_{\mathrm{pu}}(T)$ is similar for the three orientations studied, (111), (110), and (100). The measurements and modeling in the present work are used to determine the diffusivity of Si in SiGe for the three basic crystallographic orientations.

The presence of Ge at the oxidation interface may have either a catalytic or inhibitive effect on the oxidation rate of SiGe, but, any such Ge induced oxidation rate enhancement or retardation will be subject to a variety of tertiary factors. The potential influence of crystallographic orientation, Ge content, oxide and epitaxial layer strain, epitaxial layer doping, oxidation ambient, bond energies, electronegativity, electrical potential, and point defect generation on the oxidation rate of SiGe are discussed with the help of oxidation rate ratios.

The analysis, modeling, and measurements presented herein provide the framework for designing thermal oxidation processes for fabrication of nanostructures for nano- and opto-electronic applications, as well as, further studies into the oxidation of SiGe.

References

[1] N. Cabrera and N. F. Mott, "Theory of the oxidation of metals," *Rep. Prog. Phys.*, vol. 12, no. 1, pp. 163–184, 1949.

[2] J. R. Ligenza, "Effect of crystal orientation on oxidation rates of silicon in high pressure steam," *J. Phys. Chem.*, vol. 65, no. 11, pp. 2011–2014, Nov 1961.

[3] J. R. Ligenza, "Oxidation of silicon by high-pressure steam," *J. Electrochem. Soc.*, vol. 109, no. 2, pp. 73–76, Feb 1962.

[4] H. Edagawa, Y. Morita, S. ichi Maekawa, and Y. Inuishi, "Growth and structure of Si oxide films on Si surface," *Japan. J. Appl. Phys.*, vol. 2, no. 12, pp. 765–775, Dec 1963.

[5] B. E. Deal, "The oxidation of silicon in dry oxygen, wet oxygen, and steam," *J. Electrochem. Soc.*, vol. 110, no. 6, pp. 527–533, Jun 1963.

[6] B. E. Deal and A. S. Grove, "General relationship for the thermal oxidation of silicon," *J. Appl. Phys.*, vol. 36, no. 12, pp. 3770–3778, Dec 1965.

[7] H. Z. Massoud, J. D. Plummer, and E. A. Irene, "Thermal oxidation of silicon in dry oxygen: Growth-rate enhancement in the thin regime," *J. Electrochem. Soc.*, vol. 132, no. 11, pp. 2685–2693, Nov 1985.

[8] H. Z. Massoud, J. D. Plummer, and E. A. Irene, "Thermal oxidation of silicon in dry oxygen: Growth-rate enhancement in the thin regime," *J. Electrochem. Soc.*, vol. 132, no. 11, pp. 2693–2700, Nov 1985.

[9] E. H. Nicollian and J. R. Brews, *MOS (Metal Oxide Semiconductor) Physics and Technology*, ser. Wiley Classics Library. Wiley-Interscience, 2002.

[10] W. A. Pliskin, "Separation of the linear and parabolic terms in the steam oxidation of silicon," *IBM J. Res. Dev.*, vol. 10, no. 3, pp. 198–206, May 1966.

[11] E. A. Irene, "The effects of trace amounts of water on the thermal oxidation of silicon in oxygen," *J. Electrochem. Soc.*, vol. 121, no. 12, pp. 1613–1616, Dec 1974.

[12] H. Z. Massoud and J. D. Plummer, "Analytical relationship for the oxidation of silicon in dry oxygen in the thin film regime," *J. Appl. Phys.*, vol. 62, no. 8, pp. 3416–3423, Oct 1987.

[13] J. Crank, *The mathematics of diffusion*, 1st ed. London: Oxford University Press, 1967.

[14] S. A. Campbell, *Fabrication engineering at the micro- and nanoscale*, 3rd ed. New York: Oxford University Press, 2008.

[15] R. Kube, H. Bracht, J. Lundsgaard Hansen, A. Nylandsted Larsen, E. E. Haller, S. Paul, and W. Lerch, "Composition dependence of Si and Ge diffusion in relaxed $Si_{1-x}Ge_x$ alloys," *J. Appl. Phys.*, vol. 107, no. 7, p. 073520, Apr 2010.

[16] J. P. Dismukes, L. Ekstrom, and R. J. Paff, "Lattice parameter and density in germanium-silicon alloys," *J. Phys. Chem.*, vol. 68, no. 10, pp. 3021–3027, Oct 1964.

[17] E. Long, A. Azarov, F. Kløw, A. Galeckas, A. Y. Kuznetsov, and S. Diplas, "Ge redistribution in SiO_2/SiGe structures under thermal oxidation: Dynamics and predictions," *J. Appl. Phys.*, vol. 111, no. 2, p. 024308, Jan 2012.

[18] E. Long, A. Galeckas, A. Y. Kuznetsov, A. Ronda, L. Favre, I. Berbezier, and H. H. Radamson, "Nano-structuring in sige by oxidation induced anisotropic Ge self-organization," *J. Appl. Phys.*, vol. 113, no. 10, p. 104310, Oct 2012.

[19] E. Long, A. Galeckas, and A. Y. Kuznetsov, "Ge concentrations in pile-up layers of sub-100-nm SiGe films for nano-structuring by thermal oxidation," *J. Vac. Sci. Technol. B*, vol. 30, no. 4, p. 041212, Jul 2012.

[20] N. Nagasima, "Structure analysis of thermal oxide films of silicon by electron diffraction and infrared absorption," *Japan. J. Appl. Phys.*, vol. 9, no. 8, pp. 879–888, Aug 1970.

[21] S. M. Sze, *Physics of Semiconductor Devices*, 2nd ed. New York: John Wiley and Sons, 1981.

[22] Y. Taur and T. H. Ning, *Fundamentals of modern VLSI devices*, 2nd ed. Cambridge: Cambridge University Press, 1998.

[23] B. J. Skinner and D. E. Appleman, "Melanophlogite, a cubic polymorph of silica," *The American Mineralogist*, vol. 48, pp. 854–867, Jul 1963.

[24] C. M. Herzinger, B. Johs, W. A. McGahan, J. A. Woollam, and W. Paulson, "Ellipsometric determination of optical constants for silicon and thermally grown silicon dioxide via a multi-sample, multi-wavelength, multi-angle investigation," *J. Appl. Phys.*, vol. 83, no. 6, pp. 3323–3336, Mar 1998.

[25] J. W. Matthews and A. E. Blakeslee, "Defects in epitaxialmultilayers: I. misfit dislocations," *J. Cryst. Growth*, vol. 27, pp. 118–125, Dec 1974.

[26] R. People and J. C. Bean, "Calculation of critical layer thickness versus lattice mismatch for Ge_xSi_{1-x}/Si strained-layer heterostructures," *Appl. Phys. Lett.*, vol. 47, no. 3, pp. 322–324, Aug 1985.

[27] H. Stöhr and W. Klemm, "Über zweistoffsysteme mit germanium. I. germanium/aluminium, germanium/zinn und germanium/silicium," *Z. Anorg. Allg. Chem.*, vol. 241, no. 4, pp. 305–323, Jun 1939.

[28] D. C. Paine, C. Caragianis, and A. F. Schwartzman, "Oxidation of $Si_{1-x}Ge_x$ alloys at atmospheric and elevated pressure," *J. Appl. Phys.*, vol. 70, no. 9, pp. 5076–5084, Nov 1991.

[29] E. C. Frey, N. Yu, B. Patnaik, N. R. Parikh, M. L. Swanson, and W. K. Chu, "Transition between Ge segregation and trapping during high-pressure oxidation of Ge_xSi_{1-x}/Si," *J. Appl. Phys.*, vol. 74, no. 7, pp. 4750–4755, Oct 1993.

[30] S. J. Kilpatrick, R. J. Jaccodine, and P. E. Thompson, "A diffusional model for the oxidation behavior of $Si_{1-x}Ge_x$ alloys," *J. Appl. Phys.*, vol. 81, no. 12, pp. 8018–8028, Jun 1997.

[31] J. M. Madsen, Z. Cui, and C. G. Takoudis, "Low temperature oxidation of SiGe in ozone: Ultrathin oxides," *J. Appl. Phys.*, vol. 87, no. 4, pp. 2046–2051, Feb 2000.

[32] I. W. Boyd, V. Craciun, and A. Kazor, "Vacuum-ultra-violet and ozone induced oxidation of silicon and silicon-germanium," *Japan. J. Appl. Phys.*, vol. 32, pp. 6141–6146, Dec 1993.

[33] V. Craciun, I. W. Boyd, A. H. Reader, W. J. Kersten, F. J. G. Hakkens, P. H. Oosting, and D. E. W. Vandenhoudt, "Microstructure of oxidized layers formed by the low-temperature ultraviolet-assisted dry oxidation of strained $Si_0.8Ge_0.2$ layers on Si," *J. Appl. Phys.*, vol. 75, no. 4, pp. 1972–1976, Feb 1994.

[34] V. Craciun, R. K. Singh, and I. W. Boyd, "Photonic effects during low-temperature ultraviolet-assisted oxidation of SiGe," *J. Electron. Mater.*, vol. 31, no. 12, pp. 1325–1329, Aug 2002.

[35] S. I. Raider, R. A. Gdula, and J. R. Petrak, "Nitrogen reaction at a silicon-silicon dioxide interface," *Appl. Phys. Lett.*, vol. 27, no. 3, pp. 150–152, Aug 1975.

[36] J. P. Zhang, P. L. F. Hemment, S. M. Newstead, A. R. Powell, T. E. Whall, and E. H. C. Parker, "A comparison of the behaviour of $Si_{0.5}Ge_{0.5}$ alloy during dry and wet oxidation," *Thin Solid Films*, vol. 222, no. 1-2, pp. 141–144, Dec 1992.

[37] M. Spadafora, G. Privitera, A. Terrasi, S. Scalese, C. Bongiorno, A. Carnera, M. Di Marino, and E. Napolitani, "Oxidation rate enhancement of SiGe epitaxial films oxidized in dry ambient," *Appl. Phys. Lett.*, vol. 83, no. 18, pp. 3713–3715, Nov 2003.

[38] F. K. LeGoues, R. Rosenberg, T. Nguyen, F. Himpsel, and B. S. Meyerson, "Oxidation studies of SiGe," *J. Appl. Phys.*, vol. 65, no. 4, pp. 1724–1728, Feb 1989.

[39] J. Eugène, F. K. LeGoues, V. P. Kesan, S. S. Iyer, and F. M. d'Heurle, "Diffusion versus oxidation rates in silicon-germanium alloys," *Appl. Phys. Lett.*, vol. 59, no. 1, pp. 78–80, Jul 1991.

[40] M. Spadafora, A. Terrasi, S. Mirabella, A. Piro, M. G. Grimaldi, S. Scalese, E. Napolitani, M. Di Marino, D. De Salvador, and A. Carnera, "Dry oxidation of MBE-SiGe films: rate enhancement, Ge redistribution and defect injection," *Mater. Sci. Semicond. Process.*, vol. 8, no. 1-3, pp. 219–224, 2005.

[41] D. K. Nayak, K. Kamjoo, J. S. Park, J. C. S. Woo, and K. L. Wang, "Rapid isothermal processing of strained GeSi layers," *IEEE Trans. Electron Devices*, vol. 39, no. 1, pp. 56–63, Jan 1992.

[42] D. K. Nayak, K. Kamjoo, J. S. Park, J. C. S. Woo, and K. L. Wang, "Wet oxidation of GeSi strained layers by rapid thermal processing," *Appl. Phys. Lett.*, vol. 57, no. 4, pp. 369–371, Jul 1990.

[43] W. S. Liu, E. W. Lee, M. A. Nicolet, V. Arbet-Engels, K. L. Wang, N. M. Abuhadba, and C. R. Aita, "Wet oxidation of GeSi at 700 °C," *J. Appl. Phys.*, vol. 71, no. 8, pp. 4015–4018, Apr 1992.

[44] G. L. Patton, S. S. Iyer, S. L. Delage, E. Ganin, and R. C. Mcintosh, "Oxidation of strained Si-Ge layers grown by MBE," *MRS Proc.*, vol. 102, pp. 295–299, 1988.

[45] O. W. Holland, C. W. White, and D. Fathy, "Novel oxidation process in Ge+-implanted Si and its effect on oxidation kinetics," *Appl. Phys. Lett.*, vol. 51, no. 7, pp. 520–522, Aug 1987.

[46] P. E. Hellberg, S. L. Zhang, F. M. d'Heurle, and C. S. Petersson, "Oxidation of silicon-germanium alloys. I. an experimental study," *J. Appl. Phys.*, vol. 82, no. 11, pp. 5773–5778, Dec 1997.

[47] S. G. Park, W. S. Liu, and M. A. Nicolet, "Kinetics and mechanism of wet oxidation of Ge_xSi_{1-x} alloys," *J. Appl. Phys.*, vol. 75, no. 3, pp. 1764–1770, Feb 1994.

[48] F. K. LeGoues, R. Rosenberg, and B. S. Meyerson, "Kinetics and mechanism of oxidation of SiGe: dry versus wet oxidation," *Appl. Phys. Lett.*, vol. 54, no. 7, pp. 644–646, 1989.

[49] E. Long, A. Galeckas, and A. Y. Kuznetsov, "A comparative analysis of oxidation rates for thin films of SiGe versus Si," *Phys. Status Solidi A*, vol. 209, no. 10, pp. 1934–1939, Oct 2012.

[50] Y. Zhang, C. Li, K. Cai, Y. Chen, S. Chen, H. Lai, and J. Kang, "Experimental evidence of oxidant-diffusion-limited oxidation of SiGe alloys," *J. Appl. Phys.*, vol. 106, no. 6, p. 063508, 2009.

[51] J. Xiang, N. Herbots, H. Jacobsson, P. Ye, S. Hearne, and S. Whaley, "Comparative study on dry oxidation of heteroepitaxial $Si_{1-x}Ge_x$ and $Si_{1-x-y}Ge_xC_y$ on Si(100)+," *J. Appl. Phys.*, vol. 80, no. 3, pp. 1857–1866, Aug 1996.

[52] C. Tètelin, X. Wallart, J. P. Nys, L. Vescan, and D. J. Gravesteijn, "Kinetics and mechanism of low temperature atomic oxygen-assisted oxidation of SiGe layers," *J. Appl. Phys.*, vol. 83, no. 5, pp. 2842–2846, Mar 1998.

[53] Y. S. Lim, F. Bassani, A. Portavoce, A. Ronda, S. Nozaki, and I. Berbezier, "The effect of Sb on the oxidation of Ge quantum dots," *Mater. Sci. Eng. B*, vol. 101, no. 1-3, pp. 190–193, Aug 2003.

[54] E. J. Jaquez, A. E. Bair, and T. L. Alford, "Cu enhanced oxidation of sige and sigec," *Appl. Phys. Lett.*, vol. 70, no. 7, pp. 874–876, Feb 1997.

[55] Z. Atzmon, A. E. Bair, T. L. Alford, D. Chandrasekhar, D. J. Smith, and J. W. Mayer, "Wet oxidation of amorphous and crystalline $Si_{1-x-y}Ge_xC_y$ alloys grown on (100)Si substrates," *Appl. Phys. Lett.*, vol. 66, no. 17, pp. 2244–2246, Apr 1995.

[56] T. Shimura, Y. Okamoto, T. Inoue, T. Hosoi, and H. Watanabe, "Residual order in the thermal oxide of a fully strained SiGe alloy on Si," *Phys. Rev. B*, vol. 81, no. 3, p. 033308, Jan 2010.

[57] A. R. Srivatsa, S. Sharan, O. W. Holland, and J. Narayan, "Nature of interfaces and oxidation processes in Ge+-implanted Si," *J. Appl. Phys.*, vol. 65, no. 10, pp. 4028–4032, May 1989.

[58] T. Shimura, Y. Okamoto, D. Shimokawa, T. Inoue, T. Hosoi, and H. Watanabe, "Interface reaction and rate enhancement of SiGe thermal oxidation," *ECS Trans.*, vol. 33, no. 6, pp. 893–899, 2010.

[59] D. Nayak, K. Kamjoo, J. C. S. Woo, J. S. Park, and K. L. Wang, "Rapid thermal oxidation of GeSi strained layers," *Appl. Phys. Lett.*, vol. 56, no. 1, pp. 66–68, Jan 1990.

[60] M. A. Rabie, Y. M. Haddara, and J. Carette, "A kinetic model for the oxidation of silicon germanium alloys," *J. Appl. Phys.*, vol. 98, no. 7, p. 074904, Oct 2005.

[61] L. Pauling, *The nature of the chemical bond*, 3rd ed. Ithaca, New York: Cornell University Press, 1960.

[62] R. J. Jaccodine, "Surface energy of germanium and silicon," *J. Electrochem. Soc.*, vol. 110, no. 6, pp. 524–527, 1963.

[63] J. Drowart, G. De Maria, A. J. H. Boerboom, and M. G. Inghram, "Mass spectrometric study of inter-group IVB molecules," *J. Phys. Chem.*, vol. 30, no. 1, pp. 308–313, Jan 1959.

[64] J. Drowart and R. E. Honig, "A mass spectrometric method for the determination of dissociation energies of diatomic molecules," *J. Phys. Chem.*, vol. 61, no. 7, pp. 980–985, Jul 1957.

[65] R. Viswanathan, R. W. S. Jr., and K. A. Gingerich, "Molar atomization enthalpies and molar enthalpies of formation of GeSi, $GeSi_2$, Ge_2Si, and Ge_2Si_2 by Knudsen-effusion mass spectrometry," *J. Chem. Thermodyn.*, vol. 27, no. 7, pp. 763–770, Jul 1995.

[66] P. Wielgus, S. Roszak, D. Majumdar, J. Saloni, and J. Leszczynski, "Theoretical studies on the bonding and thermodynamic properties of Ge_nSi_m $(m+n=5)$ clusters: The precursors of germanium/silicon nanomaterials," *J. Chem. Phys.*, vol. 128, no. 14, p. 144305, 2008.

[67] A. L. Allred and E. G. Rochow, "Electronegativities of carbon, silicon, germanium, tin and lead," *J. Inorg. Nucl. Chem.*, vol. 5, no. 4, pp. 269–288, Jun 1958.

[68] A. G. Revesz, "Noncrystalline structure and electronic conduction of silicon dioxide films," *Phys. Status Solidi B*, vol. 24, no. 1, pp. 115–126, 1967.

[69] P. J. Jorgensen, "Effect of an electric field on silicon oxidation," *J. Chem. Phys.*, vol. 4, no. 37, pp. 874–877, Aug 1962.

[70] R. People, "Indirect band gap of coherently strained Ge_xSi_{1-x} bulk alloys on <001> silicon substrates," *Phys. Rev. B*, vol. 32, no. 2, pp. 1405–1408, Jul 1985.

[71] M. M. Rieger and P. Vogl, "Electronic-band parameters in strained $Si_{1-x}Ge_x$ alloys on $Si_{1-y}Ge_y$ substrates," *Phys. Rev. B*, vol. 48, no. 19, pp. 14 276–14 287, Nov 1993.

[72] C. G. Van de Walle and R. M. Martin, "Theoretical calculations of heterojunction discontinuities in the Si/Ge system," *Phys. Rev. B*, vol. 34, no. 8, pp. 5621–5634, Oct 1986.

[73] H. Statz, G. deMars, L. Davis, and A. Adams, "Surface states on silicon and germanium surfaces," *Phys. Rev.*, vol. 101, no. 4, pp. 1272–1281, Feb 1956.

[74] H. Statz, G. deMars, L. Davis, and A. Adams, "Surface states on silicon and germanium surfaces," *Phys. Rev.*, vol. 106, no. 3, pp. 455–464, May 1957.

[75] F. K. LeGoues, R. Rosenberg, and B. S. Meyerson, "Dopant redistribution during oxidation of SiGe," *Appl. Phys. Lett.*, vol. 54, no. 8, pp. 751–753, Feb 1989.

[76] A. Seeger, "Self-diffusion in silicon - change of a paradigm," *Phys. Status Solidi B*, vol. 248, no. 12, pp. 2772–2774, 2011.

[77] A. Seeger and K. P. Chik, "Diffusion mechanisms and point defects in silicon and germanium," *Phys. Status Solidi B*, vol. 29, no. 2, pp. 455–542, 1968.

[78] G. N. Wills, "The orientation dependent diffusion of boron in silicon under oxidizing conditions," *Solid-State Electron.*, vol. 12, no. 2, pp. 133–134, Feb 1969.

[79] G. Masetti, S. Solmi, and G. Soncini, "Temperature dependence of boron diffusion in (111), (110) and (100) silicon," *Solid-State Electron.*, vol. 19, no. 6, pp. 545–546, Jun 1976.

[80] P. M. Fahey, P. B. Griffin, and J. D. Plummer, "Point defects and dopant diffusion in silicon," *Rev. Mod. Phys.*, vol. 61, no. 2, pp. 289–384, Apr 1989.

[81] S. Balakumar, K. D. Buddharaju, B. Tan, S. C. Rustagi, N. Singh, R. Kumar, G. Q. Lo, S. Tripathy, and D. L. Kwong, "Germanium-rich SiGe nanowires formed through oxidation of patterned SiGe FINs on insulator," *J. Electron. Mater.*, vol. 38, no. 3, pp. 443–448, 2009.

[82] F.-J. Ma, B. S. Chia, S. C. Rustagi, and G. C. Samudra, "Study on SiGe nanowire shape engineering and Ge condensation," in *ESciNano*, ser. Int. Conf. on Enabling Sci. and Nanotechnology, Dec 2010, pp. 1–2.

[83] E. P. EerNisse, "Stress in thermal SiO_2 during growth," *Appl. Phys. Lett.*, vol. 35, no. 1, pp. 8–10, Jul 1979.

[84] E. Kobeda and E. A. Irene, "Intrinsic SiO_2 film stress measurements on thermally oxidized si," *J. Vac. Sci. Technol. B*, vol. 5, no. 1, pp. 15–19, Feb 1987.

[85] A. Fargeix and G. Ghibaudo, "Dry oxidation of silicon: A new model of growth including relaxation of stress by viscous flow," *J. Appl. Phys.*, vol. 54, no. 12, pp. 7153–7158, Dec 1983.

[86] D.-B. Kao, J. P. McVittie, W. D. Nix, and K. C. Saraswat, "Two-dimensional thermal oxidation of silicon - I. experiments," *IEEE Trans. Electron Devices*, vol. 34, no. 5, pp. 1008–1017, May 1987.

[87] D.-B. Kao, J. P. McVittie, W. D. Nix, and K. C. Saraswat, "Two-dimensional thermal oxidation of silicon - II. modeling stress effects in wet oxides," *IEEE Trans. Electron Devices*, vol. 35, no. 1, pp. 25–37, Jan 1988.

[88] E. A. Irene, D. W. Dong, and R. J. Zeto, "Residual stress, chemical etch rate, refractive index, and density measurements on SiO_2 films prepared using high pressure oxygen," *J. Electrochem. Soc.*, vol. 127, no. 2, pp. 396–399, 1980.

[89] K. Imai and K. Yamabe, "Stress effect on oxidation kinetics of silicon with different surface orientations," *MRS Proc.*, vol. 239, pp. 107–112, 1991.

[90] E. A. Lewis and E. A. Irene, "the effect of surface orientation on silicon oxidation kinetics," *J. Electrochem. Soc.*, vol. 134, no. 9, pp. 2332–2339, Sep 1987.

[91] K. E. Bean and P. S. Gleim, "The influence of crystal orientation on silicon semiconductor processing," *Proc. IEEE*, vol. 57, no. 9, pp. 1469–1476, Sep 1969.

[92] M. Uematsu, H. Kageshima, and K. Shiraishi, "Microscopic mechanism of thermal silicon oxide growth," *Comp. Mater. Sci.*, vol. 24, no. 1-2, pp. 229–234, May 2002.

[93] P. Ramanarayanan, K. Cho, and B. M. Clemens, "Effect of composition on vacancy mediated diffusion in random binary alloys: First principles study of the $Si_{1-x}Ge_x$ system," *J. Appl. Phys.*, vol. 94, no. 1, pp. 174–185, Jul 2003.

Chapter 5

Future work and potential applications

5.1 Benefits of using low Ge contents in as-grown layers

The present work used thin films of $Si_{0.80}Ge_{0.20}$ and $Si_{0.85}Ge_{0.15}$ as a raw material. However, over the course of the research presented here, it has become evident that there are a number of advantages to using $Si_{1-X}Ge_X$ with a small X as a starting material for experimenting with oxidation induced Ge condensation. The most trivial of these is that many of the physical properties of SiGe vary between those of Si and those of Ge (see chapter 2), and after more than half a century of intense research and industrial use, Si is much better understood than Ge. Using smaller values of X will likely lead to less uncertainty in the results obtained by the empiricist and will minimize the temptation to explain away various phenomena by attributing them to the poorly characterized properties of Ge or high values of X in the starting material. There are also a number of more concrete (and less philosophical) reasons why it is beneficial to use SiGe with low Ge contents as a starting material. These include:

- Starting with a small value of X allows more room to increase X_{pu} for one or more pile-up layers (*i.e.* bigger differences between X and X_{pu}).
- Low strain levels between Si substrates and epitaxial SiGe layers.
- Relatively thick initial SiGe layers can be grown epitaxially without reaching the critical thickness.
- Thick initial SiGe layers allows for thicker pile-up layers which may be used for growing multiple pile-up layers with multiple oxidations.
- Due to the relatively low diffusivity of Si in Si (as compared to the diffusivity of Si in Ge), starting with low Ge contents will result in more abrupt barriers between layers of increasing Ge content.

- The same low diffusivity of Si in $Si_{1-X}Ge_X$ where X is small will minimize the diffusion of Si from the substrate, into, and through the initial SiGe layer.
- Less ambiguity about the oxidation rates and less potential for the initial Ge content to alter the oxidation kinetics.
- Any variations in the oxidation rate due to initial Ge contents will have a minimal influence on the thickness of the pile-up region due to very small t_{pu}/t_{ox} ratios. This will make it easier to achieve accurate and small values of t_{pu}, despite any extant uncertainties in the oxidation rate (*i.e.* thin pile-up layers can be formed by growing thick oxide layers).
- Reduced strain levels between the substrate and the SiGe layers will minimize the risk of defects developing during high temperature oxidations.

5.2 Variable temperature, vacuum-UV, pressure, and ambient chemistry

The relationship between the Ge content in the pile-up and the oxidation temperature has been explored in some depth in the present work and is expressed by equation 4.2. Still, the oxidation conditions may be manipulated in a number of ways in order to change the oxidation rate, and hence the Ge content in the pile-up layer.

All of the experiments done for the publications in the present work were done with one or more oxidations at a variety of fixed temperatures. It should be clear that multiple pile-up layers can be grown one upon the other by conducting multiple oxidations at progressively lower fixed temperatures. The logical extention of this would be to conduct a single oxidation with a temperature that varies with time in such a way as to control the gradient of the Ge content in the pile-up layer. The way in which temperature should be modified as a function of time in order to achieve any given Ge profile is not trivial and could be the subject of further investigations.

Ambient chemistry, oxidant partial pressure, and illumination by vacuum-ultra-violet (V-UV) radiation are all oxidation conditions that could be used to manipulate the Ge content at the oxidation interface, but which haven't been investigated. Investigation of ambient chemistry would be most useful in illuminating the mechanisms behind the enhanced oxidation rates that have been observed in so many publications on oxidation of SiGe. A study of the influence of trace amounts of H_2O, similar to what was done by Irene [1], would be of particular utility. A study of the influence of oxidant partial pressures on Ge redistribution would be useful in determining whether pressure, instead of temperature, could be used to control the Ge content at the oxidation interface. It would be advantageous to limit the thermal budget for processing by using pressure as a process control, but, pressure will only alter the oxidation rate, and may result in unacceptably long processing times. Illumination of the sample with UV light may allow for

much lower process temperatures to be used, while still resulting in fast oxidation times. This is a result of the potential for UV illumination to alter the activation energies for both oxidation and the diffusivity of Si in SiGe.

5.3 SiSn and SiGeSn oxidation

The Gibbs free energies for formation of SiO_2, GeO_2, and SnO_2 from their constituent elements are shown in figure 5.1. Considering the similarity between the Gibbs free energies for formation of GeO_2 and SnO_2 and the exclusive formation of SiO_2 during SiGe oxidations, it is likely that oxidation of SiSn and SiGeSn will also result in an oxide of composed exclusively of SiO_2, while Ge and Sn accumulate at the interface between the oxide and the underlying SiSn or SiGeSn crystal. This is supported by XPS measurements in multiple studies indicating a thermodynamic preference for SiO_2 over SnO_2 [2, 3]. This will be important for application of tin oxide or indium tin oxide as transparent contacts for solar cells, as well as applications in photonics and opto-electronics that take advantage of the direct bandgap of SiGeSn alloys [4]. A proposal for tin based confinement modulated gap transistors (CMGT) relies on using the orientation and diameter of a nanowire to manipulate the bandgap of the transistor channel material (Sn) between $\sim$2.7 and 0 eV [5]. Such CMGT's, as well as other multi-gate transistor architectures, could be constructed using Sn or GeSn condensation by thermal oxidation of SiSn or SiGeSn. It is possible that ohmic contacts to source and drain regions of transistors could be improved and that contact implants could be eliminated by using Sn condensation. If the source and drain regions are composed of SiSn with a low Sn content, selective oxidation could be used to create a metallic contact by condensing a thin layer of Sn at surface of the source and drain regions.

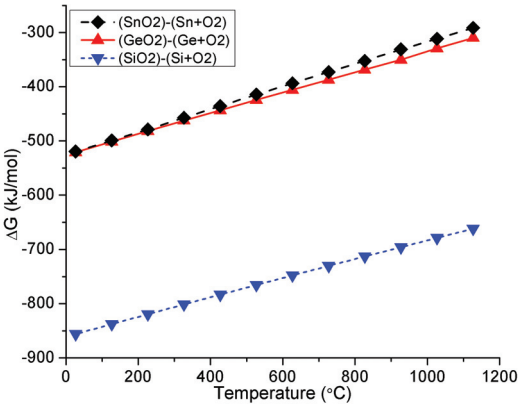

Figure 5.1: *Gibbs energies for oxidation of Si, Ge, and Sn [6].*

5.4 Dopant and alloy gradients by differential diffusion

Grove *et al* [7] described the redistribution of dopants in oxidizing Si. They demonstrated that the n-type dopants (phosphorus, arsenic, and antimony) tend to become depleted at the oxidation interface, while the p-type dopants (boron, gallium, and indium) tend to pile-up at the oxidation interface. LeGoues *et al* [8] showed that diffusion of boron in oxidizing SiGe is retarded with respect to Si. Dopant diffusion in SiGe has been shown to be a function of Ge content in non-oxidizing conditions as well. Phosphorus [9], arsenic [10], and antimony [11] have been shown to diffuse faster as the Ge content is increased, while results for boron and gallium diffusion are mixed; boron and gallium diffusion are reported either to be independent of Ge content, or to decrease as Ge content increases [12–15]. Indications that Sn increases the diffusivity of antimony in Si [16] might suggest that SiSn and SiGe behave similarly.

The tendency of Ge to pile up at the oxidation interface during thermal oxidation should exaggerate the accumulation or depletion of dopants at the same interface, and could be used to build opto-electronic devices. For example, if a layer of SiGe is uniformly doped with both n and p-type dopants, oxidizing the material may cause the p-type dopants to pile-up at the oxidation interface, while the n-type dopants are depleted, creating a p-n diode. This might be done to form shallow junctions in photovoltaic cells.

Another application could be in formation of ohmic contacts for the source and drain of transistors. Contact implants have been used in integrated circuit fabrication to create a highly doped region where the metal contacts meet the source and drain of a transistor in order to minimize the contact resistance. Differential diffusion could be used to form ohmic source and drain contacts in PMOS transistors by piling up the p-type dopant at the surface of the source and drain regions. This might be particularly convenient in transistors that use Ge in the source and drain to manipulate channel strain and reduce drain induced barrier lowering (DIBL). If the source and drain use a SiSn alloy, it might be possible to grade the Sn content such that both the dopant and Sn content increase towards the contact interface such that a metal to metal (rather than semiconductor to metal) contact is made.

References

[1] E. A. Irene, “The effects of trace amounts of water on the thermal oxidation of silicon in oxygen,” *J. Electrochem. Soc.*, vol. 121, no. 12, pp. 1613–1616, Dec 1974.

[2] J. H. Thomas and A. Catalano, “Auger electron and x-ray photoelectron spectroscopy analysis of the hydrogenated amorphous silicon-tin oxide interface: Evidence of a plasma-induced reaction,” *Appl. Phys. Lett.*, vol. 43, no. 1, pp. 101–102, Apr 1983.

[3] S. Badrinarayanan, S. Sinha, and A. P. B. Sinha, "Evidence for a solid state reaction at the a-Si-SnO_x interface: An x-ray photoelectron spectroscopy study," *Thin Solid Films*, vol. 144, no. 1, pp. 133–137, May 1986.

[4] P. Moontragoon, R. A. Soref, and Z. Ikonic, "The direct and indirect bandgaps of unstrained $Si_xGe_{1-x-y}Sn_y$ and their photonic device applications," *J. Appl. Phys.*, vol. 112, no. 7, p. 073106, Oct 2012.

[5] L. Ansari, G. Fagas, and J. C. Greer, "Tin nanowire field effect transistor," in *Proc. of the Eur. Solid State Device Research Conf.*, Sep 2012, pp. 294–297.

[6] I. Barin, *Thermochemical Data of Pure Substances*, 2nd ed. Weinheim: VCH, 1993.

[7] A. S. Grove, O. Leistiko, and C. T. Sah, "Redistribution of acceptor and donor impurities during thermal oxidation of silicon," *J. Appl. Phys.*, vol. 35, no. 9, pp. 2695–2701, Sep 1964.

[8] F. K. LeGoues, R. Rosenberg, and B. S. Meyerson, "Dopant redistribution during oxidation of SiGe," *Appl. Phys. Lett.*, vol. 54, no. 8, pp. 751–753, Feb 1989.

[9] J. S. Christensen, H. H. Radamson, A. Y. Kuznetsov, and B. G. Svensson, "Diffusion of phosphorus in relaxed $Si_{1-x}Ge_x$ films and strained $Si/Si_{1-x}Ge_x$ heterostructures," *J. Appl. Phys.*, vol. 94, no. 10, pp. 6533–6540, Nov 2003.

[10] P. Laitinen, I. Riihimäki, and J. Räisänen, "Arsenic diffusion in relaxed $Si_{1-x}Ge_x$," *Phys. Rev. B*, vol. 68, no. 15, p. 155209, Oct 2003.

[11] A. N. Larsen and P. Kringhøj, "Diffusion of Sb in relaxed $Si_{1-x}ge_x$," *Appl. Phys. Lett.*, vol. 68, no. 19, pp. 2684–2686, Feb 1996.

[12] N. R. Zangenberg, J. Fage-Pedersen, J. Lundsgaard Hansen, and A. Nylandsted Larsen, "Boron and phosphorus diffusion in strained and relaxed Si and SiGe," *J. Appl. Phys.*, vol. 94, no. 6, pp. 3883–3890, Sep 2003.

[13] I. Riihimäki, A. Virtanen, H. Kettunen, P. Pusa, and J. Räisänen, "Diffusion properties of Ga in $Si_{1-x}Ge_x$ alloys," *J. Appl. Phys.*, vol. 104, no. 12, p. 123510, Dec 2008.

[14] J. Bang, J. Kang, W.-J. Lee, K. J. Chang, and H. Kim, "Chemical bonding effect of Ge atoms on B diffusion in Si," *Phys. Rev. B*, vol. 76, no. 6, p. 064118, Aug 2007.

[15] C. C. Wang, Y. M. Sheu, S. Liu, R. Duffy, A. Heringa, N. E. B. Cowern, and P. B. Griffin, "Boron diffusion in strained and strain-relaxed SiGe," *Mater. Sci. Eng. B*, vol. 124-125, no. 0, pp. 39–44, Dec 2005.

[16] J. Fage-Pedersen, A. Nylandsted Larsen, P. Gaiduk, J. Lundsgaard Hansen, and M. Linnarsson, "Sn-background-induced diffusion enhancement of Sb in Si," *Phys. Rev. Lett.*, vol. 81, no. 26, pp. 5856–5859, Dec 1998.

Chapter 6

Overview of articles

6.1 Article I

New data for the dry O_2 oxidation of MBE grown thin films of $Si_{0.80}Ge_{0.20}$ and $Si_{0.85}Ge_{0.15}$ is presented along with data for Si control samples. The new data is compared to data for dry O_2 oxidation of SiGe from the literature as well as common models for oxidation of Si. The article addresses the fact that there are a variety of claims about the role of the Ge content in the as-grown SiGe layer in determining the oxidation rate. This is coupled with the observation that there is wide variation in the oxidation rates for SiGe between studies and in the models for Si oxidation. The point is made that since Ge piles up in the region where oxidation occurs, discussion of the oxidation rate's dependence on the Ge content in the as-grown layer is inherently flawed. Both VASE and XRD are used to characterized the oxide thicknesses and pile-up Ge concentrations for the samples from the present study.

6.2 Article II

XPS is used to characterize the chemical composition of oxides formed on SiGe by thermal oxidation and to confirm the preferential formation of SiO_2. XPS and RBS are used to confirm that Ge piles up at the oxidation interface. The theoretical foundation for the modeling that lead to the equations describing the thickness of the pile-up region (equation 4.5) and the Ge content in the pile-up region (equation 4.4) is established and explained. This includes a detailed discussion of the requirement that the flux of Si into the oxide be balanced by the flux of Si through the pile-up layer. The modeling is also used to evaluate the influences of oxide thickness and oxidation temperature on the Ge content in the pile-up layer.

6.3 Article III

XRD and VASE are used to fully characterize the Ge content in the pile-up region for a variety of oxidation times and temperatures. Both simulation and empiric results are used to show that the Ge content in the pile-up is linearly dependent on oxidation temperature and to support equation 4.4. Measurements are presented that help confirm that Ge content in the pile-up is largely independent of oxide thickness but highly dependent on oxidation temperature; this includes measurements showing the correlation between oxide thickness and pile-up layer thickness. The relative influence of oxidation temperature and the Ge content in the as-grown SiGe layer on the oxidation rate is addressed and oxidation rates of SiGe samples are compared to results from an established model for the oxidation of Si.

6.4 Article IV

The diffusivity of Si in (111), (110), and (100) oriented oxidizing SiGe is determined by combining VASE measurements of oxide thickness, XRD measurements of the Ge content in the pile-up region, and equation 4.4. The Ge content in the pile-up region is shown to be dependent on orientation, though, the temperature dependence is nearly identical for the three orientations. The linear relationship between oxidation temperature and the Ge content in the pile-up layer is explained by assumption of Arrhenius relations to describe both diffusion of Si in the pile-up layer and the oxidation rate of SiGe, resulting in equation 4.2. Oxidation rate ratios between SiGe and Si samples and between samples of different orientations are used to evaluate the relative importance of orientation and Ge content on the oxidation rate of SiGe. Oxidation rate ratios are also used to discuss various physical mechanisms for oxidation of SiGe. The integrity of equations 4.2 and 4.4 are verified by demonstrating the predictability of the Ge content in the pile-up layer for samples subjected to multiple oxidations at progressively higher temperatures. It is also demonstrated that, by choosing an appropriate oxidation temperature, the Ge content at the oxidation interface can be kept static or reduced. The ability to reduce the Ge content at the oxidation interface is consistent with the predictions made by equations 4.2 and 4.4.

Article I

A comparative analysis of oxidation rates for thin films of SiGe *versus* Si

---

E. Long, A. Galeckas, and A. Yu. Kuznetsov

Physica Status Solidi A, **209**(10), 1934-1939 (2012)

Article II

Ge redistribution in SiO_2/SiGe structures under thermal oxidation: Dynamics and predictions

E. Long, A. Azarov, F. Kløw, A. Galeckas, A. Yu. Kuznetsov, and S. Diplas
Journal of Applied Physics **111**, 024308 (2012)

Ge redistribution in SiO_2/SiGe structures under thermal oxidation: Dynamics and predictions

Ethan Long,[1,a)] Alexander Azarov,[1] Frode Kløw,[1] Augustinas Galeckas,[1] Andrej Yu Kuznetsov,[1] and Spyridon Diplas[2]
[1]*Department of Physics/Center for Materials Science and Nanotechnology, University of Oslo, P.O. Box 1048 Blindern, Oslo N-0316, Norway*
[2]*SINTEF Materials and Chemistry, Oslo N-0314, Norway and Department of Chemistry/Center for Materials Science and Nanotechnology, University of Oslo, P.O. Box 1048 Blindern, Oslo N-0316, Norway*

(Received 29 August 2011; accepted 15 December 2011; published online 24 January 2012)

Several fundamental aspects of the oxidation-induced redistribution of Ge in thin films of SiGe are studied. This includes the incorporation of Ge into the oxide and the formation of what is alternatively referred to as pile-up, snow-plow, or a germanium-rich layer. Experimental data from the present work shows longer oxidation times leading to an increase of Ge content in the pile-up region and eventually creating a single high Ge content pile-up layer by entirely consuming the initial SiGe layer. The pile-up effect was shown to occur at the oxidation interface, with the highest Ge content occurring at the same interface. For a given oxide thickness, the redistribution of Ge and the formation of a pile-up region was shown experimentally to be independent of temperature in the range between 800 °C and 1000 °C. Simulations using common models for the oxidation of Si and diffusion of Si in SiGe indicate that temperature does have an influence on the composition of the pile-up layer, though the range of achievable compositions is limited. The flux of Si due to diffusion of Si in SiGe relative to the oxidation-induced flux of Si out of the SiGe is integral to the formation and dimensions of a pile-up region. Two predictive relations were derived for describing the dynamics of oxidation of SiGe. The first relation is given for determining the pile-up layer thickness as a function of oxide thickness and the composition of the pile-up layer. The second relation assumes a limited supply of Si and is for determination of the minimum initial thickness of a SiGe layer to avoid oxidation of Ge. The validity of these equations was confirmed experimentally by RBS and XPS data from the present work. The proposed models may be used in nanostructuring of thin films of SiGe by oxidation and in the design of core-shell structures and transistors. This is all done with a focus on oxidation of epitaxial thin films (< 100 nm) of $Si_{1-X}Ge_X$ in dry O_2 at 1 atm between 800 °C and 1000 °C. © *2012 American Institute of Physics*. [doi:10.1063/1.3677987]

I. INTRODUCTION

The importance of SiGe in IC design and fabrication is increasing due to demand for higher speed and lower power electronics, recent commercialization of FINFETs, advances in the fabrication of SiGe-on-insulator[1–3] (sapphire or SiO_2), and the proliferation of RF applications in the marketplace. Incorporation of Ge into Si CMOS processing has been motivated by SiGe's utility in creating high mobility channels,[4] reduction of parasitic effects, like drain-induced barrier lowering,[5] and creation of other novel gate architectures and nanowire transistors.[6,7] Yet another promising application of SiGe is its use in core-shell structures for photovoltaics.[8] Nanostructuring of SiGe by oxidation is an effective method for construction of a wide variety of SiGe-based electronic devices, a fact which highlights the importance of research into the dynamics of oxidation of SiGe and the subsequent redistribution of Ge in the SiGe.

The use of dry O_2 oxidation to create SiGe core-shell structures relies on the selective oxidation of Si, which acts to separate Si from Ge and creates a graded Ge concentration in the SiGe. Such concentration gradients are typically characterized by a Ge-rich region adjacent to the SiO_2 growth front and are variously referred to as a pile-up region, snow plow effect, or germanium-rich layer (GRL). The pile-up effect, resulting from dry oxidation of SiGe, has been reported to occur in numerous publications,[9–23] but these observations are frequently limited to the acknowledgment of the existence of a pile-up layer. Furthermore, the reports do not provide sufficient information to understand how modification of the oxidation conditions may lead to variations in the profile of Ge concentration in the SiGe.

The present work addresses the dynamics of oxidation of thin films of SiGe by considering dry O_2 oxidation with various times and temperatures. The focus on sub-100-nm films ensures that the discussion is pertinent to modern technological applications.

The driving factors in the formation of a pile-up layer are, first, the susceptibility for incorporation of Ge into the oxide and, second, the relative diffusion of O, Si, and Ge in the oxidizing material. The Ge content of the oxide is evaluated here using analysis of x ray photoelectron spectroscopy (XPS) data.

[a)]Author to whom correspondence should be addressed. Electronic mail: ethanl@smn.uio.no.

The role of Gibbs energies in the formation of oxides is reviewed to provide a better understanding of the influence of temperature on the incorporation of Ge into the oxide. The relative diffusion of oxidant in SiO_2 and that of Si in SiGe or Ge forms the basis of several models that have been proposed to describe the oxidation processes in SiGe.[23–26] The present work uses Rutherford backscattering spectroscopy (RBS) data to evaluate the role of oxidation time and temperature in the formation of a pile-up region and to provide experimental support for two descriptive relations. The proposed relations describe the pile-up layer thickness as a function of oxide thickness and allow prediction of the initial SiGe layer thickness required to avoid oxidation of Ge. These models may be useful in making first order estimates in the design of core-shell structures and transistors using oxidized SiGe.

II. EXPERIMENTAL

Epitaxial layers of $Si_{1-X}Ge_X$ on a 100-nm Si buffer layer were grown on (100)-oriented Si substrates. The $Si_{1-X}Ge_X$ layer thicknesses for the two wafers used were 80 nm and 70 nm for $X = 0.15$ and $X = 0.20$, respectively. The thermal oxidation was done using a tube furnace at ambient pressure flushed with dry O_2 at 800 °C, 850 °C, 900 °C, 950 °C, and 1000 °C. The native oxides were not removed prior to oxidation.

X ray photoelectron spectroscopy (XPS) was performed with a *Kratos Axis Ultra DLD* system using Al Kα x ray excitation ($h\nu = 1486.6$ eV). Compositional profiles were acquired by combining XPS measurements with Ar+ cation etching. The XPS compositional profiles were correlated to physical depths using profilometer measurements of the milled craters. The resolution of XPS measurements is given by the detection depth, $d = 3\lambda\cos\theta$, where λ is the inelastic mean free path of photoelectrons and θ is the angle of emission. In this case, θ is 0°, so the detection depth is 3.5 nm for the Ge2p photoelectrons, which is significantly less than the detection depth of 11.7 nm for Ge3d photoelectrons. These detection depth values were derived assuming that the photoelectrons are traveling through an SiO_2 layer and by using data from the Tanuma, Powell, and Penn algorithm.[27,28]

Rutherford backscattering spectroscopy (RBS) measurements were done with 2 MeV 4He+ ions backscattered into the detector at 100° relative to the incident beam direction. This glancing-angle detector geometry was used to provide enhanced depth resolution for accurate analysis of films near the surface region. Oxide and pile-up layer thicknesses were determined by fitting simulated curves to the experimentally determined RBS spectra.

Oxide thicknesses were also measured by ellipsometry at 632.8 nm and 830.0 nm wavelengths and 70° angle of incidence, with each sample repeatedly measured at each wavelength in order to account for random error in the measurements. The analysis used a three-layer model and treated the oxide, pile-up, and SiGe layer thicknesses as well as the index of refraction for the pile-up layer as unknowns. For the purpose of comparing the oxide thicknesses determined by ellipsometry to those determined by RBS, the certainty in the ellipsometry measurements may be calculated while presuming the RBS values to be the actual values. With such a presumption, the sample standard deviation in the ellipsometry measurements was calculated to be 3.8 nm.

III. RESULTS AND DISCUSSION

A. Oxide composition

A critical factor in the manipulation of Ge concentrations in SiGe thin films by oxidation is the degree to which Ge is incorporated into the oxide. Considering this, Fig. 1 shows an XPS depth profile of the oxide of a $Si_{0.85}Ge_{0.15}$ sample oxidized at 950 °C for 25 min. Ar+ cation etching was used to expose progressively deeper levels of the sample to create the depth profile of the sample composition shown. A short etch time was used for this sample to highlight the composition of the oxide. In the XPS profiles, metallic and oxidized Si appear at binding energies of ~97 eV and ~102 eV, while metallic and oxidized Ge appear at ~1215 eV and ~1219 eV, respectively. Noting that Ge2p photoelectrons have low kinetic energy and arise from shallow depths, the surface sensitive Ge2p peak indicates that the native oxide contains some oxidized Ge, which is consistent with other reports in the literature.[29] The remainder of the oxide is devoid of any form of Ge until the SiO_2 to SiGe interface is reached.

XPS data in Fig. 2 illustrates very similar behavior for a sample with a comparable oxide thickness, but oxidized at 850 °C. A long etch time was used for this sample, so the XPS profile shows the sample composition from the surface

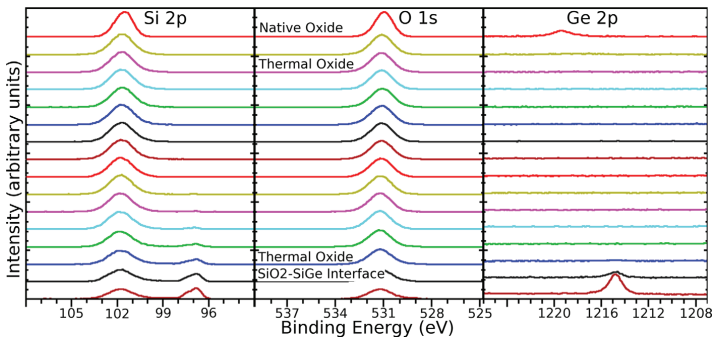

FIG. 1. (Color online) XPS depth profile of a $Si_{0.85}Ge_{0.15}$ thin film oxidized at 950 °C for 25 min. The oxide thickness as measured by ellipsometry is 392 Å. The topmost profile is for the surface of the unetched sample. The bottommost profile is at the SiGe layer, as indicated by the presence of metallic Si and Ge.

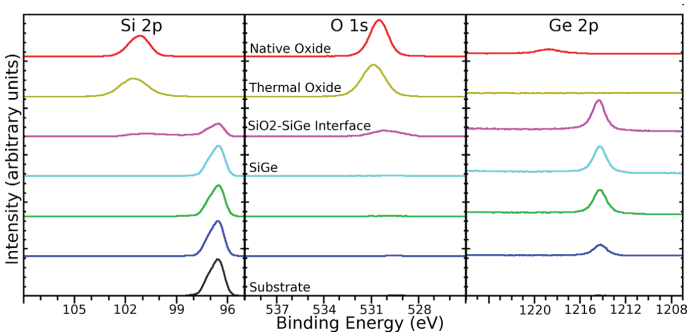

FIG. 2. (Color online) XPS depth profile of $Si_{0.85}Ge_{0.15}$ thin film oxidized at 850 °C for 75 min. The oxide thickness as measured by ellipsometry is 356 Å. The topmost profile is for the unetched sample surface. The bottommost profile is at the substrate, as indicated by the presence of metallic Si and the absence of either O or Ge.

all the way to the substrate. It can be seen that GeO_2 appears in the region of the native oxide, while only SiO_2 occurs in the bulk of the oxide. Metallic Ge can be seen in the SiGe layer, and no Ge is present in the substrate. However, when compared to the sample in Fig. 1, the longer etching times used between XPS measurements for the sample in Fig. 2 result in less detailed probing of the interface between the oxide and pile-up layers.

Figure 3 presents a depth profile showing the relative concentrations of O, Si, and Ge constructed from the same XPS data as was used for Fig. 2; the lines connecting data points in Fig. 3 are for illustrative purposes only. The depth profile uses the Ge3d signal, which is less surface sensitive than the Ge2p signal, but allows better comparison to the O and Si data due to the fact that the signals arise from similar depths.

Figure 3 does indicate the presence of Ge in the region of the native oxide, but considering the limited resolution of the Ge3d peak, the concentration of Ge in this region is negligibly small. Both Figs. 1 and 2 also indicate that the GeO_2 is limited to the native oxide. This is consistent with experimental evidence presented in the literature showing GeO_2 in very thin or low temperature oxides, including native oxides.[30–32] Also, there is a point of high Ge concentration at the interface between the oxide and SiGe layers, which is indicative of a Ge pile-up layer with a Ge concentration that is roughly double that of the intrinsic SiGe.

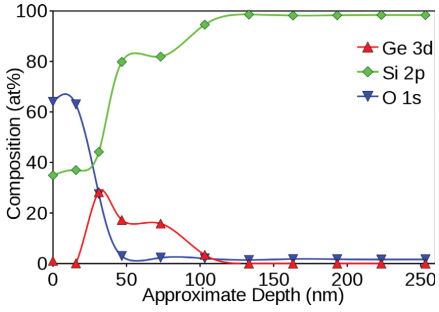

FIG. 3. (Color online) Profile of $Si_{0.85}Ge_{0.15}$ oxidized at 850 °C for 75 min showing relative atomic composition vs depth from XPS measurements. The oxide thickness as measured by ellipsometry is 356 Å.

The preferential oxidation of Si over that of Ge is a critical characteristic of SiGe oxidation and can be explained using the Gibbs energies, G, of the constituent reactants.[32] Thus, an understanding of the Gibbs energies involved will help explain whether Ge will be incorporated into the oxide during thermal oxidation.

The change in Gibbs energy due to a reaction between several reactants is given by $\Delta G_P = G_P - (G_{R1} + G_{R2})$, where G_P, G_{R1}, and G_{R2} are the Gibbs energies of the reaction product and two separate reactants, respectively.[33] A negative value for ΔG_P indicates that the reaction will occur spontaneously. The values of ΔG_{SiO2} and ΔG_{GeO2} for the formation of oxide from Si, Ge, and O_2 for temperatures between 27 °C and 1127 °C are in the range of −856 kJ/mol to −661 kJ/mol and −521 kJ/mol to −310 kJ/mol,[33] respectively. It is clear that, although both SiO_2 and GeO_2 formation are exergonic, the SiO_2 reaction is more so than that of GeO_2, leading to the preferential formation of SiO_2. This point may be emphasized by the data in Fig. 4, showing ΔG_{SiO2} for the formation of SiO_2 from GeO_2 and Si, which is equivalent to the difference between ΔG_{SiO2} and ΔG_{GeO2}. The data in Fig. 4 shows that SiO_2 is preferred over GeO_2, at least for temperatures between 27 °C and 1127 °C, and that any occurrence of GeO_2 may be converted to SiO_2, given elemental Si.[34] This preference is exaggerated at higher temperatures, but ΔG is consistently and substantially negative between temperatures where native oxides might occur and the upper end of common oxidation temperatures. This and other published analyses[32] indicate that Ge will not be oxidized if elemental Si is present.

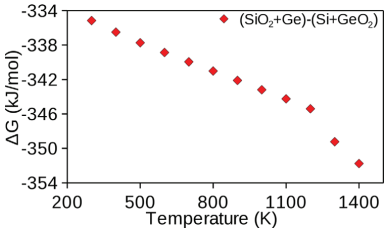

FIG. 4. (Color online) Gibbs energies for the formation of SiO_2 from GeO_2 and Si (Ref. 33).

The analysis of the thermodynamics of Si and Ge oxidation is useful in determining whether Ge will be oxidized in such a tertiary system, but it does not address the question of whether there is a tertiary system, that is, whether Si is present at the oxidation interface. The supply of Si to the oxidizing interface, and thus the exclusive oxidation of Si versus oxidation of both Si and Ge, depends on the diffusion of the constituent species in the thin films. This has been examined by modeling the flows of oxidant through the oxide and of Si through a Ge-rich region adjacent to the oxidizing interface.[22,23,32] Low relative Si flows induced by low temperatures or high oxidant pressures have been recognized as leading to formation of GeO_2.[30,32] Kilpatrick *et al.*[23] have determined a so-called crossover temperature for various oxide thicknesses and oxidation conditions, below which GeO_2 is formed and above which the oxide is exclusively SiO_2. For dry oxidation at 1 atm, this crossover temperature is listed as ~380 °C for very thin oxides and not exceeding ~650 °C for oxides of a few micrometers or more.[23]

The presence of oxidized Ge in the native oxide, as demonstrated in Figs. 1 and 2, may be due to the low diffusion rates of Si and Ge as compared to O at such low temperatures. If Si is fixed due to low diffusion rates at low temperatures during the formation of the native oxide, the surface of the SiGe film would be denuded of metallic Si, allowing for the oxidation of Ge. The very fast oxidation rates for ultrathin oxides during subsequent thermal oxidation may prevent diffusion of enough Si to the outermost surface of the oxide to convert the oxidized Ge to SiO_2 according to the thermodynamics presented in Fig. 4. The Si2p line at the sample surface in both Figs. 1 and 2 confirm the absence of metallic Si in this layer. This may be contrasted to the interface region between the thermal oxide and the SiGe layer. In this interface region, the Si2p and O1s lines indicate the coexistence of Si and SiO_2, while the Ge2p line indicates the absence of any oxidized Ge, which lends further credence to the conclusions presented in Fig. 4 and the accompanying discussion.

The oxidation temperatures used in this study and those that appear most commonly in the literature are between 800 °C and 1000 °C. This is motivated in part by the fact that lower temperatures increase the probability of Ge incorporation into the oxide, which will reduce the pile-up effect and potentially compromise the electrical integrity of the oxide. On the other hand, higher temperatures could lead to melting of the pile-up region, which may have an adverse effect on the oxidation process;[21–23] the melting temperature for Ge is ~940 °C, with the solidus curve passing $Si_{0.25}Ge_{0.75}$ at ~1000 °C.[35]

B. Ge redistribution and the pile-up layer

Given that Ge incorporation into the oxide is not significant under the oxidation conditions considered here, our focus on evaluation of the Ge concentration profile shifts to the SiGe layer, from which Si is leached during oxidation. Figure 3 has shown that a region of elevated Ge concentration occurs at the oxidation front. This pile-up effect has been reported at temperatures as low as 600 °C[23] and as high as 1125 °C.[13] Li *et al.*[20] examined the Ge concentration at the oxidation interface for different oxidation temperatures and times and qualitatively compared the influence of temperature on the oxidation rate to the diffusion of Ge. However, the authors did not examine the Ge concentration away from the interface to give a better description of the overall Ge distribution. A few reports present profiles of Ge distributions for various oxidation times at individual temperatures;[18–21] an approach which is useful for understanding the progression of the pile-up effect over time. Figure 5 takes this approach by presenting data from the present study, showing RBS profiles from $Si_{0.80}Ge_{0.20}$ samples oxidized for various times at 900 °C with an emphasis on the Ge signal. The RBS profiles represent samples with oxide thicknesses between the native oxide for the un-oxidized sample and 575 Å for a sample oxidized for 150 min at 900 °C. The inset shows a wide view of two RBS spectra, including the O, Si, and Ge signals for the un-oxidized and most oxidized samples. In the case of oxidation for 25 min resulting in a 196 Å oxide, there is a distinct pile-up region that is clearly differentiated from the bulk of the SiGe layer. At 67 min (356 Å oxide), the pile-up continues to enhance the Ge concentration and, although there is a Ge gradient, there are not two distinct regions of Ge concentration. At 150 min (575 Å oxide), there is only a single region of high Ge concentration. In the latter sample, there is clearly a pile-up effect, but the resulting stoichiometry is fundamentally different from the dual concentration regions frequently associated with the terms pile-up, snow plow, and germanium-rich layer (GRL) and that are required by core-shell structures.

Figure 6 shows the RBS profiles for $Si_{0.85}Ge_{0.15}$, wherein the channel number has been normalized in such a way as to align the oxide to SiGe interface for all of the samples. This is done in order to illustrate more clearly the development of the pile-up region. The tendency for longer oxidation times to induce higher Ge concentrations is clearly visible. Furthermore, whereas in the non-oxidized sample, the Ge concentration near the oxidation front gradually increases to a plateau value, the longer the sample is oxidized, the steeper the RBS profile becomes at the oxide to SiGe interface. This indicates that the RBS resolution is not

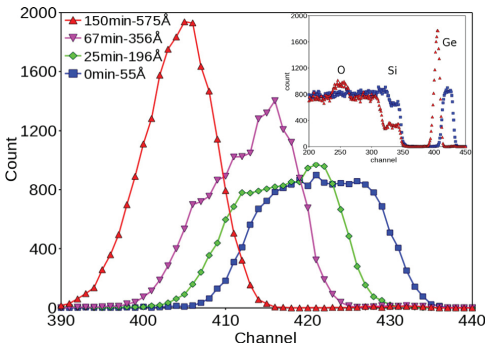

FIG. 5. (Color online) RBS profiles of Ge concentration for $Si_{0.80}Ge_{0.20}$ oxidized at 900 °C for various times, including an un-oxidized sample. The inset shows two spectra with a broader range, including signals for O, Si, and Ge for two samples with very thin and thick oxides. The spectra are labeled by oxidation time and oxide thickness (from ellipsometry.)

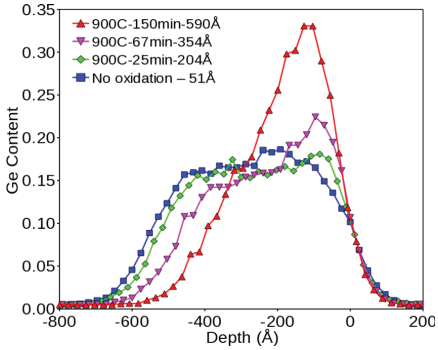

FIG. 6. (Color online) Ge content vs depth from RBS measurements for $Si_{0.85}Ge_{0.15}$ samples with various oxide thicknesses. Excepting the unoxidized sample, the oxidation temperature was 900 °C. The profiles are aligned with the oxidation front at depth zero. The spectra are labeled by oxidation temperature, time, and oxide thickness (from ellipsometry.)

the sole cause for the gradual increase in Ge for the intrinsic samples and that oxidation serves to maximize the Ge concentration at the oxidation front. In contrast, the slope of the RBS profile for the Ge at the interface with the substrate remains reasonably constant with oxidation time. This along with the fact that the depth of the Ge profile decreases with time indicates that there is little or no diffusion of Ge into the substrate. It is possible that oxidation of thicker intrinsic SiGe layers would demonstrate this more clearly by ensuring a longer plateau and distance between the pile-up region and the substrate.

Another approach is presented by Jang *et al.*,[14] who look at pile-up effects at multiple temperatures for a single oxidation time. Although most authors conclude that temperature does influence the Ge profile, they do not effectively compare one temperature to another, because the use of one oxidation time for multiple temperatures results in different amounts of Si having been removed from the SiGe layer by oxidation. To fully appreciate the influence of temperature on the Ge distribution, samples with similar oxide thicknesses should be compared such that the Si removed from the SiGe layer by oxidation is similar for all samples and temperatures. Figure 7 shows such data from $Si_{0.85}Ge_{0.15}$ samples with similar oxide thicknesses which were oxidized at temperatures between 800 °C and 1000 °C. There is no clearly discernible influence of temperature on the Ge concentration profile for a given oxide thickness.

C. Empirical relations for layer thicknesses

The thicknesses of the pile-up and oxide layers that result from thermal oxidation may be determined using ellipsometry, RBS, or TEM. However, it is useful for the experimentalist or technologist to have a simple predictive tool for determining these values before an oxidation is done. To that end, the following discussion presents two relations that may be used in designing nanostructures in oxidized thin films of SiGe.

The term "pile-up" is in fact poorly defined in the literature and can only be described reliably as the tendency to increase the Ge concentration in a region adjacent to the oxidation front. This does not define the Ge profile other than to state that it is higher than it was prior to oxidation. The magnitude and profile of the germanium concentration in the pile-up region will depend on a balance between the oxidation rate and the rate of diffusion of Si through the pile-up region toward the oxidation front. If, however, this system is simplified by removing the effect of the diffusion of Si and also assuming that the pile-up region is 100% Ge, then the thickness of the pile-up region can be calculated directly.

Considering the oxidation of Si; the depth of Si consumed, $t_{Si\text{-}consumed}$, in order to provide enough Si for the formation of an oxide with thickness t_{ox}, is described as

$$t_{Si-consumed} = t_{ox}N_{ox}/N_{Si}, \tag{1}$$

where N_{ox} and N_{Si} are the molecular and atomic densities of the oxide and Si, respectively. Similarly, for the oxidation of SiGe, the depth of SiGe from which Si is extracted to form the oxide layer, $t_{SiGe\text{-}consumed}$, is

$$t_{SiGe-consumed} = t_{ox}N_{ox}/N_{Si-SiGe}, \tag{2}$$

where $N_{Si\text{-}SiGe}$ is the atomic density of Si in the SiGe layer; this assumes exclusive oxidation of Si. If the composition of the initial SiGe layer is described by X, the number of Ge atoms in the SiGe as a fraction of the total, while the total atomic density of the SiGe is N_{SiGe}, then the atomic densities of Si and Ge in the SiGe are

$$N_{Si-SiGe} = N_{SiGe}(1-X) \text{ and } N_{Ge-SiGe} = N_{SiGe}X \tag{3}$$

or

$$N_{Ge-SiGe} = N_{Si-SiGe}X(1-X)^{-1}. \tag{4}$$

If all of the Si atoms are removed from the SiGe layer to a depth of $t_{SiGe\text{-}consumed}$, leaving a layer of pure Ge (i.e., no Si), then

$$N_{Ge-SiGe}t_{SiGe-consumed} = N_{Ge}t_{pileup}, \tag{5}$$

where N_{Ge} is the atomic density of Ge and t_{pileup} is the thickness of the pile-up region. The pile-up thickness may then be found by substitution as

$$t_{pileup} = Xt_{ox}N_{ox}[(1-X)N_{Ge}]^{-1}. \tag{6}$$

Here, the pile-up layer is composed only of Ge, and so t_{pileup} is at its minimum possible value. As the pile-up layer will inevitably contain some Si, Eq. (6) may be rewritten as

$$\begin{aligned} t_{pileup} &= Xt_{ox}N_{ox}[(1-X)N_{Ge-pileup}]^{-1} \\ &= Xt_{ox}N_{ox}[(1-X)X_{pileup}N_{SiGe-pileup}]^{-1}, \end{aligned} \tag{7}$$

where $N_{Ge\text{-}pileup}$ is the atomic density of Ge in the pile-up layer, $N_{SiGe\text{-}pileup}$ is the atomic density of the pile-up layer, and X_{pileup} is the fraction of Ge in the pile-up layer. Equation (7) is a more

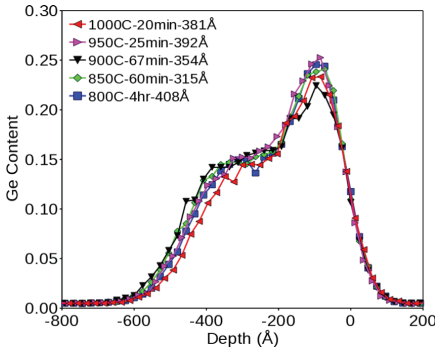

FIG. 7. (Color online) Ge content vs depth from RBS measurements for oxidized $Si_{0.85}Ge_{0.15}$ samples with similar oxide thicknesses but varying oxidation temperatures. The profiles are aligned with the oxidation front at depth zero and labeled according to oxidation temperature, time, and oxide thickness (from ellipsometry.)

general expression and is equivalent to Eq. (6) when $X_{pileup} = 1$.

Equation (6), wherein the pile-up layer is composed entirely of Ge, may serve as a limiting condition, particularly when considering oxidation of SiGe-on-insulator or when oxidizing nanorods. These are situations in which there will be no diffusion of Si from the substrate and, thus, a limited supply of Si for oxidation. Oxidation of such structures beyond a given oxide thickness will lead to the oxidation of Ge due to the absence of Si for oxidation. Three cases can be defined for SiGe-on-insulator systems (with the pre-oxidation SiGe layer thickness written as $t_{SiGe\text{-}initial}$):

i. $t_{ox} > [t_{SiGe\text{-}initial}(1-X)N_{SiGe}/N_{ox}]$; formation of GeO_2;
ii. $t_{ox} = [t_{SiGe\text{-}initial}(1-X)N_{SiGe}/N_{ox}]$; maximum pile-up before GeO_2 formation;
iii. $t_{ox} < [t_{SiGe\text{-}initial}(1-X)N_{SiGe}/N_{ox}]$; Ge pile-up and only SiO_2.

The minimum initial SiGe thickness required to avoid formation of GeO_2 in SiGe-on-insulator systems is then

$$t_{SiGe-initial} = t_{SiGe-consumed} = t_{ox}N_{ox}[(1-X)N_{SiGe}]^{-1}, \quad (8)$$

where N_{SiGe} may be determined through a quadratic fit to the data presented in Dismukes *et al.*,[36] $N_{SiGe} = (5.0214 - 0.5286X - 0.0517X^2)10^{22}$ atoms/cm^3. The assumptions made in arriving at Eq. (8) mandate that absolutely all of the Si in the SiGe layer is oxidized prior to oxidation of Ge. However, Kilpatrick *et al.*[23] point out that Ge and Si will oxidize simultaneously when the flow of O to the oxidation interface outweighs the flow of Si to the same interface. So, in practice, the minimum initial SiGe layer thickness to avoid formation of GeO_2 will be somewhat larger than is predicted by Eq. (8), but it will not be any smaller. For the fabrication of nanowires, consideration of the dimensions of the nanowire must take into account the fact that oxidation will occur from multiple dimensions as well as the likelihood that oxidation will occur at different rates for different crystal facets. This is a similar problem for FINFETS, but, in this case, an oxidation barrier like a SiN cap may be placed on top of the fin in order to limit oxidation to two sides.

The discussion so far has not incorporated diffusion of Si from the substrate. In the event that Si does diffuse toward the oxide from the substrate, some of the Si from the SiGe layer that has been incorporated into the oxide during oxidation will effectively be replaced by Si diffusing from the substrate into the SiGe layer. This effect can be expressed by rearranging Eq. (7) to show the dose of Si in the oxide and that removed from the SiGe layer with the addition of the dose of Si from the substrate, Q_{sub},

$$Q_{sub} + t_{pileup}N_{SiGe-pileup}X_{pileup}(1-X)/X = t_{ox}N_{ox}. \quad (9)$$

The present work and other studies[15–17,37] have used samples with SiGe on Si and provide enough data to give a cursory validation of Eq. (9). Figure 8 uses data from this study as well as data extracted from published work to plot the dose of Si in the oxide, $t_{ox}N_{ox}$, versus the dose of Si removed from the SiGe, $t_{pileup}N_{SiGe\text{-}pileup}X_{pileup}(1-X)/X$. The value used for N_{ox} in Fig. 8 is 2.21×10^{22} Si atoms/cm^3, and the data therein is separated and labeled by the Ge content of the pre-oxidation SiGe layer and the data source.

In the event that Q_{sub} is 0, the dose in the oxide should exactly equal the dose from the pile-up region, and the correlation between the two should have a slope of 1. The data in Fig. 8 shows that this is the case for the small oxide thicknesses, but that the data for larger oxide thicknesses indicate a non-zero value for Q_{sub}. This is quite sensible for the case of small oxide thicknesses, as very little if any of the Si from the substrate will have reached the pile-up or oxide due to the relatively thick SiGe layer it must pass through and the short oxidation time associated with the thin oxide. Regarding the thicker oxides; if all other values are correct, then the value of Q_{sub} indicated would have to be negative, which is not easily explicable, given that Si from the substrate should diffuse into and not out of the SiGe. However, the accuracy with which the variables in Eq. (9) are determined is not perfect, and the results are particularly susceptible to variation in the value used for X. Furthermore, what constitutes the

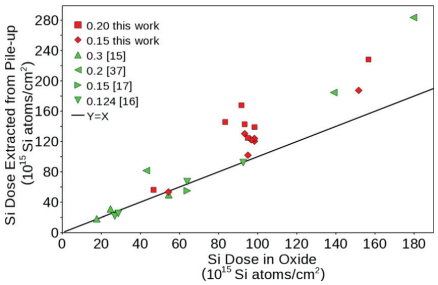

FIG. 8. (Color online) Si dose extracted from the pile-up region, $t_{pileup}N_{SiGe\text{-}pileup}X_{pileup}(1-X)/X$, vs that in the oxide, $t_{ox}N_{ox}$, from Eq. (9) with data from this study and other works (Refs. 15–17 and 37). All data points are labeled by the initial Ge content. The oxide and pile-up thickness data from this study are extracted from RBS measurements. The black diagonal in the plot indicates where the x-values equal the y-values.

thickness of the pile-up region is not well defined in the literature. Smaller values of the pile-up thickness, concentration, or density would help to account for the apparent negative value of Q_{sub} in Fig. 8. The same is true of larger values of the oxide thickness or density or of the initial SiGe concentration. It is clear though that there is no evidence of diffusion of Si from the substrate making any substantial contribution to the dimensions of the oxide or pile-up layer.

D. Determination of the pile-up Ge concentration

The system being discussed can be described by three fundamental fluxes of Si. The first is the flux of Si being consumed by the oxide, J_{ox}, the second is the flux of Si from the SiGe region through the pile-up toward the oxidation front, J_{pileup}, while the third is the flux of Si from the substrate into the SiGe region, $J_{substrate}$.

The relationship between J_{ox} and J_{pileup} is integral to the formation of the pile-up region. Where $J_{ox} > J_{pileup}$, a pile-up region will form, and if this condition remains true for long enough, both Si and Ge will be oxidized and X_{pileup} will be 1, whereas $J_{ox} < J_{pileup}$ will lower the Ge concentration at the oxidation front. The case in which $J_{ox} = J_{pileup}$ will affect a constant Ge concentration at the oxidation front.

The diffusivity of Si in Ge is reported as being five to six orders of magnitude higher than the diffusivity of Si in Si.[38] This will tend to create an abrupt transition between the SiGe region and the pile-up region with nearly constant Ge concentration in the pile-up region. If at first a pile-up region composed entirely of Ge is formed and J_{ox} is both independent of X_{pileup} and less than J_{pileup}, the Ge concentration in the pile-up region will decrease, thereby decreasing J_{pileup} until either $J_{pileup} = J_{ox}$ or until the pile-up concentration equals the concentration of the infinite source (the initial SiGe concentration in this case.) In this way, X_{pileup} is determined by balancing the flux of silicon to the oxidation front and the flux of silicon consumed by oxidation and can be considered a single value because of the assumption of an abrupt transition between the SiGe layer and the pile-up layer. This makes the oxidation rate a determining factor in the formation of the pile-up region.

The relationship between $J_{substrate}$ and J_{pileup} are synonymous to that between J_{pileup} and J_{ox}. Given that the diffusivity of Si in Ge is orders of magnitude higher than it is in Si and that a pile-up region exists with a Ge concentration that is higher than the initial SiGe concentration, the condition where $J_{substrate} > J_{pileup}$ should never occur. It would then also be true that lower initial Ge concentrations will minimize the contribution of $J_{substrate}$ to the formation of the pile-up region. More precisely, the contribution of $J_{substrate}$ to the formation of the pile-up will decrease as the ratio X/X_{pileup} goes from 1 to 0. In the extreme case where $X = 1$ and $J_{substrate} = 0$, there is no Si to be oxidized and no pile-up region. This situation may be extended to any condition in which $X/X_{pileup} > 1$, whether $X = 1$ or $X_{pileup} < X < 1$. The implication of this is that, if J_{ox} acts to limit the value of X_{pileup} to less than 1, then there will exist a maximum value of X, below which a pile-up region may form and above which no pile-up will occur. The case where X is very close to 0 will minimize the influence of $J_{substrate}$ and will maximize the pile-up effect by maximizing the contrast between the Ge concentration in the initial SiGe layer and the pile-up region (i.e., minimizing the X/X_{pileup} ratio). Thicker initial layers of SiGe will also minimize the influence of $J_{substrate}$.

If the Ge concentration is constant throughout the pile-up region and the entirety of the Si in the pile-up region and the oxide is considered to be supplied by diffusion of Si, then the post oxidation Ge content may be written as the sum of doses from diffusion and the doses in the resulting oxide and pile-up region,

$$\begin{aligned} Q_{diffusion} &= Q_{ox} - Q_{sub} + Q_{pileup} \\ &= (Q_{ox} - Q_{sub})\{1 + (1 - X_{pileup})X/[X_{pileup}(1 - X)]\}, \end{aligned} \tag{10}$$

where $Q_{diffusion}$ is the dose of Si supplied to the pile-up from J_{pileup} (i.e., from the initial SiGe layer), $Q_{ox} = t_{ox}N_{ox}$ is the dose of Si in the oxide, and $Q_{pileup} = t_{pileup}N_{SiGe\text{-}pileup}(1 - X_{pileup})$ is the dose of Si remaining in the pile-up region after oxidation. Substitution of t_{pileup} from Eq. (9) allows the simplification of Eq. (10).

Figure 9 shows the values of X_{pileup} that satisfy Eq. (10) versus the oxide thickness; the data presented is for five temperatures and is labeled accordingly. The value of t_{ox}, and thus Q_{ox}, for various oxidation times and temperatures is found by modeling the oxide thickness with the Massoud[39] model while using oxidation rate constants for Si published therein. The value of $Q_{diffusion}$ is determined using a pre-deposition diffusion model while defining the initial SiGe layer as the infinite source and the pile-up layer as the medium into which Si is diffusing. The diffusivity of Si in the said medium is defined by X_{pileup} and is estimated from published values.[38] The initial SiGe region is thick (e.g., ~100 nm) and has a low value of X (0.05), such that the contribution of $J_{substrate}$ to the formation of the oxide and pile-up layer may be neglected. Use of a Ge concentration, X, of 5% for the initial SiGe layer also ensures that the assumptions of an infinite source associated with a pre-deposition model and Si oxidation constants are appropriate approximations. The flatness of the curves in Fig. 9 reflect a close correlation between J_{ox} and J_{pileup}, except for oxide thicknesses very close to 0.

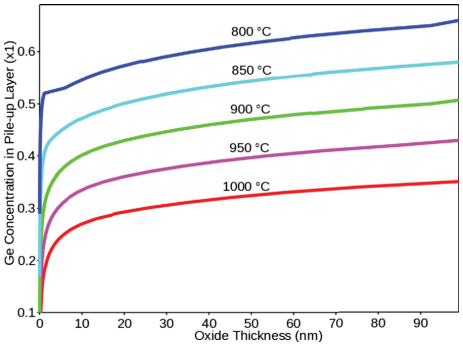

FIG. 9. (Color online) Ge concentration in the pile-up layer, X_{pileup}, that satisfies Eq. (10) vs the oxide thickness.

The influence of X_{pileup} on the relationship between J_{ox} and J_{pileup} may be seen by considering the ratio between the left- and right-hand sides of Eq. (10). Figure 10 shows this ratio as a function of oxide thickness (analogous to oxidation time), as determined by the Massoud[39] model. The data presented is for five values of X_{pileup} and is labeled accordingly, while X is fixed at 0.05 and the temperature is fixed at 1000 °C. A value of 1 indicates the Ge concentration for which Eq. (10) is satisfied. Small changes in X_{pileup} cause a drastic deviation from the equilibrium condition, where the scaled ratio of doses is 1. The value of X_{pileup} that satisfies Eq. (10) remains quite stable over a range of oxide thicknesses.

Figure 11 shows the same scaled ratio of doses for the same five values of X_{pileup} as in Fig. 10, but plotted against temperature and for a fixed oxide thickness of 50 nm. Figure 11 suggests that X_{pileup} has a limited dependence on temperature, though the data in Fig. 7 suggest that this dependence is substantially smaller. The stability of the value of X_{pileup} over a range of oxidation thicknesses suggested by Figs. 9 and 10 and the results in Fig. 11 suggest that there is a limited range of pile-up concentrations that may be achieved by oxidation in the sub-100-nm region and particularly in the linear oxidation regime, which is dominated by a nearly constant oxidation rate.

This analysis suggests that variation of the oxidation temperature during the oxidation could be a realistic means to control the pile-up concentration, but that the range of achievable pile-up concentrations is limited. In discussion of their own modeling results, Kilpatrick *et al.*[23] also mention the limited dependence of X_{pileup} on temperature, but they do not demonstrate the point. If temperature variation is used to control the pile-up concentration, the pile-up thickness could be controlled by modification of the oxidation time and the initial SiGe concentration. However, wet oxidation or controlled oxidant pressure would be more effective methods of controlling X_{pileup}, as they act to modify the oxidation rate without simultaneously altering the diffusion of Si in SiGe, as happens with temperature changes.

E. Oxidation rate dependence on pile-up concentration

The discussion, so far, has assumed that the oxidation rate of SiGe alloys is the same as or close to that of Ge-free

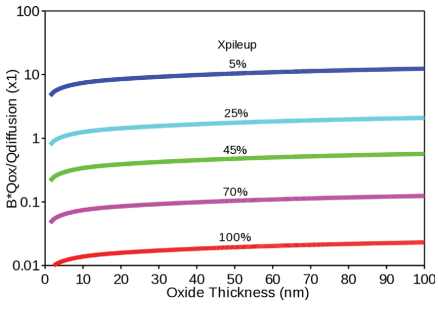

FIG. 10. (Color online) A plot of the scaled ratio of doses from Eq. (10) vs oxide thickness. Here, $B = \{1 + (1 - X_{pileup})X/[X_{pileup}(1 - X)]\}$.

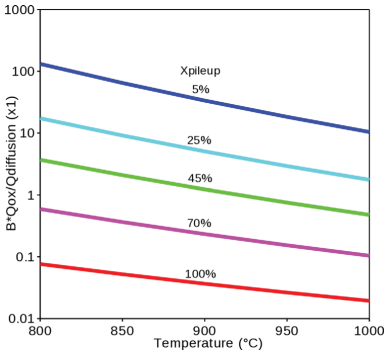

FIG. 11. (Color online) A plot of the scaled ratio of doses from Eq. (10) vs temperature. Here, $B = \{1 + (1 - X_{pileup})X/[X_{pileup}(1 - X)]\}$.

Si and may be described by the Massoud[39] or Deal and Grove[40] models. If the oxidation rate of SiGe is enhanced or slowed as a function of Ge concentration, then the pile-up layer concentration will be integral to determining the oxidation rate. Recognizing that higher Ge concentrations act as a catalyst for diffusion of Si in SiGe alloys, if variation in Ge concentrations influence the oxidation rate of SiGe, then the two effects will create a feedback loop between J_{ox} and J_{pileup}. With the starting assumption that $J_{ox} = J_{pileup}$ and since higher Ge concentrations lead to higher fluxes of Si in SiGe, there are five cases to consider for comparison of the rate of change of flux with respect to Ge concentration in the pile-up:

i. $dJ_{pileup}/dX_{pileup} < dJ_{ox}/dX_{pileup}$; the thermodynamic preference for oxidation of Si will initiate an increase in X_{pileup}, leading to $J_{ox} > J_{pileup}$ and then to $X_{pileup} = 1$ and the oxidation of Ge
ii. $dJ_{pileup}/dX_{pileup} = dJ_{ox}/dX_{pileup}$; published values[38] for diffusivity of Si in SiGe and a common model, like the pre-deposition model, would lead to orders of magnitude difference in the oxidation rate of SiGe between $X = 0$ and $X = 1$. The data from this study does not support this case.
iii. $dJ_{pileup}/dX_{pileup} > dJ_{ox}/dX_{pileup} > 0$; an increase in X_{pileup} causes a smaller value of J_{ox}/J_{pileup}, which leads to a disproportionately large drop in X_{pileup}
iv. $dJ_{pileup}/dX_{pileup} > dJ_{ox}/dX_{pileup} = 0$; although an increase in X_{pileup} will increase J_{pileup}, no feedback occurs and J_{ox} is unaffected
v. $-dJ_{pileup}/dX_{pileup} < dJ_{ox}/dX_{pileup} < 0$; an increase in X_{pileup} causes a larger value of J_{ox}/J_{pileup}, which leads to a disproportionately large increase in X_{pileup}
vi. $-dJ_{pileup}/dX_{pileup} > dJ_{ox}/dX_{pileup}$; an initial increase in X_{pileup} leads to a lower oxidation rate, J_{ox}/J_{pileup}, and X_{pileup}. The associated drop in J_{pileup} is not sufficient to compensate for the drop in J_{ox}, and X_{pileup} is forced toward X, making the pile-up layer disappear.

If Ge acts as either a catalyst or inhibitor for the oxidation of Si in SiGe alloys, then the oxidation rate will vary as a function of X_{pileup}. Holland *et al.*[26] recognize this point and

suggest that a difference in binding energy of Si to Si and Si to Ge at the oxidation front is responsible for Ge acting as a catalyst. However, their analysis relies on correlation of Ge implant doses (i.e., X) to oxide thickness rather than explicitly correlating oxidation rate to X_{pileup}. The influence of X, temperature, time, pressure, and the oxidation ambient on oxidation rate must be decoupled from their influence on X_{pileup} in order to determine how and whether Ge acts as a catalyst or inhibitor for oxidation of Si.

IV. SUMMARY AND CONCLUSIONS

This study addresses several fundamental aspects of the oxidation-induced redistribution of Ge in thin films of SiGe, including the incorporation of Ge into the oxide and the formation of what is alternatively referred to as pile-up, snowplow, or a germanium-rich layer. The dynamics of the formation of a pile-up layer are explored, with attention given to the influence of oxidation temperature on Ge redistribution and formation of a pile-up region. This is done with novel observations and is motivated by the use of thermal oxidation for nanostructuring and device fabrication with SiGe. The analysis is supported by experimental evidence from RBS, XPS, and ellipsometry measurements, as well as simulations. The focus of the study is on oxidation of epitaxial thin films (< 100 nm) of $Si_{1-X}Ge_X$ in dry O_2 at 1 atm and 800 °C, 850 °C, 900 °C, 950 °C, and 1000 °C.

The oxidization of SiGe in the temperature range between 800 °C and 1000 °C at ambient pressures has been demonstrated to avoid the incorporation of Ge into the SiO_2 layer. As predicted by an analysis of the Gibbs free energies, the preferential oxidation of Si is supported by observations made by XPS. The XPS profiles show limited oxidized Ge in the native oxide, while no oxidized Ge is present in the thermal oxide or the Si-rich region of the SiGe to SiO_2 interface.

RBS data shows longer oxidation times, leading to an increase of Ge content in the pile-up region and eventually creating a single high Ge content pile-up layer by entirely consuming the initial SiGe layer. The pile-up effect was shown to occur at the oxidation interface, with the highest Ge content occurring at the same interface. For a given oxide thickness, the redistribution of Ge and the formation of a pile-up region was shown by RBS data to be independent of temperature in the range between 800 °C and 1000 °C. Simulations using common models for the oxidation of Si and diffusion of Si in SiGe indicate that temperature does have an influence on the composition of the pile-up layer, though the range of achievable compositions is limited. The flux of Si due to diffusion of Si in SiGe relative to the oxidation-induced flux of Si out of the SiGe is integral to the formation and dimensions of a pile-up region.

Two predictive relations were derived for describing the dynamics of oxidation of SiGe. The first relation is given for determining the pile-up layer thickness as a function of oxide thickness and the composition of the pile-up layer. The second relation assumes a limited supply of Si and is for determination of the minimum initial thickness of a SiGe layer to avoid oxidation of Ge. The validity of these equations was confirmed by RBS and XPS data from this study as well as values from TEM and XRD from other studies. The proposed models may be used in nanostructuring thin films of SiGe by oxidation and in the design of core-shell structures and transistors.

ACKNOWLEDGMENTS

The authors gratefully acknowledge the NSE-IM2NP team and NanoTecMat platform for providing the SiGe samples and the Norwegian Research Council for financial support by way of the FRINAT program.

[1]Y. Park, G. C. King, and S. H. Choi, J. Cryst. Growth **310**, 2724 (2008).
[2]I. Lagnado and P. R. de la Houssaye, Microelectron. Eng. **59**, 455 (2001).
[3]H. S. Gamble, B. M. Armstrong, P. T. Baine, Y. H. Low, P. V. Rainey, Y. W. Low, D. W. McNeill, S. J. N Mitchell, J. H. Montgomery, and F. H. Ruddell, Mater. Sci. Semicond. Process. **11**, 195 (2008).
[4]K. L. Wang, S. G. Thomas, and M. O. Tanner, J. Mater. Sci: Mater. Electron. **6**, 311 (1995).
[5]S. E. Thompson, M. Armstrong, C. Auth, M. Alavi, M. Buehler, R. Chau, S. Cea, T. Ghani, G. Glass, T. Hoffman, C.-H. Jan, C. Kenyon, J. Klaus, K. Kuhn, Z. Ma, B. Mcintyre, K. Mistry, A. Murthy, B. Obradovic, R. Nagisetty, P. Nguyen, S. Sivakumar, R. Shaheed, L. Shifren, B. Tufts, S. Tyagi, M. Bohr, and Y. El-Mansy, IEEE Trans. Electron Devices **51**(11), 1790 (2004).
[6]S. Balakumar, K. D. Buddharaju, B. Tan, S. C. Rustagi, N. Singh, R. Kumar, G. Q. Lo, S. Tripathy, and D. L. Kwong, J. Electron. Mater. **38**(3), 443 (2009).
[7]N. Singh, K. D. Buddharaju, S. K. Manhas, A. Agarwal, S. C. Rustagi, G. Q. Lo, N. Balasubramanian, and D.-L. Kwong, IEEE Trans. Electron Devices **55**(11), 3107 (2008).
[8]A. I. Hochbaum and P. Yang, Chem. Rev. **110**(1), 527 (2010).
[9]M. Spadafora, A. Terrasi, S. Mirabella, A. Piro, M. G. Grimaldi, S. Scalese, E. Napolitani, M. Di Marino, D. De Salvador, and A. Carnera, Mater. Sci. Semicond. Process. **8**, 219 (2005).
[10]F. K. LeGoues, R. Rosenberg, and B. S. Meyerson, Appl. Phys. Lett. **54**(7), 644 (1989).
[11]Y. S. Lim, J. S. Jeong, J. Y. Lee, H. S. Kim, H. K. Shon, H. K. Kim, and D. W. Moon, Appl. Phys. Lett. **79**(22), 3606 (2001).
[12]Z. Di, P. K. Chu, M. Zhang, W. Liu, Z. Song, and C. Lin, J. Appl. Phys. **97**, 064504 (2005).
[13]D. Nayak, K. Kamjoo, J. C. S. Woo, J. S. Park, and K. L. Wang, Appl. Phys. Lett. **56**(1), 66 (1990).
[14]J. H. Jang, S. Y. Son, W. Lim, M. S. Phen, K. Siebein, S. J. Pearton, and V. Craciun, Appl. Phys. Lett. **94**, 202104 (2009).
[15]B. G. Min, J. H. Yoo, H. C. Sohn, D. H. Ko, M. H. Cho, K. B. Chung, and T. W. Lee, Thin Solid Films **518**, 2065 (2010).
[16]Y. S. Lim, J. S. Jeong, J. Y. Lee, H. S. Kim, H. K. Shon, H. K. Kim, and D. W. Moon, J. Electron. Mater. **31**(5), 529 (2002).
[17]M. Spadafora, G. Privitera, A. Terrasi, S. Scalese, C. Bongiorno, A. Carnera, M. Di Marino, and E. Napolitani, Appl. Phys. Lett. **83**(18), 3713 (2003).
[18]J. P. Zhang, P. L. F. Hemment, S. M. Newstead, A. R. Powell, T. E. Whall, and E. H. C. Parker, Thin Solid Films **222**, 141 (1992).
[19]B.-G. Min, Y. H. Pae, K. S. Jun, D.-H. Ko, H. Kim, M.-H. Cho, and T.-W. Lee, J. Appl. Phys. **100**, 016102 (2006).
[20]C. Li, K. Cai, Y. Zhang, H. Lai, and S. Chen, J. Electrochem. Soc. **155**(3), H156 (2008).
[21]T. Shimura, M. Shimizu, S. Horiuchi, H. Watanabe, K. Yasutake, and M. Umeno, Appl. Phys. Lett. **89**, 111923 (2006).
[22]Y. Zhang, C. Li, K. Cai, Y. Chen, S. Chen, H. Lai, and J. Kang, J. Appl. Phys. **106**, 063508 (2009).
[23]S. J. Kilpatrick, R. J. Jaccodine, and P. E. Thompson, J. Appl. Phys. **81**(12), 8018 (1997).
[24]M. A. Rabie, Y. M. Haddara, and J. Carette, Nanotechnology **3**, 21 (2005).
[25]M. A. Rabie, Y. M. Haddara, and J. Carette, J. Appl. Phys. **98**, 074904 (2005).
[26]O. W. Holland, C. W. White, and D. Fathy, Appl. Phys. Lett. **51**(17), 520 (1987).
[27]S. Tanuma, C. J. Powell, and D. R. Penn, Surf. Interface Anal. **20**, 77 (1993).

[28]C. J. Powell and A. Jablonski, *NIST Electron Inelastic Mean Free Path Database, Version 1.1* (National Institute of Standards and Technology, Gaithersburg, MD, 2000).
[29]I.-M. Lee and C. G. Takoudis, J. Vac. Sci. Technol. A **15**(6), 3154 (1997).
[30]S. J. Kilpatrick, R. J. Jaccodine, and P. E. Thompson, J. Appl. Phys. **93**(8), 4896 (2003).
[31]R. J. Jaccodine and S. J. Kilpatrick, Proc. Electrochem. Soc. **2005-05**, 542 (2005).
[32]D. C. Paine, C. Caragianis, and A. F. Schwartzman, J. Appl. Phys. **70**(9), 5076 (1991).
[33]I. Barin, *Thermochemical Data of Pure Substances*, 2nd ed. (VCH, Weinheim, 1993).
[34]J. E. Castle, H. D. Liu, and N. Saunders, Surf. Interface Anal. **20**(2), 149 (1993).
[35]H. Stöhr and W. Klemm, Z. Anorg. Allg. Chem. **241**(4), 305 (1939).
[36]J. P. Dismukes, L. Ekstrom, and R. J. Paff, J. Phys. Chem. **68**(10), 3021 (1964).
[37]N. Daval, E. Guiot, K. K. Bourdelle, M. Kennard, I. Cayrefourcq, T. Akatsu, C. Mazure, H. Cerva, and A. Rucki, ECS DECON **2005-10**, 42 (2005).
[38]R. Kube, H. Bracht, J. Lundsgaard Hansen, A. Nylandsted Larsen, E. E. Haller, S. Paul, and W. Lerch, J. Appl. Phys. **107**, 073520 (2010).
[39]H. Z. Massoud, J. D. Plummer, and E. A. Irene, J. Electrochem. Soc. **132**(11), 2685 (1985).
[40]B. E. Deal and A. S. Grove, J. Appl. Phys. **36**(12), 3770 (1965).

Article III

Ge concentrations in pile-up layers of sub-100-nm SiGe films for nano-structuring by thermal oxidation

E. Long, A. Galeckas, and A. Yu. Kuznetsov

Journal of Vacuum Science and Technology B **30**(4), 041212 (2012)

Ge concentrations in pile-up layers of sub-100-nm SiGe films for nano-structuring by thermal oxidation

Ethan Long,[a] Augustinas Galeckas, and Andrej Yu Kuznetsov
Department of Physics/Centre for Materials Science and Nanotechnology, University of Oslo, P.O. Box 1048 Blindern, N-0316 Oslo, Norway

(Received 8 April 2012; accepted 23 June 2012; published 10 July 2012)

The data and analysis presented herein aims to facilitate the design and manufacture of SiGe based nanostructures and devices by describing the enhancement of Ge concentration in sub-100-nm thin films of SiGe by dry thermal oxidation. Thin films of SiGe were restructured by using thermal oxidation induced self-organization of Si and Ge atoms to create a layer of enhanced Ge concentration. The dry thermal oxidations were carried out at temperatures between 800 °C and 1000 °C. The influence of temperature on the Ge content at the oxidation front, as measured by x-ray diffraction, is examined and supported by simulation results. A model for determination of the Ge content in the pile-up layer is presented along with appropriate values for the activation energy and pre-exponential constant for diffusion of Si in $Si_{1-X}Ge_X$. This model may also be used for determination of the diffusivity of Si in $Si_{1-X}Ge_X$ by fitting the model results to the measured Ge concentration in the pile-up layer. It is observed that the Ge content at the oxidation front is a function of temperature and varies linearly between 64% at 800 °C and 36% at 1000 °C. However, the Ge content is largely independent of oxide thickness and the Ge content in the initial SiGe layer. When the Ge concentration at the oxidation front is considered, the experimental results presented here indicate that the oxidation rates of SiGe closely match those of Si and provide evidence that the presence of Ge in very thin films of SiGe does not lead to enhanced or retarded oxidation rates as compared to Si. © *2012 American Vacuum Society*. [http://dx.doi.org/10.1116/1.4736982]

I. INTRODUCTION

There has been substantial interest in the oxidation of silicon germanium (SiGe) as it pertains to transistor and nanowire design and fabrication. Commercialization of multiple gate field effect transistors and incorporation of Ge into Si CMOS processing has been motivated by SiGe's utility in creating high mobility channels,[1] reduction of parasitic effects like drain induced barrier lowering in deep sub-micron devices,[2] and creation of other novel gate architectures and nanowire transistors.[3,4] The potential of SiGe core-shell constructions in photovoltaics is also a new and promising application.[5]

An integral aspect of the thermal oxidation of SiGe is the tendency towards self-organization of Si and Ge atoms within the SiGe and oxide structure. The selective oxidation of Si tends to separate Si from Ge and creates a region of enhanced Ge concentration in the SiGe. This Ge rich region occurs adjacent to the SiO_2 growth front and is alternately referred to as a pile-up region, snow plow effect, or germanium rich layer. Such manipulation of the Ge content in SiGe is concomitant with manipulation of the bandgap. Furthermore, by taking advantage of the variable dependencies of the diffusivities of common dopants (e.g., B, P, As, and Sb) on Ge concentration, creation of Ge concentration gradients by thermal oxidation could allow for creation of dopant profiles, and thus electronic or opto-electronic devices. However, this sort of nanostructure design and fabrication requires a thorough understanding of the mechanisms and dependencies governing the formation of the pile-up region.

Understanding the redistribution of Ge due to thermal oxidation requires knowledge of the dependence of the oxidation rate on the Ge concentration at the oxidation front. Although the oxidation of Si is described by the well established Deal–Grove[6] and Massoud[7] models, the oxidation of SiGe is not as well characterized. A variety of oxidation conditions have been investigated including dry,[8] wet,[9] ozone,[10] fluorine[11] ambients, oxygen plasma,[12] UV assisted oxidation,[13] a variety of pressures,[14] initial germanium concentrations,[15] and oxide thicknesses, as well as SiGe-on-insulator.[15] Several models have been proposed to describe the oxidation processes in SiGe,[11,16–19] all of which consider the relative diffusion of O in SiO_2 and that of Si in SiGe and Ge. There have been several publications which discuss oxidation rates for SiGe in dry O_2, though, each of them focuses on a limited range of conditions and oxide thicknesses.[8,15,20–33] Despite the work that has been done to study oxidation of SiGe, a lack of consensus remains regarding oxidation rates for SiGe as compared to that of Si. This lack of consensus becomes clear if one considers reports of the oxidation rate of SiGe in dry O_2 being the same as,[8,23,24] faster than,[20–22,28,29] and slower than[15,32,33] that of Si. It is obvious that there is substantial variation in the data between published works which is aggravated by the limited range of temperatures and oxide thicknesses as well as the sometimes exotic oxidation conditions in individual studies. More importantly, those studies that have investigated the influence of Ge concentration on the oxidation rate of SiGe have only considered the Ge concentration in the initial SiGe layer

[a]Author to whom correspondence should be addressed; electronic mail: ethanl@smn.uio.no

and not the concentration at the oxidation interface. If the Ge concentration influences the oxidation rate of SiGe, then the critical concentration will be that at the oxidation front, rather than that in the initial SiGe layer. This serves as a fundamental motivation for the present work's effort to characterize the Ge concentration in the pile-up region.

The present study focuses on description of the Ge content in the pile-up layer of sub-100-nm films of SiGe that have been subjected to dry thermal oxidation. A linear dependence of the Ge content in the pile-up layer on the oxidation temperature is shown using data measured by x-ray diffraction and supported by simulation. A model for determination of the Ge content in the pile-up layer, based on the diffusivity of Si in SiGe, oxidation time and temperature, and oxide thickness, is presented and compared to measured data. The model and measured data for the Ge concentration in the pile-up layer are used to determine the activation energy and pre-exponential constant for diffusion of Si in SiGe. The present work in combination with previous work[19] provides the empiric relations, theory, and analysis necessary to design and construct nanostructured thin films of SiGe by dry thermal oxidation.

II. EXPERIMENT

Fully strained epitaxial layers of $Si_{1-X}Ge_X$ on a 100 nm Si buffer layer were grown on (100) oriented Si substrates by molecular beam epitaxy. The $Si_{1-X}Ge_X$ layer thicknesses for the two wafers used were 80 nm and 70 nm for $X = 0.15$ and $X = 0.20$, respectively. A third Si (100) wafer was used as a control sample. The thermal oxidation was done using a tube furnace at ambient pressure and flushed with dry O_2. For a given oxidation time and temperature, three samples, Si, $Si_{0.85}Ge_{0.15}$, and $Si_{0.80}Ge_{0.20}$, were oxidized simultaneously in order to ensure identical oxidation conditions for the three stoichiometries. Oxidation was carried out at 800 °C, 850 °C, 900 °C, 950 °C, and 1000 °C with the oxidation times adjusted to provide a series of oxide thicknesses between the native oxide and 60 nm for each temperature. The native oxides were not removed prior to oxidation but their thicknesses have been taken into account when calculating oxidation rates.

Oxide thicknesses were measured by ellipsometry at 632.8 nm and 830.0 nm wavelengths and 70° angle of incidence with each sample being measured five times at each wavelength in order to account for random error in the measurements. The ellipsometry analysis was carried out using a three layer model and treating the oxide, pile-up layer, and SiGe layer thicknesses as well as the index of refraction for the pile-up layer as unknowns. The modeled and measured delta and psi data were analyzed by calculating the minimum mean squared error for the stated unknowns.

A subset of 16 samples was used to check the ellipsometry results against those found using Rutherford backscattering spectrometry (RBS). RBS measurements were done with 2 MeV 4He+ ions backscattered into the detector at 100° relative to the incident beam direction. This glancing-angle detector geometry was used to provide enhanced depth resolution for accurate analysis of films near the surface region. The oxide thicknesses were determined by fitting simulated curves to the experimentally determined RBS spectra. For the purpose of comparing the oxide thicknesses determined by ellipsometry to those determined by RBS, the uncertainty in the ellipsometry measurements may be calculated while presuming the RBS values to be the actual values. With such a presumption the sample standard deviation in the ellipsometry measurements was calculated to be 3.8 nm.

The thickness and Ge concentration of the SiGe layers were measured using x-ray diffraction (XRD). A Bruker AXS x-ray diffractometer in double axis configuration and CuKα1 radiation was used to conduct 2θ-ω scans of the (004) peak for each sample. The incident beam was conditioned to remove CuKα2 radiation using a Göbel mirror and Ge monochromator. A point source detector in "1 D" mode was used on the secondary side to maximize the count rates. The profiles from the 2θ-ω scans were fit using a three layer model and the Leptos simulation software with data for lattice constants from Dismukes *et al.*[34] Reciprocal space maps focusing on the $\pm(113)$ and $\pm(224)$ peaks from a limited number of samples were used to confirm that the SiGe layers were fully strained before and after oxidation.

III. RESULTS AND DISCUSSION

In order to design and construct nanostructures in SiGe by using thermal oxidation to create a layer of enhanced Ge concentration, or to evaluate the influence of Ge on the oxidation rate of SiGe, it is first necessary to estimate the degree to which Ge is concentrated at the oxidation front. To this end, XRD is used to provide a measure of the Ge concentration in the pile-up layer by measuring the lattice constant in the various layers of the oxidized SiGe samples. As an example of the XRD measurements used, Fig. 1 shows the 2θ-ω scans of the (004) peak of several samples of $Si_{0.80}Ge_{0.20}$ oxidized at five temperatures between 800 °C and 1000 °C as well as the scan for an unoxidized sample (labeled pre-oxidation in the graph). The three peaks for each sample correspond to three distinct layers in the sample, those three layers being the substrate, the primary SiGe layer, and the pile-up layer. The primary SiGe layer is synonymous with the initial SiGe layer except that the initial SiGe layer is specific to the layer prior to any oxidation. Reciprocal space mapping of selected samples showed layer peaks that indicate no relaxation in the layers, and as such, the positions of the peaks along the 2θ axis in Fig. 1 correlate to the lattice spacing, and hence the Ge concentration, in the respective layer. The peak from the Si substrate, visible on the right hand side at about 69.129°, was used to align the samples to one another. The peak from the pile-up layer occurs on the far left, the lower angles indicating higher Ge concentrations. There are two critical aspects of the pile-up layer peaks. First, the peak for the pile-up layer is shifted substantially and consistently to the left of the peak for the primary SiGe layer, confirming the presence of a distinct pile-up layer. Second, as the oxidation temperature is

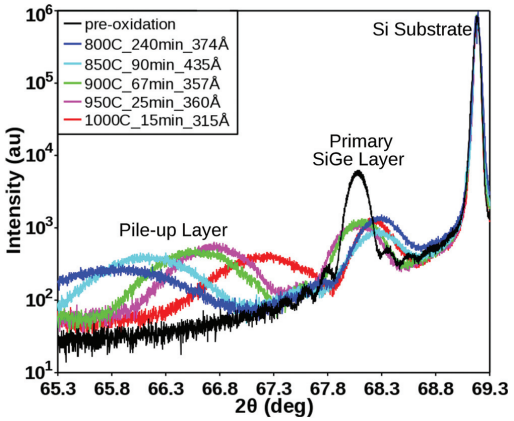

FIG. 1. (Color) XRD intensity profiles of the (004) peaks of $Si_{0.8}Ge_{0.2}$ samples oxidized at various temperatures and times as well as an unoxidized sample. Intensity peaks for the Si substrate, primary SiGe layer, and the pile-up layer are shown. The samples are labeled by oxidation temperature, time, and oxide thickness, while the unoxidized sample is labeled "pre-oxidation."

lowered, the Ge concentration in the pile-up layer increases, as is indicated by the pile-up peak shifting to lower 2θ angles. The sample that was not oxidized does not show a peak for the pile-up layer and has a more intense peak for the primary SiGe layer than is present for the oxidized samples, indicating the absence of a pile-up layer and a relatively thick primary SiGe layer.

The data for the Ge concentration in the pile-up layers that was extracted from the XRD measurements and the oxide thicknesses, as measured by ellipsometry, are presented in Fig. 2. With regard to the Ge content in the pile-up layer, since there was no discernible difference between the samples with an initial layer Ge content of 15% and those with 20%, this distinction is not made in Fig. 2. This leaves oxidation temperature and time as the two oxidation parameters that may influence the Ge content in the pile-up layer. For any given temperature, oxide thickness is a reflection of the oxidation time, and so, comparing Ge concentration in the pile-up layer to the oxide thickness will highlight the role of oxidation time in determining the Ge content in the pile-up layer. If the data in Fig. 2 is viewed without regard to temperature, the scattering of data makes it clear that any correlation between the Ge concentration in the pile-up layer and the oxide thickness is negligible for the range of oxide thicknesses considered here. The lack of correlation between Ge content in the pile-up and the oxide thickness remains true when the oxidation temperature is considered. Furthermore, consideration of the oxidation temperature highlights that the influence of temperature on Ge content is substantially more important than that of oxidation time. For any given temperature, the data in Fig. 2 appears at a roughly constant value of Ge concentration in the pile-up. As the oxidation temperature decreases, the value of Ge concentration in the pile-up increases. The importance of temperature in determining the Ge content in the pile-up layer is related to the role of temperature in determining the diffusivity of oxidant in the oxide relative to that of Si in SiGe.

The Si that composes the oxide is drawn from the pile-up region and must translate into either a higher Ge content in the pile-up or an increased pile-up layer thickness. So, it is logically correct that, whereas the Ge content in the pile-up is essentially independent of the oxide thickness, the thickness of the pile-up layer is well correlated to the oxide thickness. The empirical data in Fig. 3 supports this conclusion and provides perspective on the magnitude of the pile-up layer thicknesses being discussed. Figure 3 shows the pile-up thickness as measured by XRD versus the oxide thickness

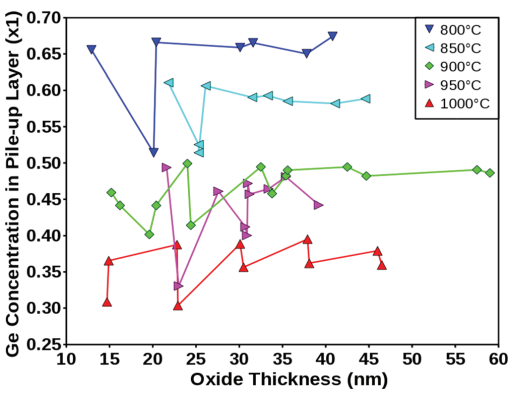

FIG. 2. (Color online) Ge concentration in the pile-up layer plotted against oxide thickness for samples oxidized at various temperatures and labeled accordingly. Ge concentrations are determined by XRD; oxide thicknesses are determined by ellipsometry. The lines connecting the measured data points are for visual guidance only.

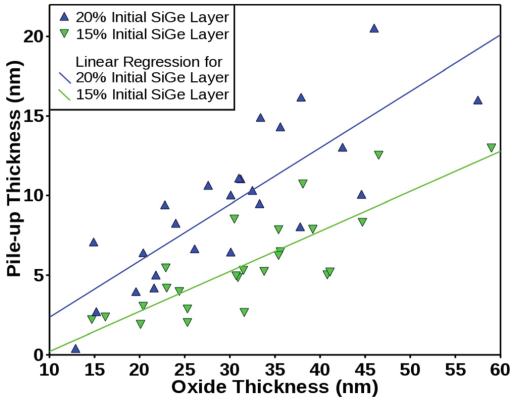

FIG. 3. (Color online) Pile-up layer thicknesses of $Si_{0.85}Ge_{0.15}$ and $Si_{0.8}Ge_{0.2}$ samples plotted against oxide thickness. The pile-up layer thicknesses are determined by XRD; oxide thicknesses are determined by ellipsometry. Linear fits to the measured data are included to aid in visual interpretation of the data.

from ellipsometry. The pile-up thicknesses tend to be lower for the 15% Ge initial layers than for the 20% Ge initial layers which is sensible considering the dynamics of formation of the pile-up layer. In both cases, longer oxidation times, represented by larger oxide thicknesses, lead to thicker pile-up layers.

Measuring the Ge content in ultra thin layers of SiGe using XRD does involve some degree of uncertainty. As the thickness of a layer of SiGe approaches zero, the signal from the layer in an XRD scan becomes vanishingly small and confounded by noise. As such, the instrumental setup used in this study was designed to maximize the signal and minimize the noise in order to highlight even thin layers of SiGe. Even so, there remains some uncertainty in the measurements, and noting that oxide thickness correlates to the thickness of the pile-up layer, this uncertainty is evident in the increased scattering of Ge concentration data at very small oxide thicknesses in Fig. 2.

A direct comparison between oxidation temperature and Ge content in the pile-up layer is warranted here. Figure 4 shows the Ge concentration in the pile-up layer from XRD for samples oxidized at various temperatures and with a variety of oxide thicknesses. The measured data is presented alongside values determined by simulation. The simulations were conducted by using a predeposition model to calculate the dose of Si diffusing through the pile-up layer toward the oxidation front and comparing this to separately calculated doses of Si being consumed by oxidation as calculated by the Massoud[7] model. Values for the diffusivity of Si in SiGe were taken from a previous work.[35] A more detailed description of the simulation method and its results is presented in an earlier work.[19] Both the data and the simulations show that the Ge concentration in the pile-up layer varies between about 64% at 800 °C and 36% at 1000 °C. For all of the temperatures considered here, the Ge concentration in the pile-up layer is substantially higher than that in the initial SiGe layer. The simulations indicate that lower Ge concentrations in the initial SiGe layer will result in lower concentrations in the pile-up layer, but this effect is minor in comparison to the influence of temperature and is not apparent in the measured data. The simulation results showed a weak correlation between Ge content in the pile-up layer and oxide thickness; however, as shown in Fig. 2, no clear correlation was evident in the data. In fact, any such correlation that may exist is small enough to be obscured by the experimental error in the measured data.

A significant feature of Fig. 4 is the linear correlation between the Ge content in the pile-up layer and the oxidation temperature. A linear fit to the measured data, shown in Fig. 5, gives a correlation that may be written as

$$X_{\mathrm{pu}} = 1.74 - (1.38 \times 10^{-3}/^{\circ}\mathrm{C})T, \tag{1}$$

where X_{pu} is the Ge content in the pile-up layer and T is the oxidation temperature in Celsius. For various initial Ge concentrations and oxide thicknesses, although linear fits to the measured data and simulations give values of $X_{\mathrm{pu}}(T=0)$ between about 1.5 and 1.8, the slope of the fits is very nearly constant at about $-1.38 \times 10^{-3}/^{\circ}\mathrm{C}$. This would infer that, for any given initial Ge concentration and target oxide thickness, if the range of oxidation temperatures is limited by practical concerns, then the range of values of X_{pu} will also be limited to a nearly constant range. Inducing high Ge concentrations in the pile-up layer by using low oxidation temperatures is limited by the onset of formation of GeO_2 (Ref. 11) and long oxidation times. Inducing low Ge concentrations in the pile-up layer using high oxidation temperatures is limited by difficulty controlling the temperature and oxide thickness due to high oxidation rates; this is particularly true for thin oxides. An additional limiting factor, which is not explored here, is the potential for defects or relaxation in the films due to oxidation temperature and large

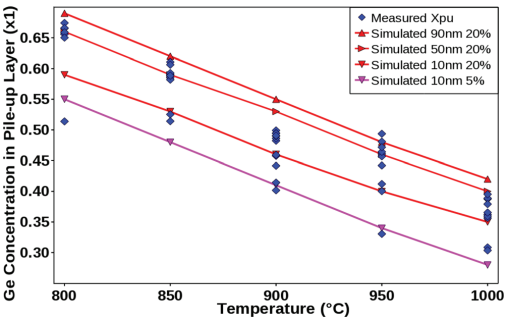

FIG. 4. (Color online) Ge concentration in the pile-up layer of SiGe samples plotted against oxidation temperature. Data measured by XRD is presented alongside simulation results. The measured data is for samples with initial layers of both 15% and 20% Ge (presented as a single series) while the simulated points are for initial SiGe layers of 20% and 5% Ge and labeled accordingly. Simulated results are presented for three oxide thicknesses and labeled accordingly. The lines connecting the simulated points are for visual guidance only.

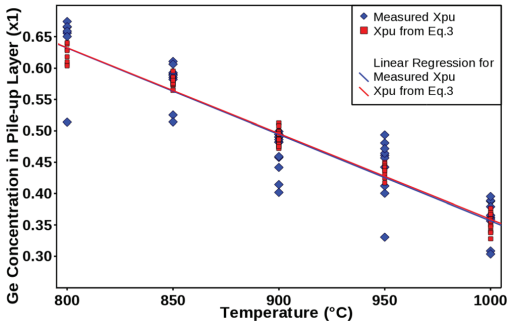

FIG. 5. (Color online) Ge concentration in the pile-up layer of SiGe samples plotted against oxidation temperature. Data measured by XRD is presented alongside modeled data determined by Eq. (3), using oxide thicknesses determined by ellipsometry. The linear fit to the measured data was used to determine Eq. (1). The coefficients of the activation energy and pre-exponential for the diffusivity of Si in SiGe were determined by matching the linear regressions for the modeled and measured data. The measured and modeled data is for samples with initial layers of both 15% and 20% Ge (presented as a single series.)

Ge concentration gradients between the primary SiGe layer and the pile-up layer.

The melting point of SiGe is not a major factor when manipulating the Ge concentration in the pile-up region with dry thermal oxidation. Following Eq. (1), the oxidation temperatures that will induce values of 1 and 0 for X_{pu} are 533 °C and 1258 °C, respectively. Given that the melting point of SiGe varies between ~940 °C for Ge and ~1400 °C for Si,[36] and that the Ge concentration in the pile-up layer is reduced as oxidation temperature is increased, melting of the pile-up layer is unlikely for dry thermal oxidations at 1 atm. Melting of the pile-up layer may be a concern when high Ge concentrations in the pile-up are induced by accelerating the oxidation using, for example, high oxidant pressures and wet oxidation while also using high oxidation temperatures, but then Eq. (1) would need to be redetermined with regard to the appropriate oxidation conditions.

The linear relationship between Ge concentration in the pile-up layer and the oxidation temperature is an observation of measured data and is supported by values determined by simulation. It is useful, however, to have a predictive model that will allow for explicit determination of the Ge concentration in the pile-up. To derive such a model, we start with the assumption that the dose of Si arriving at the oxidation front through diffusion of Si in SiGe, $Q_{\text{Si-SiGe}}$, is equal to the dose of Si consumed by oxidation, Q_{ox}. If a predeposition model is used to model the diffusion, the doses may be written as

$$Q_{\text{Si-SiGe}} = 2C_0\sqrt{\frac{Dt}{\pi}} = Q_{ox} = N_{ox}t_{ox}, \tag{2}$$

where C_0 is the density of Si in the initial layer of SiGe, D is the diffusivity of Si in the pile-up layer, t is the oxidation time, N_{ox} is the density of Si in the oxide, and t_{ox} is the oxide thickness. If an Arrhenius relation wherein the activation energy is a linear function of the Ge concentration in the pile-up is used, the diffusivity of Si in the pile-up layer may be written as $D = D_0\exp[-(E_m X_{pu} + E_{Si})/kT]$. Here, D_0 is the pre-exponential factor, k is Boltzmann's constant, T is the temperature in Kelvin, X_{pu} is the Ge concentration in the pile-up layer, and the activation energy is $E_a = E_m X_{pu} + E_{Si}$. [Although the Arrhenius relation includes an activation energy that is typically treated as a constant value, this is not possible for evaluating the diffusion of Si in SiGe where the Ge concentration is unknown. The value of the activation energy for the diffusion of Si in $Si_{1-X}Ge_X$ is a function of X (in this case X_{pu}) and a linear relationship is supported by published data.[35] The physical phenomena responsible for the nearly linear relationship between E_a and X is not obvious, but, it is perhaps not surprising given the nearly linear relationship between the lattice constant of $Si_{1-X}Ge_X$ and X as described by Vegard's law. Both E_m and E_{Si} are in units of eV.]

The use of a linear relation to describe E_a as a function of X_{pu} is significant here, in that it allows for a direct solution for X_{pu} as shown in

$$X_{pu} = \frac{\left[\ln\left(\frac{N_{ox}^2 t_{ox}^2 \pi}{4C_0^2 t}\right) - \ln(D_0)\right]kT + E_{Si}}{-E_m}. \tag{3}$$

Equation (3) can be used either to determine the value of X_{pu} using known values for the diffusivity of Si in SiGe, or to determine the values of D_0, E_m, and E_{Si} using known values of X_{pu}.

For the former case, Eq. (3) may be used in process design and simulations for the construction of electronic or photovoltaic devices using thermal oxidation to manipulate the Ge concentration in thin films or nanorods of SiGe.

For the latter case, measured values of t_{ox}, t, T, and C_0 from this study were used along with starting estimates for the values of D_0, E_m, and E_{Si} to solve for X_{pu}. These modeled values for X_{pu} were compared to the values measured by XRD, and the values of D_0, E_m, and E_{Si} were subsequently adjusted in order to optimize the agreement between the modeled and measured values and to arrive at final values for D_0, E_m, and E_{Si}. This resulted in values for D_0, E_m, E_{Si} of 1339 cm^2/s, −1.8 eV, and 5.12 eV, respectively. These values are in close agreement with data for the diffusivity of Si in SiGe determined by measuring diffusion of Si isotopes using TOF-SIMS[35] as well as previous observations regarding the binding energy of Si to Si being higher than that of Si to Ge.[18] Figure 5 presents the data from this work as measured by XRD, values modeled using Eq. (3), and the linear fits to both measured and modeled data. The linear fit to the measured data is described by Eq. (1). The agreement between the linear fits in Fig. 5 shows that the empiric relation given by Eq. (1) and the model in Eq. (3) are accurate representations of the relationship between the Ge concentration in the pile-up and the oxidation temperature. Furthermore, this analysis is a demonstration of the feasibility of measuring the diffusivity of Si in SiGe by dry thermal oxidation of SiGe and subsequent measurement of the oxide thickness and Ge concentration in the pile-up layer.

Use of dry thermal oxidation in device and nanostructure construction still requires a reliable estimate of the rate at which SiGe will oxidize. As stated in the introduction, the role of the Ge concentration at the oxidation front in determining the oxidation rate has not been adequately addressed.

Comparison of the oxidation rate to the oxide thickness for multiple temperatures was used to great affect by Massoud[7] to demonstrate and model oxidation rates in Si for very thin oxides. A similar approach is taken in Fig. 6 in order to evaluate the influence of Ge on the oxidation rate of SiGe. Although the samples in the present study have 15% or 20% Ge in the initial SiGe layers, the Ge content in the pile-up region is substantially higher and primarily dependent on the oxidation temperature. So, it is appropriate to treat all of the data from SiGe that is oxidized at a given temperature as having the same Ge content at the oxidation interface and comparing that data to the Si data points for the same temperature. Figure 6 shows data for SiGe and Si alongside predictions for Si using the Massoud[7] model and assuming the presence of a native oxide layer. The model constants used are as previously published,[6,7] except for the linear rate

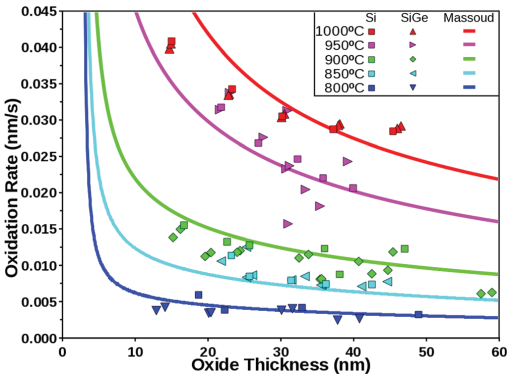

FIG. 6. (Color online) Oxidation rates for Si and SiGe vs the oxide thickness as measured by ellipsometry. Data from the present work is presented along with simulation results. The simulations used the Massoud (Ref. 7) model and published model parameters (Refs. 6 and 7) with the exception of the linear rate constant, B/A, which was determined from the data from the present work.

coefficient (B/A), which was estimated from the data in this study. The values for B/A used here were 0.00487 nm/s, 0.00933 nm/s, 0.01512 nm/s, 0.02991 nm/s, and 0.03363 nm/s for 800 °C, 850 °C, 900 °C, 950 °C, and 1000 °C, respectively. The most important aspect of the data presented in Fig. 6 is that the oxidation rates for SiGe do not differ in any meaningful way from those of Si. Despite Ge contents at the oxidation front between about 64% and 36% for 800 °C and 1000 °C, respectively, the oxidation rate of the SiGe samples is the same as that of the Si control samples. Furthermore, both the SiGe and Si oxidation rates are in close agreement with what is predicted by the Massoud[7] model for Si.

IV. SUMMARY AND CONCLUSIONS

The present work adds to the general understanding of SiGe oxidation by measuring the Ge content in the pile-up region and the oxide thickness that result from simple and nonexotic oxidation conditions (dry O_2 at 1 atm.) Data is presented, showing that the Ge content in the pile-up layer is primarily determined by the oxidation temperature, while it is largely independent of oxide thickness and the Ge content in the initial SiGe layer. The Ge content in the pile-up layer is determined to vary linearly as a function of temperature and is measured to be about 64% at 800 °C and 36% at 1000 °C. Despite elevated Ge content at the oxidation front where oxidation occurs, the weight of the evidence indicates that Ge content does not influence the oxidation rate of SiGe for sub-100-nm thin films. Use of the established models and parameters for Si give very reasonable and practical estimations for the oxidation of thin films of SiGe. A model that allows for the explicit determination of the Ge concentration in the pile-up layer based on other known or measured values is presented. This model may be used either as a predictive tool in the design and manufacture of nanostructures and devices or as a tool for determination of the diffusivity of Si in SiGe. The model has been supported by data from the present work as well as data from the literature.

ACKNOWLEDGMENTS

The authors gratefully acknowledge Alexander Azarov and Frode Kløw at the University of Oslo for performing RBS measurements and associated simulations, the NSE-IM2NP team, and NanoTecMat platform for providing the SiGe samples, and the Norwegian Research Council for financial support by way of the FRINAT program.

[1]K. L. Wang, S. G. Thomas, and M. O. Tanner, J. Mater. Sci.: Mater. Electron. **6**, 311 (1995).
[2]S. E. Thompson *et al.*, IEEE Trans. Electron Devices **51**, 1790 (2004).
[3]S. Balakumar, K. D. Buddharaju, B. Tan, S. C. Rustagi, N. Singh, R. Kumar, G. Q. Lo, S. Tripathy, and D. L. Kwong, J. Electron. Mater. **38**, 443 (2009).
[4]N. Singh, K. D. Buddharaju, S. K. Manhas, A. Agarwal, S. C. Rustagi, G. Q. Lo, N. Balasubramanian, and D.-L. Kwong, IEEE Trans. Electron Devices **55**, 3107 (2008).
[5]A. I. Hochbaum and P. Yang, Chem. Rev. (Washington, D.C.) **110**, 527 (2010).
[6]B. E. Deal and A. S. Grove, J. Appl. Phys. **36**, 3770 (1965).
[7]H. Z. Massoud, J. D. Plummer, and E. A. Irene, J. Electrochem. Soc. **132**, 2685 (1985).
[8]F. K. LeGoues, R. Rosenberg, and B. S. Meyerson, Appl. Phys. Lett. **54**, 644 (1989).
[9]F. K. LeGoues, R. Rosenberg, T. Nguyen, F. Himpsel, and B. S. Meyerson, J. Appl. Phys. **65**, 1724 (1989).
[10]J. M. Madsen, Z. Cui, and C. G. Takoudis, J. Appl. Phys. **87**, 2046 (2000).
[11]S. J. Kilpatrick, R. J. Jaccodine, and P. E. Thompson, J. Appl. Phys. **81**, 8018 (1997).
[12]P. C. Chen, J. Y. Lin, Y. J. Hsu, and H. L. Hwang, Mater. Res. Soc. Symp. Proc. **281**, 485 (1993).
[13]L.-P. Chen, Y.-C. Chan, S.-J. Chang, G.-W. Huang, and C.-Y. Chang, Jpn. J. Appl. Phys., Part 2 **37**, L122 (1998).
[14]D. C. Paine, C. Caragianis, and A. F. Schwartzman, J. Appl. Phys. **70**, 5076 (1991).
[15]T. Shimura, M. Shimizu, S. Horiuchi, H. Watanabe, K. Yasutake, and M. Umeno, Appl. Phys. Lett. **89**, 111923 (2006).
[16]M. A. Rabie, Y. M. Haddara, and J. Carette, NSTI-Nanotech **3**, 21 (2005).
[17]M. A. Rabie, Y. M. Haddara, and J. Carette, J. Appl. Phys. **98**, 074904 (2005).
[18]O. W. Holland, C. W. White, and D. Fathy, Appl. Phys. Lett. **51**, 520 (1987).
[19]E. Long, A. Azarov, F. Kløw, A. Galeckas, A. Y. Kuznetsov, and S. Diplas, J. Appl. Phys. **111**, 024308 (2012).
[20]S. J. Kilpatrick, R. J. Jaccodine, and P. E. Thompson, J. Appl. Phys. **93**, 4896 (2003).
[21]M. Spadafora, G. Privitera, A. Terrasi, S. Scalese, C. Bongiorno, A. Carnera, M. Di Marino, and E. Napolitani, Appl. Phys. Lett. **83**, 3713 (2003).
[22]M. Spadafora *et al.*, Mater. Sci. Semicond. Process. **8**, 219 (2005).
[23]D. K. Nayak, K. Kamjoo, J. S. Park, J. C. S. Woo, and K. L. Wang, IEEE Trans. Electron Devices **39**, 56 (1992).
[24]D. Nayak, K. Kamjoo, J. C. S. Woo, J. S. Park, and K. L. Wang, Appl. Phys. Lett. **56**, 66 (1990).
[25]Y. S. Lim, J. S. Jeong, J. Y. Lee, H. S. Kim, H. K. Shon, H. K. Kim, and D. W. Moon, Appl. Phys. Lett. **79**, 3606 (2001).
[26]Y. S. Lim, J. S. Jeong, J. Y. Lee, H. S. Kim, H. K. Shon, H. K. Kim, and D. W. Moon, J. Electron. Mater. **31**, 529 (2002).
[27]N. Daval, E. Guiot, K. K. Bourdelle, M. Kennard, I. Cayrefourcq, T. Akatsu, C. Mazure, H. Cerva, and A. Rucki, *Crystalline Defects and Contamination: Their Impact and Control in Device Manufacturing IV DECON 2005*, edited by B. O. Kolbesen (Electrochemical Society, Pennington, 2005), Vol. 2005–10, pp. 42–51.
[28]T. Shimura, Y. Okamoto, D. Shimokawa, T. Inoue, T. Hosoi, and H. Watanabe, ECS Trans. **33**, 893 (2010).

[29]T. Shimura, Y. Okamoto, T. Inoue, T. Hosoi, and H. Watanabe, Phys. Rev. B **81**, 033308 (2010).
[30]M. K. Bera *et al*., J. Vac. Sci. Technol. A **24**, 84 (2006).
[31]B. G. Min, J. H. Yoo, H. C. Sohn, D. H. Ko, M. H. Cho, K. B. Chung, and T. W. Lee, Thin Solid Films **518**, 2065 (2010).
[32]J. P. Zhang, P. L. F. Hemment, S. M. Newstead, A. R. Powell, T. E. Whall, and E. H. C. Parker, Thin Solid Films **222**, 141 (1992).
[33]Y. Zhang, C. Li, K. Cai, Y. Chen, S. Chen, H. Lai, and J. Kang, J. Appl. Phys. **106**, 063508 (2009).
[34]J. P. Dismukes, L. Ekstrom, and R. J. Paff, J. Phys. Chem. **68**, 3021 (1964).
[35]R. Kube, H. Bracht, J. Lundsgaard Hansen, A. Nylandsted Larsen, E. E. Haller, S. Paul, and W. Lerch, J. Appl. Phys. **107**, 073520 (2010).
[36]H. Stöhr and W. Klemm, Z. Anorg. Allg. Chem. **241**, 305 (1939).

Article IV

Nano-structuring in SiGe by oxidation induced anisotropic Ge self-organization

E. Long, A. Galeckas, A. Kuznetsov, A. Ronda, L. Favre, I. Berbezier, and H. Radamson

Journal of Applied Physics **113**, 104310 (2013)

JOURNAL OF APPLIED PHYSICS **113**, 104310 (2013)

Nano-structuring in SiGe by oxidation induced anisotropic Ge self-organization

Ethan Long,[1,a)] Augustinas Galeckas,[1] Andrej Yu Kuznetsov,[1] Antoine Ronda,[2] Luc Favre,[2] Isabelle Berbezier,[2] and Henry H. Radamson[3]
[1]*University of Oslo, Blindern, 0316 Oslo, Norway*
[2]*Univ. Aix Marseille, Campus St. Jérôme, 13397 Marseille Cedex 20, France*
[3]*Royal Institute of Technology (KTH), Electrum 29, 16440 Kista, Sweden*

(Received 31 January 2013; accepted 25 February 2013; published online 14 March 2013)

The present study examines the kinetics of dry thermal oxidation of (111), (110), and (100) silicon-germanium (SiGe) thin epitaxial films and the redistribution of Ge near the oxidation interface with the aim of facilitating construction of single and multi-layered nano-structures. By employing a series of multiple and single step oxidations, it is shown that the paramount parameter controlling the Ge content at the oxidation interface is the oxidation temperature. The oxidation temperature may be set such that the Ge content at the oxidation interface is increased, kept static, or decreased. The Ge content at the oxidation interface is modeled by considering the balance between Si diffusion in SiGe and the flux of Si into the oxide by formation of SiO_2. The diffusivity of Si in SiGe under oxidation is determined for the three principal crystal orientations by combining the proposed empirical model with data from X-ray diffraction and variable angle spectroscopic ellipsometry. The orientation dependence of the oxidation rate of SiGe was found to follow the order: $(111) > (110) > (100)$. The role of crystal orientation, Ge content, and other factors in the oxidation kinetics of SiGe versus Si are analyzed and discussed in terms of relative oxidation rates. © *2013 American Institute of Physics*. [http://dx.doi.org/10.1063/1.4794991]

I. INTRODUCTION

There is significant research and industrial interest in silicon-germanium (SiGe) based nano-structures and devices.[1] Among numerous examples of how SiGe, in general, and Ge condensation by thermal oxidation of SiGe, in particular, may be used for fabrication of nano-scale devices are: monolithically integrated optical interconnects and waveguides,[2] nano-antennas,[3] bolometers for uncooled infrared photodetectors,[4,5] nano-crystals for use in high density non-volatile memories,[6,7] multiple gate field effect transistors (including FinFETs),[8–11] and nano-wires.[12,13] Achieving a direct bandgap in SiGe core-shell nanowires depends on, among other things, the nanowire's orientation and shell thickness.[14–16] Local oxidation of SiGe has long been proposed as a method to manipulate the Ge content in the channel or source/drain regions of transistors, which, in addition to the performance benefits, may help reduce manufacturing costs and cycle times by eliminating steps from SiGe CMOS processes.[17] SiGe-on-insulator (SGOI) is a viable replacement for bulk Si in deep sub-micron CMOS applications,[18] and the fabrication of SGOI wafers using Ge condensation by thermal oxidation[19] as well as by thermally induced Ge dilution[20] has been suggested. Use of thermal oxidation for SGOI fabrication may also allow for endotaxial growth of high Ge content layers and Ge nano-crystals at the interface between a buried oxide and a SiGe layer.[21] A sound understanding of the oxidation of SiGe in multiple crystallographic orientations will be required to develop processes for using SiGe in such applications.

The two phenomena commonly discussed in the literature about oxidation of SiGe are the potential for Ge to act as a catalyst or inhibitor for oxidation, and the formation of a Ge-rich layer between the oxide and the underlying SiGe, referred to as Ge condensation, pile-up, or snow plowing.[22–30] A common explanation for the presumed catalytic effect of Ge relies on the dissociation energy for a Si-Ge bond being lower than that of a Si-Si bond,[31–35] while others explain Ge's role as a catalyst in terms of the generation of vacancies and interstitials in the SiGe layers.[22–25,36–38] However, conclusions about the role of Ge in determining the oxidation rate vary widely, and the Ge content at the oxidation interface is rarely characterized in a systematic way.[39] Furthermore, except for an early study using (111) oriented material,[40] oxidation of SiGe has been studied with an exclusive focus on (100) material. The orientation dependence of oxidation of Si[41–43] may be an indication that SiGe will exhibit similar behaviour, but it is not obvious that SiGe and Si are perfectly synonymous in this respect. It has been established that oxidation enhanced diffusion of dopants in Si is tied to both point defects and crystallographic orientation.[44,45] If point defects play a role in Si diffusion in SiGe,[22,38,46] then it is likely that any oxidation enhanced diffusion of Si in SiGe due to point defects is also orientation dependent. By virtue of the dependence of the Ge condensation on the diffusivity of Si in SiGe,[26,27] any orientation dependence in the latter will have a direct consequence on the Ge content at the oxidation interface.

The present study evaluates the kinetics of oxidation of SiGe with (111), (110), and (100) oriented thin epitaxial films of SiGe. The possibility to increase, keep stable, or decrease the Ge content at the oxidation interface is demonstrated by using

[a)]Electronic mail: ethanl@smn.uio.no.

X-ray diffraction (XRD) characterization of SiGe samples after multiple oxidations. Characterization of samples with a range of oxide thicknesses and oxidation temperatures shows that the Ge content in the pile-up region is strongly dependent on oxidation temperature and only weakly dependent on the Ge content in the underlying SiGe. Lower oxidation temperatures are shown to be linearly correlated to higher Ge contents, though the linear temperature dependence of Ge content varies with crystallographic orientation. The Ge content at the oxidation interface is modeled by an empirical relationship which considers the balance between Si diffusion in SiGe and Si flux into the oxide by formation of SiO_2. The diffusivity parameters of Si in SiGe under oxidation are determined for the principal crystal orientations. The oxidation rates of both Si and SiGe are found to be dependent on the crystallographic orientation as well as the presence of Ge at the oxidation interface. The degree of growth rate enhancement or reduction is discussed in terms of oxidation rate ratios.

II. EXPERIMENTAL

Epitaxial layers of $Si_{1-X}Ge_X$ were grown on (111), (110), and (100) oriented Si substrates by molecular beam epitaxy (MBE). The as-grown SiGe layers were composed of 20% Ge, while a supplementary set of (100) oriented samples contained 15% Ge. Additionally, a set of (100) oriented samples with $Si_{0.8}Ge_{0.2}$ layers were grown by chemical vapor deposition (CVD). The CVD grown samples were used exclusively for experiments involving repeated oxidations. Those samples which were subjected to repeated oxidations had their oxides removed by a timed buffered hydrofluoric acid etch between each oxidation. All as-grown $Si_{1-X}Ge_X$ layers had thicknesses of ~80 nm. Bare Si substrates were used as reference samples for all oxidation runs.

The thermal oxidations were carried out at ambient pressure (1 atm) in a tube furnace flushed with dry O_2. For any given oxidation time and temperature, all samples were processed simultaneously in order to ensure identical oxidation conditions between samples with various characteristics (i.e., SiGe, Si, crystal orientation). Oxidations for (111), (110), and (100) oriented samples were carried out at 900, 950, and 1000 °C with oxidation times chosen to target 20, 40, 60, 80, and 100 nm thick oxides. Supplementary (100) oriented $Si_{0.85}Ge_{0.15}$ and $Si_{0.80}Ge_{0.20}$ samples were oxidized at 780, 820, 870, 920, or 960 °C to grow oxides between 0 and 60 nm thick.

XRD measurements were made with a diffractometer in double axis configuration. The incident beam was composed of Cu-$K_{\alpha 1}$ radiation, while Cu-$K_{\alpha 2}$ and Cu-K_β radiation was removed with a Göbel mirror and Ge monochromator. The peaks for the 2θ-ω scans were chosen according to sample orientation, i.e., the (004) peak for (100), the (333) peak for (111), and both (022) and (044) peaks for (110) oriented material. The profiles from the 2θ-ω scans were fit using a 3-layer model, lattice constants from Dismukes *et al.*[47] and the LEPTOS simulation software. Reciprocal space maps of a limited number of samples confirmed that the SiGe layers were pseudomorphically strained before and after oxidation.

Oxide thicknesses were measured by variable angle spectroscopic ellipsometry. Measurements were recorded at 65°, 70°, and 75° with photon energies varied between 1.39 and 3.25 eV in increments of 0.01 eV. Oxide thicknesses were determined using a multi-layer model, optical constants for SiO_2, Si, and SiGe from literature,[48,49] and the COMPLETEEASE software.

III. RESULTS AND DISCUSSION

A. Ge content in the pile-up

A series of multi-step oxidations was performed to highlight the relative influence of temperature and initial Ge content on the pile-up of Ge at the oxidation interface. Figure 1 shows XRD scans for $Si_{0.8}Ge_{0.2}$ samples subjected to one, two, and three separate oxidations at progressively lower temperatures. The XRD scans are aligned to the Si substrate peak at 69.13°. The peak at 68.10° arises from the as-grown SiGe layer and reflects the 20% Ge content of the layer. The left most peaks correspond to the Ge pile-up layers that form as a result of the oxidations. After oxidation, the intensity of the XRD peak for the as-grown layer will be reduced as a result of the thinning of the layer. For the oxidized samples in Fig. 1, the oxide and pile-up layers were thick enough so that any extant signal from the as-grown layer is obscured. The shift in the 2θ position of the pile-up peaks from high to low angles indicates an increase in the Ge content of the pile-up layer, X_{pu}. The first sample was subjected to a single-step oxidation at 1000 °C, which resulted in $X_{pu} = 0.310$. The second sample was subjected to a two-step oxidation: the same oxidation at 1000 °C and a subsequent second oxidation at 900 °C, resulting in $X_{pu} = 0.466$. The third sample underwent a three-step oxidation at 1000, 900, and then 800 °C, resulting in $X_{pu} = 0.572$. Despite the Ge content at the oxidation interface increasing with multiple oxidations at progressively lower temperatures, T, these results are consistent with what is predicted by empirical relations for $X_{pu}(T)$ that are based on single oxidations of $Si_{0.80}Ge_{0.20}$ and

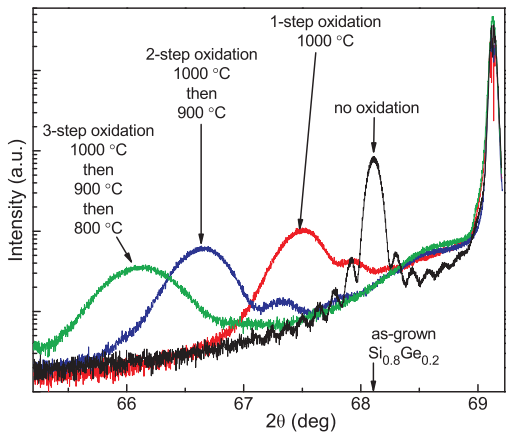

FIG. 1. XRD scans of the (004) peaks of (100) oriented SiGe samples after multi-step oxidations with decreasing temperatures. The 2θ position for the as-grown sample is marked for reference.

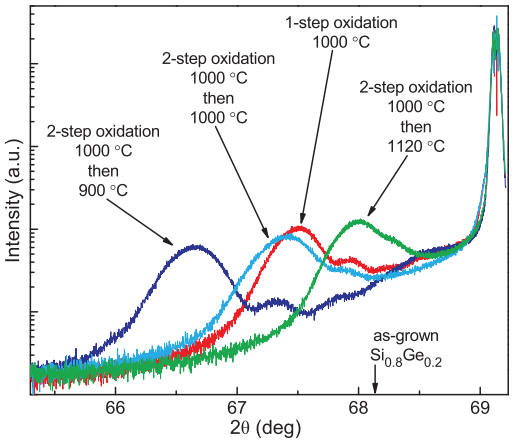

FIG. 2. XRD scans of the (004) peaks of (100) oriented SiGe samples after various multi-step oxidation schemes. The 2θ positions of the peaks indicate an increase, no change, and a decrease in X_{pu}. The scan for the as-grown sample is omitted for clarity, but its 2θ position is marked for reference.

$Si_{0.85}Ge_{0.15}$ alloys.[27] That is, the value of X_{pu} depends critically on the oxidation temperature, and is largely independent of the Ge content in the underlying SiGe. In the case of multiple oxidations at progressively lower temperatures, the Ge content at the oxidation interface, X_{pu}, is primarily determined by the temperature of the last oxidation performed, despite the progressively increasing X_{pu}.

Figure 2 shows XRD scans of $Si_{0.8}Ge_{0.2}$ samples subjected to a similar scheme of multi-step oxidations. A set of four samples was first oxidized at 1000 °C in order to create a thick pile-up layer with $X_{pu} = 0.310$. Three samples were subsequently subjected to an additional oxidation step at 1120, 1000, or 900 °C. These temperatures were chosen to induce a decrease, no change, and an increase in X_{pu} by following the previously published analysis for single oxidations of SiGe(100).[27] Indeed, the XRD scans in Fig. 2 reveal that the secondary oxidations at 1120, 1000, and 900 °C have caused X_{pu} to shift from 0.310 to 0.217, 0.331, and 0.466, respectively. As stated above, X_{pu} is determined primarily by the temperature of the last oxidation conducted. However, the Ge content at the oxidation interface is increased from 0.20 to 0.31 after the first oxidation at 1000 °C. The higher Ge content at the oxidation interface at the start of the second oxidation had the consequence of increasing X_{pu} by ~2% after the second oxidation at 1000 °C. This effect is evident in the empirical relation for $X_{pu}(T, N_{SiGe})$[27] (also in Eq. (1)), where N_{SiGe} is the Si density in the primary SiGe layer.

An additional series of oxidations was conducted on SiGe and Si samples to investigate the influence of crystallographic orientation on the formation of the pile-up region and on the oxidation kinetics of SiGe. These oxidation runs involved a single oxidation of as-grown $Si_{0.8}Ge_{0.2}$ and Si samples, though a variety of oxidation temperatures and times were used for different oxidation runs. Figure 3 shows the oxide thickness versus oxidation time for 900, 950, and 1000 °C. The oxidation rates are ordered as (111) > (110) > (100) for both Si and SiGe. Most of the oxidation runs performed at 900 and 1000 °C result in SiGe oxidizing faster than Si, but the longer oxidations at 950 °C and the 360 min oxidation at 900 °C show Si oxidizing faster than SiGe.

Figure 4 shows typical results of XRD measurements performed to quantify X_{pu} for the samples described in Fig. 3. There are three distinct peak positions: the substrate peak at ~95°, the peaks at ~93.8° from the primary SiGe layers, and the leftmost peaks corresponding to the pile-up layers. The pile-up layer peaks are distinguished by their separation according to oxidation temperature, while oxide thickness does not have a profound influence on X_{pu}.

The dependence of X_{pu} on crystallographic orientation and temperature is illustrated in Fig. 5. Even though $X_{pu}(T)$ is orientation dependent, linear fits to the measured values reveal nearly identical slopes for all three orientations.

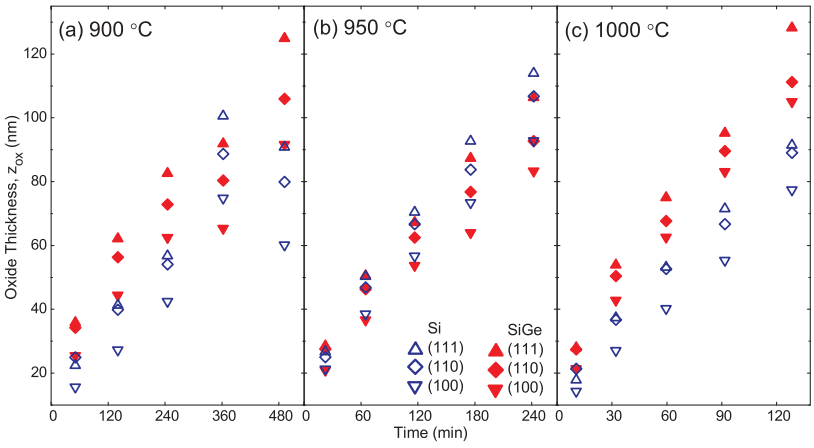

FIG. 3. Oxide thickness versus oxidation time at (a) 900, (b) 950, and (c) 1000 °C. The data are for (111), (110), and (100) oriented $Si_{0.8}Ge_{0.2}$ and Si.

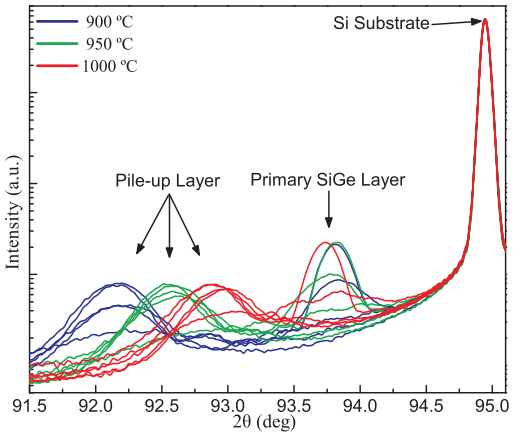

FIG. 4. XRD 2θ-ω scans of the (333) peaks of (111) oriented $Si_{0.8}Ge_{0.2}$ oxidized at various temperatures and times. Five samples with oxide thicknesses between 20 and 100 nm are shown for each temperature.

B. Diffusivity of Si in SiGe and the oxidation rate

As detailed in earlier publications,[26,27] the magnitude of X_{pu} results from the diffusion induced flux of Si towards the oxidation front, J_{pu}, and the flux of Si into the oxide due to formation of SiO_2, J_{ox}, being balanced such that $J_{ox}/J_{pu} = 1$. Thus, changes to the oxidation rate must be matched by changes to the diffusion of Si in SiGe, which appears as a change in X_{pu}. It is well established in the literature that the oxidation rate of Si depends on its crystallographic orientation,[41,50–53] and the data in Fig. 3 confirm that this is also true for SiGe. Furthermore, the orientation dependent diffusivity of dopants observed in Si under oxidation[44,45] may indicate that the diffusivity of Si in SiGe is also orientation dependent. Consequently, the orientation dependence of both the oxidation rate of SiGe and the diffusivity of Si in SiGe will alter the flux balance, $J_{ox}/J_{pu} = 1$, and thus, modify $X_{pu}(T)$.

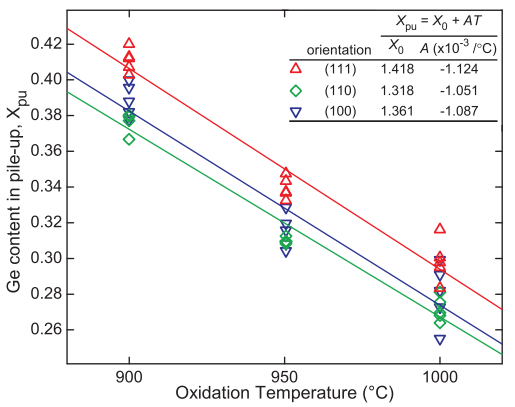

FIG. 5. XRD measurements of the Ge content in the pile-up layer, X_{pu}, versus oxidation temperature, T, along with linear fits to the data.

TABLE I. Parameters for diffusivity of Si in SiGe for different orientations.

Orientation	E_m (eV)	D_0(cm^2/s)
111	−1.81	199
110	−1.89	219
100	−1.70	239

The diffusivities of Si in (111), (110), and (100) oriented SiGe are determined by comparing values for X_{pu} as measured by XRD to values calculated with the empirical relation[27]

$$X_{pu} = \frac{k_B T \ln\left(\frac{4N_{SiGe}^2 D_0 t}{\pi N_{ox}^2 z_{ox}^2}\right) - E_{Si}}{E_m}, \quad (1)$$

where z_{ox} is the oxide thickness from ellipsometry, T is the oxidation temperature, t is the oxidation time, $N_{ox} = 2.21 \times 10^{22}\,cm^{-3}$ is the atomic density of Si in SiO_2, N_{SiGe} is the Si density in the primary SiGe layer, and k_B is the Boltzmann constant. The diffusivity of Si in SiGe is described by an Arrhenius relation, $D = D_0 \exp[-(E_m X_{pu} + E_{Si})/(k_B T)]$, where the same activation energy for Si self-diffusion, $E_{Si} = 4.76\,eV$,[54] is used for all three crystallographic orientations. The diffusion parameters D_0 and E_m were determined independently for the (111), (110), and (100) orientations by fitting the calculated and measured values of X_{pu} using the method of least squares; the results are summarized in Table I. The correlation between measured and calculated results for X_{pu} is shown in Fig. 6.

The apparent linearity of $X_{pu}(T)$ in Fig. 5 can be understood if one models both the diffusivity of Si in SiGe and the oxidation rate by Arrhenius relations. Although more refined oxidation models exist, for the range of oxide thicknesses considered here, a simple Arrhenius relation is consistent with the literature[41,51–53] and appears as an obvious choice when evaluating the balance of Si fluxes, $J_{ox}/J_{pu} = 1$. Thus,

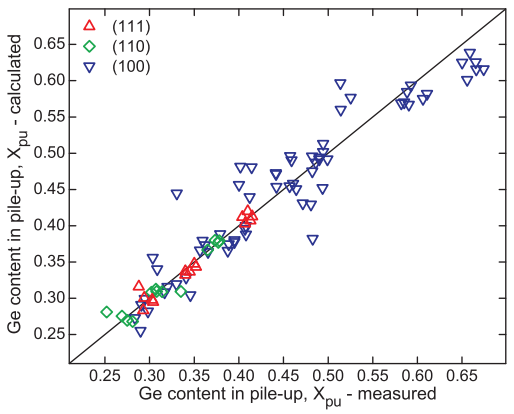

FIG. 6. Correlation between X_{pu} values measured by XRD and those calculated by Eq. (1). The diagonal line indicates where the measured and calculated values are exactly equal and is drawn for visual guidance only.

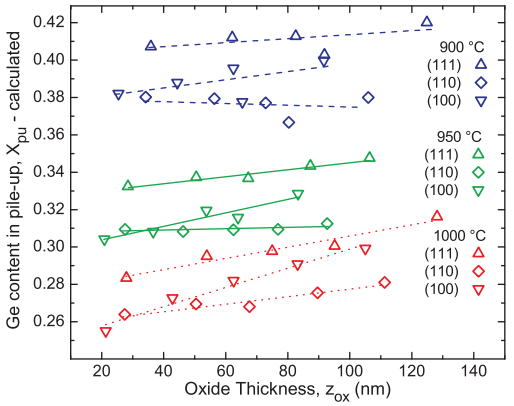

FIG. 7. The Ge content in the pile-up layer, X_{pu}, versus oxide thickness, z_{ox}. The lines are for visual guidance only.

by defining the oxidation rate as $\nu = \nu_0 \exp[-E_{ox}/(k_B T)]$, Eq. (1) can be rewritten as

$$X_{pu} = \frac{k_B T \ln\left(\frac{4N_{SiGe}^2 D_0}{\pi N_{ox}^2 \nu_0^2 t}\right) - E_{Si} + 2E_{ox}}{E_m} \quad . \qquad (2)$$

The logarithmic dependence on time is consistent with the observation that, for any given temperature and orientation, X_{pu} remains nearly constant for a variety of oxide thicknesses, as is clearly shown in Fig. 7.

C. Oxidation rate ratios

A number of factors, including crystalline orientation, Ge at the oxidation front, oxidant partial pressure, and oxidant chemistry, will have varying influences on the oxidation rate, and their influences are reflected by ν_0 and E_{ox}. Considering the ratio of two Arrhenius functions (i.e., two oxidation rates) will highlight a single factor's contribution to ν_0 and E_{ox}. So, in order to facilitate analysis of the data in Fig. 3, oxidation rate ratios are used to compare the influence of Ge content and crystal orientation on the oxidation rate. These ratios are defined here as $\rho_{a/b} = \nu_a/\nu_b$, where ν_a and ν_b are the oxidation rates for two samples with identical oxidation conditions, and a single differentiating parameter indicated by the subscripts. The average values of $\rho_{SiGe/Si}$ are listed in Table II, while the average oxidation rate ratios comparing (111), (110), and (100) material are reported in Table III.

The values of $\rho_{SiGe/Si}$ listed in Table II indicate Ge induced oxidation rate enhancement ($\rho_{SiGe/Si} > 1$) for 900 and 1000 °C, while 950 °C indicates Ge induced oxidation rate reduction ($\rho_{SiGe/Si} < 1$). The samples oxidized for 360 min at 900 °C (see Fig. 3) also show $\rho_{SiGe/Si} < 1$, while the (111) and (110) oriented samples oxidized at 950 °C for 22.5 minutes show $\rho_{SiGe/Si} > 1$. Dry oxidations are typically not completely free of H_2O or N_2 due to contamination from the room ambient by diffusion through the wall of the furnace or by back-flow from the end of the furnace.[51,53,55] So, the most likely explanation for the aberrations in the relative oxidation rates of SiGe and Si shown in Table II and Fig. 3 is contamination of the oxidizing ambient by some combination of H_2O and N_2. Furthermore, a variation in ambient chemistry seems to be the only plausible explanation for the relatively small values of $\rho_{110/100}$ and $\rho_{111/100}$ and the relatively large value of $\rho_{111/110}$ for Si at 950 °C in Table III.

TABLE II. Oxidation rate ratios, $\rho_{SiGe/Si}$, comparing SiGe to Si. The values are averages for all oxidation times for each combination of temperature and orientation.

	$\rho_{SiGe/Si}$		
T(°C)	111	110	100
780	…	…	1.02
820	…	…	1.18
870	…	…	1.07
900	1.40	1.29	1.47
920	…	…	1.17
950	0.98	0.96	0.93
960	…	…	1.19
1000	1.46	1.33	1.55

The notion that oxidant chemistry is a determining factor in the magnitude of $\rho_{SiGe/Si}$ is supported by studies of SiGe oxidation in dry, wet, N_2 diluted, fluorinated, ozone, and atomic oxygen ambients.[25,36,56,57] LeGoues *et al.*[36] demonstrated explicitly that $\rho_{SiGe/Si} > 1$ for steam oxidation, whereas an ambient with H_2O diluted by N_2 can result in $\rho_{SiGe/Si} \approx 1$. In fact, modification of the oxidation ambient chemistry may simply be viewed as a way to control the various elements and molecules present at the interface between the oxide and the underlying Si or SiGe. Introduction of impurities by doping with boron, phosphorus, arsenic, or antimony,[53,58] alloying with carbon,[59,60] or directly depositing copper[61] also have a catalytic or inhibitive effect on the oxidation of Si or SiGe, and may influence the magnitude of $\rho_{SiGe/Si}$.

The data plotted in Fig. 3 and summarized in Table III indicate that the oxidation rates of the three orientations tend to be ordered as (111) > (110) > (100). Also, a decrease in $\rho_{a/b}$ as temperature increases is an indication that E_{ox} is larger for the orientation given by b than it is for the orientation given by a.[53] It may be observed that $\rho_{a/b}$ in Table III tends to decrease as temperature increases, which would indicate that the magnitudes of E_{ox} are ordered (111) < (110) < (100) for both Si and SiGe. This is consistent with the observed ordering of the oxidation rates, however, the

TABLE III. Oxidation rate ratios, $\rho_{110/100}$, $\rho_{111/100}$, and $\rho_{111/110}$, for the stated orientations. The values are averages for Si or SiGe (as indicated) for the five oxidation times used at each temperature.

T(°C)	$\rho_{110/100}$ Si	$\rho_{110/100}$ SiGe	$\rho_{111/100}$ Si	$\rho_{111/100}$ SiGe	$\rho_{111/110}$ Si	$\rho_{111/110}$ SiGe
900	1.37	1.23	1.43	1.38	1.05	1.13
950	1.17	1.21	1.26	1.33	1.08	1.10
1000	1.30	1.14	1.28	1.23	0.99	1.09

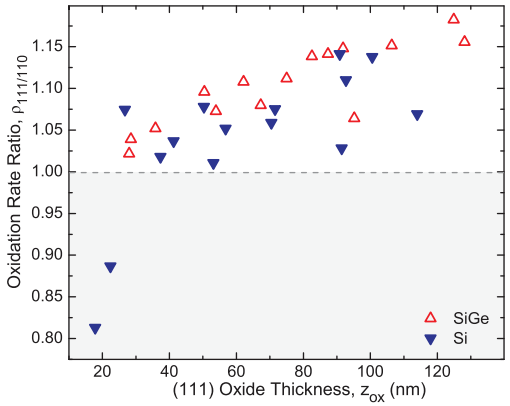

FIG. 8. Oxidation rate ratio, $\rho_{111/110}$, versus the oxide thickness of the (111) oriented sample, z_{ox}.

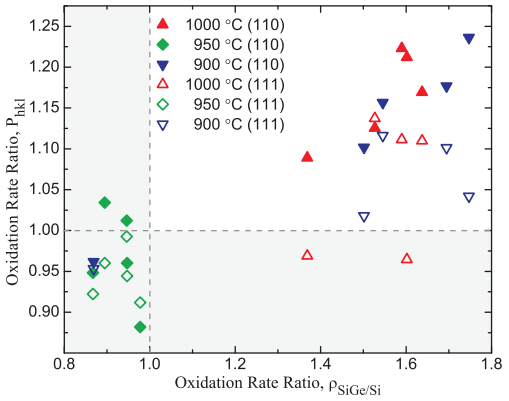

FIG. 9. The oxidation rate ratio between SiGe and Si samples of two orientations, $P_{hkl} = (\nu_{Si}^{hkl} * \nu_{SiGe}^{100})/(\nu_{Si}^{100} * \nu_{SiGe}^{hkl})$, versus the oxidation rate ratio between SiGe and Si for the (100) orientation, $\rho_{SiGe/Si} = \nu_{SiGe}^{100}/\nu_{Si}^{100}$. The data are labeled according to the oxidation temperature and the sample orientation (hkl) used to calculate P.

difference in oxidation rates between orientations is not constant. This may be seen in Fig. 8, which shows the value of $\rho_{111/110}$ decreasing towards 1 as the oxide thickness decreases, and dropping below 1 for the two points with $z_{ox} < 23$ nm. A crossover point around 20 to 25 nm and a positive slope is an indication that the oxidation proceeds from being controlled by the surface reaction rate at very small z_{ox}, to being increasingly influenced by strain and the diffusivity of oxidant in the oxide as z_{ox} increases.

It is well established that strain between the oxide and the underlying crystal reduces the oxidation rate.[42,43,50,62–64] In addition to strain, the concept of steric hindrance is integral to explaining the orientation dependence of oxidation. While the number of surface bonds on differently oriented Si or SiGe follows the order $(110) > (111) > (100)$, the number of bonds available for an oxidation reaction due to steric hindrance follows the order $(111) > (110) > (100)$.[41] On its own, the steric hindrance model predicts that the oxidation rates for dry O_2 ambients will be ordered as $(110) > (111) > (100)$,[43] but, the magnitude of strain due to oxidation has also been shown to be a function of orientation, following the order $(111) < (100) < (110)$.[42] Taken together, the influence of steric hindrance and oxide strain result in orientation dependent oxidation rates being ordered as $(110) > (111) > (100)$ or $(111) > (110) > (100)$, depending on the oxide thickness and oxidation conditions.[41,43,50,63,64] The oxide thickness where the coupling of steric hindrance and oxide strain result in the oxidation rate order switching from $(110) > (111)$ to $(111) > (110)$ has been reported as being between 5 and 50 nm,[42,43,64] which is consistent with the data from the present study.

There are a number physical mechanisms that are involved in oxidation of Si and SiGe, including point defect generation,[36,65] bond strength,[31,34] steric hindrance,[41] oxide strain,[50,63] oxidant ambient,[25] and diffusivity of Si in SiGe.[25–27] It is difficult to quantitatively differentiate between various effects and their influence on Ge induced oxidation rate enhancement or reduction. However, if Arrhenius like behaviour for ν is presumed, their various influences will be integrated into the values of ν_0 and E_{ox} and can be eliminated by considering the ratio of the oxidation rates of similar samples. For example, the influence of Ge on the oxidation rate can be removed by considering $\nu_{SiGe}^{111}/\nu_{SiGe}^{100}$, while the influence of steric hindrance may be eliminated by considering $\nu_{SiGe}^{111}/\nu_{Si}^{111}$. It follows that the ratio of oxidation rates for both Si and SiGe samples of two orientations, $P = (\nu_{Si}^{111}\nu_{SiGe}^{100})/(\nu_{Si}^{100}\nu_{SiGe}^{111})$, should be equal to 1. Such ratios comparing (111) and (110) to (100) for Si and SiGe are shown in Fig. 9 where they are plotted against $\rho_{SiGe/Si}$. It should be emphasized that each data point represents a group of samples that were oxidized simultaneously, and as such, have identical oxidation times, temperatures, and oxidant ambients. Those oxidation runs that resulted in growth rate reduction ($\rho_{SiGe/Si} < 1$) show $P \approx 1$, while those oxidation runs that resulted in growth rate enhancement ($\rho_{SiGe/Si} > 1$) show $P \gg 1$. This is an indication that simple modification of the linear rate constants may not be sufficient to model the influence of Ge on the oxidation rate.

IV. CONCLUSIONS

The results of single and multiple oxidations have confirmed the strong and predictable temperature dependence of Ge content in the pile-up layer, and its relatively weak dependence on the Ge content in the underlying SiGe. Lower oxidation temperatures have been shown to be linearly correlated to higher Ge contents. Furthermore, the possibility to increase, maintain unaffected, or to decrease Ge content at the oxidation interface by manipulating the oxidation temperature has been demonstrated. The influence of crystallographic orientation on the oxidation rate of SiGe and the Ge content in the pile-up region has been examined. The redistribution of Ge in oxidizing SiGe has been characterized and explained by the balance of the fluxes of Si due to diffusion through the pile-up layer and incorporation into the oxide. X-ray diffraction and variable angle spectroscopic

ellipsometry measurements have been used along with an empirical relation for the Ge content in the pile-up region to determine the diffusivity of Si in SiGe for the three orientations. The orientation dependence of the oxidation rate of SiGe was found to follow the order $(111) > (110) > (100)$, while the magnitude of the oxidation rate ratios between orientations is a function of the oxide thickness. The presence of Ge at the oxidation interface may have either a catalytic or inhibitive effect on the oxidation rate of SiGe; any such Ge induced oxidation rate enhancement or retardation will be subject to a number of factors, including point defect generation, bond strengths, steric hindrance, oxide strain, oxidant ambient, and the diffusivity of Si in SiGe.

ACKNOWLEDGMENTS

The Norwegian Research Council (via the FRINAT program) and CNRS are gratefully acknowledged.

[1]J. N. Aqua, I. Berbezier, L. Favre, T. Frisch, and A. Ronda, Phys. Rep. **522**, 59 (2013).
[2]Y. Kim, M. Yokoyama, N. Taoka, M. Takenaka, and S. Takagi, in *IEEE Photonics Conference* (2011), pp. 465–466.
[3]L. Cao, J.-S. Park, P. Fan, B. Clemens, and M. L. Brongersma, Nano Lett. **10**, 1229 (2010).
[4]M. Kolahdouz, A. A. Farniya, M. Östling, and H. H. Radamson, ECS Trans. **33**, 221 (2010).
[5]A. H. Z. Ahmed and R. N. Tait, J. Appl. Phys. **94**, 5326 (2003).
[6]M. Kanoun, A. Souifi, S. Decossas, C. Dubois, G. Bremond, F. Bassani, Y. Lim, A. Ronda, I. Berbezier, O. Kermarrec, and D. Bensahel, MRS Proc. **776**, Q11.34 (2003).
[7]A. G. Novikau and P. I. Gaiduk, Cent. Eur. J. Phys. **8**, 57 (2010).
[8]N. Singh, K. D. Buddharaju, S. K. Manhas, A. Agarwal, S. C. Rustagi, G. Q. Lo, N. Balasubramanian, and D.-L. Kwong, IEEE Trans. Electron Devices **55**, 3107 (2008).
[9]S. Balakumar, K. D. Buddharaju, B. Tan, S. C. Rustagi, N. Singh, R. Kumar, G. Q. Lo, S. Tripathy, and D. L. Kwong, J. Electron. Mater. **38**, 443 (2009).
[10]T.-Y. Liow, K.-M. Tan, Y.-C. Yeo, A. Agarwal, A. Du, C.-H. Tung, and N. Balasubramanian, Appl. Phys. Lett. **87**, 262104 (2005).
[11]J. Hållstedt, P. E. Hellström, and H. H. Radamson, Thin Solid Films **517**, 117 (2008).
[12]E. Sutter, F. Camino, and P. Sutter, Appl. Phys. Lett. **94**, 083109 (2009).
[13]F.-J. Ma, B. S. Chia, S. C. Rustagi, and G. C. Samudra, in *ESciNano, International Conference on Enabling Science and Nanotechnology* (2010), pp. 1–2.
[14]L. Zhang, M. d'Avezac, J.-W. Luo, and A. Zunger, Nano Lett. **12**, 984 (2012).
[15]M. Palummo, M. Amato, and S. Ossicini, Phys. Rev. B **82**, 073305 (2010).
[16]X. Peng, F. Tang, and P. Logan, J. Phys.: Condens. Matter **23**, 115502 (2011).
[17]K.-W. Ang, K.-J. Chui, A. Madan, L.-Y. Wong, C.-H. Tung, N. Balasubramanian, M.-F. Li, G. S. Samudra, and Y.-C. Yeo, IEEE Electron Device Lett. **28**, 509 (2007).
[18]C. Le Royer, Microelectron. Eng. **88**, 1541 (2011).
[19]S. Nakaharai, T. Tezuka, N. Hirashita, E. Toyoda, Y. Moriyama, N. Sugiyama, and S. Takagi, J. Appl. Phys. **105**, 024515 (2009).
[20]K. Kutsukake, N. Usami, K. Fujiwara, T. Ujihara, G. Sazaki, B. Zhang, Y. Segawa, and K. Nakajima, Jpn. J. Appl. Phys., Part 2 **42**, L232 (2003).
[21]Z. Di, P. K. Chu, M. Zhang, W. Liu, Z. Song, and C. Lin, J. Appl. Phys. **97**, 064504 (2005).
[22]F. K. LeGoues, R. Rosenberg, T. Nguyen, F. Himpsel, and B. S. Meyerson, J. Appl. Phys. **65**, 1724 (1989).
[23]M. Spadafora, G. Privitera, A. Terrasi, S. Scalese, C. Bongiorno, A. Carnera, M. Di Marino, and E. Napolitani, Appl. Phys. Lett. **83**, 3713 (2003).
[24]M. A. Rabie, Y. M. Haddara, and J. Carette, J. Appl. Phys. **98**, 074904 (2005).
[25]S. J. Kilpatrick, R. J. Jaccodine, and P. E. Thompson, J. Appl. Phys. **81**, 8018 (1997).
[26]E. Long, A. Azarov, F. Kløw, A. Galeckas, A. Y. Kuznetsov, and S. Diplas, J. Appl. Phys. **111**, 024308 (2012).
[27]E. Long, A. Galeckas, and A. Y. Kuznetsov, J. Vac. Sci. Technol. B **30**, 041212 (2012).
[28]J. H. Jang, S. Y. Son, W. Lim, M. S. Phen, K. Siebein, S. J. Pearton, and V. Craciun, Appl. Phys. Lett. **94**, 202104 (2009).
[29]I. Berbezier, M. Aouassa, A. Ronda, L. Favre, A. Delobbe, and P. Sudraud "Nanofabrication of core-shell Si1-xGex/Ge nanowires, submitted to Nanotechnology" (unpublished).
[30]A. Y. Kuznetsov, H. H. Radamson, B. G. Svensson, W. X. Ni, G. V. Hansson, and A. Nylandsted Larsen, Phys. Scr. **T79**, 202 (1999).
[31]J. P. Zhang, P. L. F. Hemment, S. M. Newstead, A. R. Powell, T. E. Whall, and E. H. C. Parker, Thin Solid Films **222**, 141 (1992).
[32]O. W. Holland, C. W. White, and D. Fathy, Appl. Phys. Lett. **51**, 520 (1987).
[33]T. Shimura, Y. Okamoto, T. Inoue, T. Hosoi, and H. Watanabe, Phys. Rev. B **81**, 033308 (2010).
[34]A. R. Srivatsa, S. Sharan, O. W. Holland, and J. Narayan, J. Appl. Phys. **65**, 4028 (1989).
[35]T. Shimura, Y. Okamoto, D. Shimokawa, T. Inoue, T. Hosoi, and H. Watanabe, ECS Trans. **33**, 893 (2010).
[36]F. K. LeGoues, R. Rosenberg, and B. S. Meyerson, Appl. Phys. Lett. **54**, 644 (1989).
[37]D. Nayak, K. Kamjoo, J. C. S. Woo, J. S. Park, and K. L. Wang, Appl. Phys. Lett. **56**, 66 (1990).
[38]F. K. LeGoues, R. Rosenberg, and B. S. Meyerson, Appl. Phys. Lett. **54**, 751 (1989).
[39]E. Long, A. Galeckas, and A. Y. Kuznetsov, Phys. Status Solidi A **209**, 1934 (2012).
[40]S. Margalit, A. Bar-Lev, A. B. Kuper, H. Aharoni, and A. Neugroschel, J. Cryst. Growth **17**, 288 (1972).
[41]J. R. Ligenza, J. Phys. Chem. **65**, 2011 (1961).
[42]E. Kobeda and E. A. Irene, J. Vac. Sci. Technol. B **5**, 15 (1987).
[43]E. A. Lewis and E. A. Irene, J. Electrochem. Soc. **134**, 2332 (1987).
[44]G. Masetti, S. Solmi, and G. Soncini, Solid-State Electron. **19**, 545 (1976).
[45]P. M. Fahey, P. B. Griffin, and J. D. Plummer, Rev. Mod. Phys. **61**, 289 (1989).
[46]A. Seeger, Phys. Status Solidi B **248**, 2772 (2011).
[47]J. P. Dismukes, L. Ekstrom, and R. J. Paff, J. Phys. Chem. **68**, 3021 (1964).
[48]C. M. Herzinger, B. Johs, W. A. McGahan, J. A. Woollam, and W. Paulson, J. Appl. Phys. **83**, 3323 (1998).
[49]J. Humlíček, M. Garriga, M. I. Alonso, and M. Cardona, J. Appl. Phys. **65**, 2827 (1989).
[50]W. A. Pliskin, IBM J. Res. Dev. **10**, 198 (1966).
[51]E. A. Irene, J. Electrochem. Soc. **121**, 1613 (1974).
[52]H. Z. Massoud and J. D. Plummer, J. Appl. Phys. **62**, 3416 (1987).
[53]E. H. Nicollian and J. R. Brews, *MOS (Metal Oxide Semiconductor) Physics and Technology*, Wiley Classics Library (Wiley-Interscience, 2002), pp. 645–707.
[54]R. Kube, H. Bracht, J. Lundsgaard Hansen, A. Nylandsted Larsen, E. E. Haller, S. Paul, and W. Lerch, J. Appl. Phys. **107**, 073520 (2010).
[55]S. I. Raider, R. A. Gdula, and J. R. Petrak, Appl. Phys. Lett. **27**, 150 (1975).
[56]C. Tètelin, X. Wallart, J. P. Nys, L. Vescan, and D. J. Gravesteijn, J. Appl. Phys. **83**, 2842 (1998).
[57]J. M. Madsen, Z. Cui, and C. G. Takoudis, J. Appl. Phys. **87**, 2046 (2000).
[58]Y. S. Lim, F. Bassani, A. Portavoce, A. Ronda, S. Nozaki, and I. Berbezier, Mater. Sci. Eng., B **101**, 190 (2003).
[59]J. Xiang, N. Herbots, H. Jacobsson, P. Ye, S. Hearne, and S. Whaley, J. Appl. Phys. **80**, 1857 (1996).
[60]Z. Atzmon, A. E. Bair, T. L. Alford, D. Chandrasekhar, D. J. Smith, and J. W. Mayer, Appl. Phys. Lett. **66**, 2244 (1995).
[61]E. J. Jaquez, A. E. Bair, and T. L. Alford, Appl. Phys. Lett. **70**, 874 (1997).
[62]A. Fargeix and G. Ghibaudo, J. Appl. Phys. **54**, 7153 (1983).
[63]D.-B. Kao, J. P. McVittie, W. D. Nix, and K. C. Saraswat, IEEE Trans. Electron Devices **34**, 1008 (1987).
[64]K. Imai and K. Yamabe, MRS Proc. **239**, 107 (1991).
[65]M. Uematsu, H. Kageshima, and K. Shiraishi, Comput. Mater. Sci. **24**, 229 (2002).